An ε_{Hf} and $\delta^{18}O$ Isotopic Study of Zircon of the Mount Osceola and Conway Granites, White Mountain Batholith, New Hampshire: Deciphering the Petrogenesis of A-Type Granites

Javier F. Matos[1], Sean Kinney[2], Michael J. Dorais[1*], Eric H. Christainsen[1]

[1] Department of Geological Sciences, Brigham Young University, Provo, Utah 84602
[2] Lamont-Doherty Earth Observatory & Department of Earth and Environmental Science, Columbia University, 61 US 9W Palisades, NY 10964

ABSTRACT

The two largest A-type granites of the Mesozoic White Mountain Batholith of New Hampshire are the Mount Osceola and Conway granites. As is typical of anorogenic granites, the granites have high K_2O, Na_2O, SiO_2, FeO_{total} and low contents of Al_2O_3, MgO, CaO, Eu, and Sr and other compatible elements and high contents of REE, Zr, Nb, and high Nb/Y ratios,. Electron microprobe analyses of biotite and amphibole in both granites are similar to those in other A-type granites, being Fe-rich, and low in MgO, and Al_2O_3.

Based on their high Nb/Y ratios, both granites could be interpreted as differentiates of mantle-derived magmas (A_1) rather than melts of depleted lower crust (A_2). In spite of their A_1 whole-rock characteristics, paired microanalyses of $\delta^{18}O$ and ε_{Hf} of zircon in both granites sampled at the Redstone Quarry at Redstone, NH show significant crustal contamination. The $\delta^{18}O$ values for zircons from the Mount Osceola are between 7.4 - 8.9‰, and for the Conway Granite are 7.0 - 8.1‰. These values are distinct from zircon crystallized from mantle derived magma ($\delta^{18}O$ 5.3 ± 0.3‰), which indicates large degrees of crustal contamination in both granites. Additionally,

these same Redstone quarry zircons have $\varepsilon_{Hf\,(188Ma)}$ values for the Mount Osceola that ranges from -1.1 to +3.4, and those from the Conway Granite range from -2.1 to +4.6. Given the high $\delta^{18}O$ values for these grains, even the most positive ε_{Hf} of 4.6 is not consistent with a primary, mantle-derived magma composition.

In contrast, zircons from both granites at other locations across the batholith show a much wider range in ε_{Hf} values. Mount Osceola zircons have values as positive as 10.3 and range as low as -6.5. One anomalous grain has an extremely negative value of -17.5. Likewise, the Concord Granite has a very positive ε_{Hf} value of 11.9 and range as low as -4.5. One grain is extraordinarily negative with a value of -27.1. The most positive of these ε_{Hf} values indicate some zircon crystallized prior to contamination or at least, reflect relatively little crustal contamination, and provide a clear view of the composition of the primary, depleted mantle component to the A-type granites. Alternatively, zircons with negative ε_{Hf} and most positive $\delta^{18}O$ values crystallized after considerable crustal contamination of mantle-derived A_1 magmas and missed capturing the signature of the mantle component. The isotopic values of the Conway and Mount Osceola zircons suggest that differentiation of basaltic magmas coupled with assimilation of Ganderian basement rocks or mixing with their partial melts produced these A-type granites.

*Corresponding author

Keywords: Conway Granite, Mount Osceola Granite, A-type granite, White Mountain Batholith

INTRODUCTION

The term “A-type granite” was introduced by Loiselle and Wones (1979), referring to granites that are alkaline, anhydrous, and occur in anorogenic settings. A-type granites have high

concentrations of REE, K_2O, Na_2O, SiO_2, FeO_{total}, Y, Nb, Ta, Hf, Zr, Th, and U, and are low in Al_2O_3, MgO, and CaO. They also have higher absolute trace-element abundances (Ga, Nb) than normal continental crust and low contents of water (Eby, 1992). These geochemical characteristics have been used to define the tectonic discriminant-diagram of Pearce (1982), where the A-type granites define the within-plate granite field.

Since the initial definition of A-type granites, there has been controversy about their petrogenesis. Some authors consider that A-type granites are the result of the differentiation of mafic mantle-derived magmas (Eby, 1990). Alternatively, other authors suggest that these rocks are generated by partial melting of previously melted crustal rocks in the lower crust (Collins et al., 1982; Murphy et al., 2018). Eby (1992) contributed to this discussion by dividing A-types into two main groups: A_1 and A_2. The A_1 group is characterized as being emplaced during intraplate rifting or being associated with hotspots or plumes, representing differentiation of mantle-derived magmas. These granites have high Nb/Y values, which is probably indicative of derivation from mantle sources, similar to sources that produce intraplate magmatism such as ocean island basalts. The A_2 group are post-collisional granites, with lower Nb/Y values than A_1 granites, having been derived from the continental crust, or with a significant crustal component. These also plot as within-plate granites in the discriminant-diagrams of Pearce et al. (1984).

An example of A_1-type granites was reviewed by Eby (1990) from the British Tertiary Igneous Province of northwest Scotland. The province consists of lavas cut by felsic and mafic intrusions. The lavas have not been contaminated by the crust, however, isotopic data for the granites show significant crustal contamination, but it does not necessarily mean they have a crustal origin. The geochemical analysis shows that both felsic and mafic materials could have a mantle-derived source.

77 In contrast, Murphy et al. (2018) studied the A-type granites in Nova Scotia which were
78 emplaced over a time span of 300 million years. They suggested that these magmas were produced
79 in the lower crust during four different tectonic events. The oldest group of A-type granites is
80 related to the accretion of Gondwana and a series of oceanic island arcs. The second group of A-
81 type granites is related to subduction and considered to represent the main tectonic phase. A third
82 magmatic event resulted from strike-slip activity and a fourth event by continental rifting. These
83 A-type magmas are associated with a variety of tectonic settings and Murphy et al. (2018) contend
84 that, independent of the tectonic environment, a given terrane will have conditions favorable to the
85 repeated production of A-type magmas as a result of dehydration of crustal sources and therefore
86 conclude that the source of these A-type magmas is in the crust. Despite all the previous studies
87 of A-type granites, the influence of continental crust in this type of granites is still debated (Creaser
88 et al., 1991; Shellnut et al., 2009; Dailey et al., 2018; Vilalva et al., 2019).
89 In this study, we present in situ $\delta^{18}O$ and ε_{Hf} isotopic compositions of zircon from two A-
90 type granites of the White Mountain Batholith in New Hampshire. These data, combined with
91 silicate mineral compositions and whole-rock geochemistry, offers insights into the characteristics
92 and petrogenesis of the magmas that form A-type granites.
93

94 **GEOLOGICAL SETTING**

95 The basement of the New England portion of the Appalachian orogen is composed of
96 Precambrian Laurentian and several peri-Gondwanan terranes. The peri-Gondwanan terrains are
97 Ganderia, Avalonia, and Meguma, accreted onto Laurentia during the Salinic (~430 Ma), Acadian
98 (~400 Ma), and Neoacadian (~360 Ma) orogenies, respectively. Cover rocks overlying much of
99 the basement terranes are Rowe-Hawley, Connecticut Valley, Central Maine, and Merrimack

terranes (Figure 1). Fragments of the peri-Gondwanan terrane Ganderia are found as the basement in New Hampshire as the Massabesic Gneiss Complex (Dorais et al., 2012), and the Red Indian Line, the boundary between Laurentian and Ganderian crust, lies beneath the Late Ordovician to Early Devonian cover rocks of the Central Maine trough (Dorais et al., 2008).

As a consequence of the collision of these peri-Gondwanan terranes with Laurentia, the Paleozoic rocks of New England contains numerous granitic intrusive suites, one of which is the Devonian New Hampshire Plutonic Suite (NHPS) (Lathrop et al., 1996; Dorais, 2003). Subsequently, during the Alleghanian orogeny, the closure between Laurentia and Gondwana formed the supercontinent Pangea to complete the Appalachian orogenic events of the eastern United States. About 200 million years ago, in the Early Mesozoic, Pangea rifted, and massive amounts of basaltic magma formed the Central Atlantic Magmatic Province (CAMP) (Hames et al., 2003). This flood basalt event was followed by a Mesozoic episode of magmatism in eastern North America and formed the Jurassic to Early Cretaceous White Mountain Magma Series (WMMS) (Eby et al., 1992), the Cretaceous New England Seamounts (Duncan, 1984; Merle et al., 2019), and other intrusions. This latest magmatic event has been attributed to two settings: 1) the Great Meteor hotspot (Kinney et al., 2021) and 2) magmatism related to tensional forces, lithospheric rifting, and structural control (McHone, 1996; Merle et al., 2019). Recently, others have favored the latter hypothesis (Matton and Jébrak, 2009; Boemmels et al., 2021) because of inconsistencies with the geologic events and the plume model predictions (McHone, 1996) and attempts to synthesize the geologic history with modern geophysical anomalies (e.g., Menke et al., 2016). However, others (e.g., Kinney et al., 2021) posit that more substantial evidence is required for outright falsification of a hotspot hypothesis.

The Central Maine terrane (CMT) extends from Connecticut to northern Maine and is composed of Silurian and Devonian metasedimentary rocks (Lyons et al., 1997), mainly schists, phyllites, quartzites, slates, and minor meta-volcanic rocks. Igneous rocks emplaced in the CMT include the Devonian New Hampshire Plutonic Suite (NHPS) (Lathrop et al., 1996; Dorais, 2003) and the Mesozoic White Mountain Plutonic-Volcanic Suite (Eby et al., 1992).

The Mesozoic White Mountain Plutonic-Volcanic Suite occurs in southwest Maine, northeast Vermont, and predominantly in New Hampshire. It consists of plutons, ring complexes, and volcanics (Creasy and Eby, 1993) intruded in the CMT. The intrusions vary in composition from gabbro to granite, and in size from small plugs and dikes to large plutons and batholiths. The age of the White Mountain Plutonic-Volcanic Suite ranges from 100 to 200 Ma (Kinney, submitted) and was emplaced over two age spans: the first group is Jurassic with ages between 160 to 200 Ma; the second is Cretaceous with ages between 100 to 125 Ma (Eby et al., 1992; Foland and Allen, 1991). Creasy and Eby (1993) divided the White Mountain Plutonic-Volcanic Suite into four petrographic associations: 1) alkali syenite-quartz syenite-granite; 2) subaluminous biotite granite; 3) gabbro-diorite-monzonite; 4) syenite-nepheline syenite. These are all attributed to anorogenic, i.e., not involving collisional or subduction-related processes.

The White Mountain Batholith (Figure 2) is a member of the White Mountain Plutonic-Volcanic Suite (Eby et al., 1992). Its geology is described in Eby et al. (1992). Granite, quartz granite, and syenite comprise ~97% of the batholith, with 3% consisting of volcanic rocks. Eby et al. (1992) portrayed the batholith as having two intrusive centers, with the western half composed of the Mount Lafayette Porphyry, Mount Garfield Porphyritic Syenite, Mount Carrigain Complex, Mount Osceola Granite, the Hart Ledge Complex, and the Conway Granite. In the eastern half, the Conway Granite, Albany Porphyritic Quartz Syenite, and the Moat Volcanics are the most

145 voluminous members. Eighty percent of the batholith consists of the Conway and the Mount
146 Osceola granites.

147 The Conway Granite is the most extensive unit of the batholith (Figure 2). It is a medium
148 to coarse-grained pink biotite two-feldspar granite and, based on intrusive relationships, is younger
149 than Mount Osceola Granite (Creasy and Eby, 1993). Biotite occurs as anhedral interstitial grains
150 with zircon, allanite, apatite, and fluorite as common accessories. In contrast with the Mount
151 Osceola Granite, the Conway Granite does not contain fayalite and ferrohedenbergite (Eby et al.,
152 1992). We sampled the Conway Granite at the Redstone Quarry at Redstone, NH located in the
153 northeast portion of the White Mountain Batholith. Kinney (2021) obtained a U-Pb zircon age of
154 188.26 ± 1.5 Ma for the Conway Granite at this location. Additional samples were obtained at Mt.
155 Willard in Crawford Notch, along the Kancamagus highway between Lincoln and Albany, NH,
156 and at Middle Mountain (Kinney, 2021). The ages of the Conway Granite at these locations
157 decreases from the western portion of the batholith (Mt. Willard; 200 Ma), to 193 Ma along the
158 Kancamagus Highway, to 183 Ma at Middle Mountain (Kinney, 2021).

159 The Mount Osceola Granite is the second-largest granite (in area; Figure 2) in the White
160 Mountain Batholith (Eby et al., 1992). The rock is medium- to coarse-grained, consisting mainly
161 of microperthite, quartz, ferrohastingsite and biotite that forms a hypidiomorphic granular texture
162 (Creasy and Eby, 1993). In contrast with the Conway Granite, fayalite, and ferrohedenbergite
163 occur as rounded grains and as inclusions within miroperthite (Eby et al., 1992). Samples were
164 obtained at the Redstone Quarry, Rattlesnake Mountain near Redstone and Humphrey's Ledge
165 near Intervale, NH (Kinney, 2021). The Mt. Osceola Granite at and near Redstone has an age of
166 185 Ma and that at Humphrey's Ledge is 183 Ma (Kinney, 2021).
167

INSTRUMENTAL METHODS

Electron microprobe

Biotite and amphibole analyses were conducted on a Cameca SX50 electron microprobe at Brigham Young University. Both minerals were analyzed with 15 KV, 10 nA, and 10μm beam. Amphibole was analyzed only for Mount Osceola Granite as no amphibole is present in the Conway granite.

Bulk-rock major and trace elements XRF were analyzed with a Rigaku ZSX Primus II at Brigham Young University (methods are described in Dailey et al., 2018). Fused disks were used for major elements and pressed pellets for trace elements. Additional trace element analyses were conducted by inductively coupled plasma mass spectrometry (ICP-MS) at ALS USA Inc. in Reno, Nevada.

Oxygen and hafnium isotopes in zircon

Two populations of zircons were studied. The first was analyzed for both oxygen and hafnium isotopic compositions. The second was the subject of detailed geochronologic study of the White Mountain Batholith (Kinney, 2021) and were analyzed only for Hf isotopic composition. For simplicity's sake, we refer to the two populations as the paired and unpaired zircons respectively.

In the paired zircon study, zircon grains were separated from the Mount Osceola and Conway granites using magnetic and density separation techniques at Brigham Young University. About one hundred zircon grains from each granite were analyzed at the University of Wisconsin-Madison; they were mounted in epoxy with the KIM-5 standard and polished until an approximately equatorial section was exposed. Zircons were imaged using panchromatic

cathodoluminescence (CL) at Brigham Young University to reveal the morphology and zoning of the grains.

These images were used as a guide to select fifteen zircon grains from each granite that were analyzed according to the textural characteristics they presented. Most grains were euhedral to subhedral and presented prismatic shapes as well as oscillatory zoning (Figure 3). Zircon grain sizes vary, averaging 250 μm with some grains up to 600 μm. All grains (thirty in total) were euhedral to subhedral and showed oscillatory zoning typical of igneous zircon. The analyzed locations were selected to target cores and rims of zircons with oscillatory zoning and thus provide the characteristics of the isotopic evolution of the magma during zircon growth.

Oxygen isotope analyses of zircon were performed on the WiscSIMS CAMECA ims-1280 multi-collector ion microprobe at the University of Wisconsin-Madison following the analytical protocols of Kita et al. (2009). A beam of 1.9-2.1 nA Cs^+ ions was used with a diameter of 12-20 μm long × 10-15 μm wide × 1 μm deep. Further details of SIMS oxygen isotope methods are found in Bonamici et al. (2015) and Page et al. (2019). Precision is typically ≤0.3‰ (Kita et al., 2009) with uncertainty within 2 standard errors (2SE); results are consequently reported to one decimal place.

The same zircon grains that were analyzed for oxygen isotopes were subsequently analyzed for Hf isotopes at the University of California Santa Barbara in one analytical session via laser ablation multi-collector inductively coupled plasma mass spectrometry (LA-MC-ICP-MS) (Kylander-Clark et al., 2013). Locations for Hf isotope analyses were adjacent to the craters for oxygen isotopes. A Photon Machines Excite laser was used with 40 μm diameter, 10Hz, ~1J/cm^2, over a 30 second period. A Nu Plasma P3D MC-ICPMS was used for Hf isotope measurement; masses 171-182 were measured on faraday cups L4-H7.

A total of sixty spots (thirty in the Mount Osceola Granite and thirty in the Conway Granite) were analyzed for both oxygen and hafnium isotopes. Precision is typically (0.035%, 2σ); results are consequently reported to one decimal place.

The unpaired zircons of Kinney (2021) produced an additional 111 analyses for Hf isotopes on a second zircon population at the LaserChron center for geochronology at the University of Arizona. Hf isotope analyses are conducted with a Nu HR ICPMS connected to a New Wave UP193HE laser (2009-2010) or a Photon Machines Analyte G2 excimer laser (2011). Instrument settings are established first by analysis of 10 ppb solutions of JMC475 and a Spex Hf solution, and then by analysis of 10 ppb solutions containing Spex Hf, Yb, and Lu. The mixtures range in concentration of Yb and Lu, with ^{176}(Yb+Lu) up to 70% of the ^{176}Hf. When all solutions yield ^{176}Hf/^{177}Hf of ~0.28216, instrument settings are optimized for laser ablation analyses and seven different standard zircons (Mud Tank, 91500, Temora, R33, FC52, Plesovice, and Sri Lanka) are analyzed. These standards are included with unknowns on the same epoxy mounts. When precision and accuracy are acceptable, unknowns are analyzed using exactly the same acquisition parameters.

Laser ablation analyses are conducted with a laser beam diameter of 40 microns, with the ablation pits located on top of the U-Pb analysis pits. CL images are used to ensure that the ablation pits do not overlap multiple age domains or inclusions. Each acquisition consists of one 40-second integration on backgrounds (on peaks with no laser firing) followed by 60 one-second integrations with the laser firing. Using a typical laser fluence of ~5 J/cm2 and pulse rate of 7 hz, the ablation rate is ~0.8 microns per second. Each standard is analyzed once for every ~20 unknowns.

Isotope fractionation is accounted for using the method of Woodhead et al. (2004): βHf is determined from the measured ^{179}Hf/^{177}Hf; βYb is determined from the measured ^{173}Yb/^{171}Yb

(except for very low Yb signals); βLu is assumed to be the same as βYb; and an exponential formula is used for fractionation correction. Yb and Lu interferences are corrected by measurement of $^{176}Yb/^{171}Yb$ and $^{176}Lu/^{175}Lu$ (respectively), as advocated by Woodhead et al. (2004). Critical isotope ratios are $^{179}Hf/^{177}Hf$ =0.73250 (Patchett and Tatsumoto, 1981); $^{173}Yb/^{171}Yb$ = 1.132338 (Vervoort et al., 2004); $^{176}Yb/^{171}Yb$ =0.901691 (Vervoort et al., 2004); $^{176}Lu/^{175}Lu$ = 0.02653 (Patchett, 1983). All corrections are done line-by-line. For very low Yb signals, βHf is used for fractionation of Yb isotopes. The corrected $^{176}Hf/^{177}Hf$ values are filtered for outliers (2-sigma filter), and the average and standard error are calculated from the resulting ~58 integrations. There is no capability to use only a portion of the acquired data.

All solutions, standards, and unknowns analyzed during a session are reduced together. The cutoff for using βHf versus βYb is determined by monitoring the average offset of the standards from their known values, and the cutoff is set at the minimum offset. For most data sets, this is achieved at ~6 mv of ^{171}Yb. For sessions in which the standards yield $^{176}Hf/^{177}Hf$ values that are shifted consistently from the know values, a correction factor is applied to the $^{176}Hf/^{177}Hf$ of all standards and unknowns. This correction factor, which is not necessary for most sessions, averages 1 epsilon unit.

The $^{176}Hf/^{177}Hf$ at time of crystallization is calculated from measurement of present-day $^{176}Hf/^{177}Hf$ and $^{176}Lu/^{177}Hf$, using the decay constant of ^{176}Lu (λ = 1.867e-11) from Scherer et al. (2001) and Söderlund et al. (2004).

Age corrections (to 188 Ma) were made for all zircon grains, using the decay constant for ^{176}Lu of 1.867×10^{-11} $year^{-1}$ (Sönderlund et al., 2004). Model ages were calculated using chondritic ratios of Bouvier et al. (2008): $^{176}Hf/^{177}Hf$ = 0.282785, and $^{176}Lu/^{177}Hf$ = 0.0336 for a chondritic uniform reservoir (CHUR). Present-day depleted mantle (DM) composition was from Andersen et

al. (2009): $^{176}Lu/^{177}Hf = 0.0388$, and Griffin et al. (2000): $^{176}Hf/^{177}Hf = 0.28325$. Depleted Mantle (Crustal) model age (T_{DM}^{c}) was calculated assuming that the parental magma of zircon was produced from average continental crust with $^{176}Lu/^{177}Hf=0.015$ from Goodge and Vervoort (2006).

RESULTS

Petrography

Mount Osceola Granite

The Mount Osceola Granite is a medium- to coarse-grained, equigranular and holocrystalline granite (Creasy and Eby, 1993). The rock consists of alkali feldspar, biotite, quartz, amphibole, biotite, and plagioclase, with zircon and apatite as accessory minerals. Riebeckite is reported from some Mount Osceola Granite locations (Creasy and Eby, 1993), but is not present in our samples. Billings (1956) gives the modal proportions of the Mount Osceola Granite as 25% quartz, 63% Kspar, 8% plagioclase, 4% amphibole and biotite, and trace amounts of olivine and pyroxene in some locations.

Alkali feldspar appears ranging from 0.5 up to 4mm. Crystals are mostly subhedral and anhedral. Quartz is present in anhedral crystals (up to 3mm) with undulatory extinction. The amphibole has greenish to brownish pleochroism and is associated with hematite and biotite. Most of the crystals are subhedral, and with sizes from 2 to 5mm.

Zircon is present in prismatic forms and euhedral crystals in sizes up to 0.2mm. Apatite occurs as an accessory mineral, and it is characterized by euhedral grains, usually as inclusions in biotite and amphibole.

Conway Granite

The Conway Granite is a medium-to coarse-grained granite (Creasy and Eby, 1993). The mineral assemblage is alkali-feldspar, quartz, biotite, with zircon and apatite as accessory minerals. The rock is equigranular and its crystals have sizes from 2 to 5mm. Billings (1956) give the mode of the granite as 29% quartz, 59% Kspar, 7% plagioclase, and 5% biotite.

Alkali-feldspar is abundant. It is present in subhedral crystals ranging from 2 to 6mm, with irregular shapes and borders. Quartz is also very abundant, characterized by anhedral crystals and undulatory extinction. They range in size from 3-5mm, with some occasional grains up to 6mm. A small quantity of subhereal biotite is up to 2mm long. Some grains of biotite have inclusions of zircon. The pleochroism of biotite is brown to light brown.

Apatite is present in euhedral grains, up to 0.2mm long. It is observable as inclusions in mafic silicates like biotite. Zircon, another accessory mineral, displays prismatic forms in euhedral crystals.

Mineral chemistry

Biotite

Biotite analyses for both granites are presented in Table 1 and plotted in the Al (cpfu) versus Fe/(Fe+Mg) diagram (Figure 4). Fields of biotite from A, I, and S-type granites are displayed in the diagram (after Christiansen et al., 1986). Biotite analyses of both granites plot within the field of A-type granites, with the Mount Osceola biotites having very high Fe/(Fe+Mg) values of ~0.97. Conway Granite biotites are also Fe-rich, but less so than the Mount Osceola Granite with Fe/(Fe+Mg) values of ~0.85.

Amphibole

Electron microprobe analyses of amphibole were only conducted for Mount Osceola Granite since no amphibole was found in the Conway Granite. The results are in Table 2 and were plotted on a Si (cpfu) versus Mg/(Mg+Fe) classification diagram of Leake et al. (1997; Figure 5). These amphiboles have low contents of Mg; the Fe-rich nature of A-type granites is reflected in the low Mg/(Mg+Fe) values of Mount Osceola Granite amphiboles. In comparison, amphiboles in I-type calc-alkaline rocks of the Sierra Nevada Batholith are more Mg-rich (Dodge et al., 1968; Dorais et al., 1990).

Whole-rock geochemistry

Major elements geochemistry

Major element compositions of the Mount Osceola and the Conway granites are given in Table 3. Both granites have high K_2O, Na_2O, SiO_2, FeO_T, but low Al_2O_3, MgO, and CaO, as is characteristic of A-type granites (Figure 6).

Both granites have over 70% SiO_2, but the Conway Granite extends to slightly higher values. The Mount Osceola Granite has lower MgO, Na_2O, and P_2O_5 than the Conway Granite, but higher CaO and K_2O.

Trace elements geochemistry

Chondrite-normalized REE patterns for both granites are presented in Figure 7A. Both the Mount Osceola and the Conway granites show very similar patterns, with the Mount Osceola Granite being more enriched than the Conway Granite. The patterns for both granites show negative slopes for the LREE, that tend to flatten out for the Mount Osceola Granite in the HREE and become flat for the Conway Granite.

The Eu anomalies for both granites were calculated using the equation $Eu_{CN}/(Sm_{CN}*Gd_{CN})^{0.5}$. The Eu anomalies are similar for both granites: Mount Osceola Granite (0.21-0.38) and Conway Granite (0.23-0.37). The depletion in Eu in the diagram indicates fractional crystallization of feldspar and is a characteristic of A-type granites. Additionally, the $(La/Yb)_N$ ratios of all analyzed samples are between 9.8-19.5.

The trace element patterns on the primitive-mantle normalized diagram (Figure 7B) of both the Mount Osceola and Conway granites are also similar, with a few variations. They are characterized by enrichments of large ion lithophile elements (LILE), especially Rb, Th, and U. Additionally, the granites have high Zr and Nb contents as typical of A-type granites (Loiselle and Wones, 1979). Patiño-Douce (1997) indicated that low Sr contents are also characteristic of A-type granites, a characteristic shown in Figure 7B for the Mount Osceola and Conway Granites (<5 ppm), lower than typical I-type granites (Patiño-Douce, 1997). The Mount Osceola Granite is richer in La, Ce, Nd, Sm, Zr and the HREE values are slightly higher than the Conway Granite that has higher values of Th and U.

Tectonic discrimination diagrams

Figure 8 shows the whole-rock compositions plotted in the discrimination diagrams of Pearce et al. (1984). Both granites plot in the field of within-plate granites (WPG) in all four diagrams. In the Rb vs. Yb+Ta diagram, the Conway Granite plots on and near the boundary between the syn-COLG (syn-collisional granite) and the WPG field. Both plutons have Nb/Y>2, (or Y/Nb < 0.5) the dividing line between A_1 and A_2 granites of Eby (1992).

The Ce/Nb versus Y/Nb and the Yb/Ta versus Y/Nb diagrams (Figure 9, Eby, 1990) distinguish ocean island basalts (OIB) and island arc basalts (IAB). Eby (1990) and Eby et al. (1992) found that the ratios in differentiates of mafic magmas remain relatively constant

throughout the evolution to A-type suites despite crustal contamination. Thus, the ratios are useful petrogenetic indicators because assimilation of crust with lower abundances of these trace elements does not radically change the initial ratios of the parental mafic magmas. Both the Mount Osceola and the Conway granites plot in the OIB field, suggesting they differentiated from mafic magmas with a mantle origin. However, the Mount Osceola Granite extends up toward the IAB field that is typical of continental crust, suggesting that the Mount Osceola Granite has a larger crustal component than the Conway Granite.

Eby (1992) used the typically incompatible elements Ce, Y, Nb, and Ga to discriminate between the two A-type groups. Continental crustal rocks tend to be Nb-poor and partial melts of such rocks are in turn, Nb-poor. Thus, A_2-type granites that are hypothetically derived from the melting of residual crust plot in the lower regions in these diagrams. In contrast, A_1-type magmas presumed to have originated primarily by differentiation of mantle-derived magmas, preserve higher Nb/Y ratios. Both the Mount Osceola and Conway granites fall within the A_1-type (primarily from mantle-derived melts) field (Figure 10), with the Mount Osceola Granite plotting closer to the border with the A_2-type (partial melting of crust) field. Both diagrams suggest that these trace element ratios for both granites are dominated by a mantle component.

Zircon saturation thermometry

Watson and Harrison (1983) formulated a zircon saturation thermometer that provides estimates of the temperatures of zircon crystallization in silicate magmas. Boehnke et al. (2013) proposed an updated thermometer that gives temperatures that are usually lower than those derived from Watson and Harrison (1983). Applying the zircon saturation temperature formulation of Boehnke et al. (2013), the highest temperatures are for the Mount Osceola Granite that range from 803-838˚C, whereas the Conway Granite has temperatures between 758-790˚C. Clemens et al.

(1986), using the zircon saturation thermometer of Watson and Harrison (1983), that gives temperatures 25-50°C higher than Boehnke et al. (2013), indicated that temperatures >830°C are higher than those of typical I and S-type granites, concluding that temperatures > 830°C (~780°C with Boehnke et al., 2013) are a characteristic of A-type granites.

Oxygen and hafnium isotopic compositions of zircon

To determine the geochemical characteristics and evolution of the magmas that formed the Mount Osceola and Conway granites from the Redstone Quarry, both cores and rims of fifteen grains (with oscillatory zoning) for each granite were analyzed for oxygen and hafnium isotopes. As a result, a total of sixty spots for oxygen and sixty spots for hafnium isotopes were analyzed for these paired grains (Tables 4 and 5; Supplementary Figure 1).

The results of zircon isotopic analyses of Hf and O are plotted in Figure 11. Zircons in the Mount Osceola Granite have higher $\delta^{18}O$ values (7.4 - 8.8‰) than zircon from the Conway Granite. Two of the analyses of zircon from the Mount Osceola Granite plot with the zircons from the Conway granite, below the main Mount Osceola group that ranges between 8.0 and 8.8‰. $\delta^{18}O$ values of zircon from the Conway Granite lie between 7.0 and 8.1‰, distinctly below the Mount Osceola Granite but considerably higher than the mantle zircon field (5.3±0.3‰, Valley, 2003).

Zircons from the Mount Osceola Granite have $^{176}Lu/^{177}Hf$ ratios from 0.000429 to 0.004210, and $^{176}Hf/^{177}Hf$ ratios from 0.282636 to 0.282778. Moreover, the Conway Granite has $^{176}Lu/^{177}Hf$ of 0.000788 to 0.009880, and $^{176}Hf/^{177}Hf$ ratios between 0.282620 to 0.282820. The calculated ε_{Hf} values at 188 Ma are given in Table 5 (and in histograms in Supplementary Figure 2). Both granites have a similar range and average $\varepsilon_{Hf.}$ The zircons paired with $\delta^{18}O$ analyses from

392 the Mount Osceola Granite have ε_{Hf} values ranging from -1.2 to +3.4, and zircons from the Conway
393 Granite have values between -2.1 to +4.6.

394 The majority of unpaired analyses of zircons from other locations across the White
395 Mountain Batholith generally show a similar range of ε_{Hf} values but extend to considerably higher
396 values (Table 6; Figures 11 and 12). Zircons from the Conway Granite are as positive as 11.9 and
397 negative as -4.6, extending the range found in the paired grains. Likewise, ε_{Hf} values zircons from
398 the Mount Osceola Granite extend the range defined by the paired zircons, plotting between 10.31
399 and -6.52. Two zircon analyses are anomalous; one Mt. Osceola grain has a strongly negative ε_{Hf}
400 value of -17.5. The other analysis, on a Conway Granite zircon, has the most negative value of -
401 27.1. Both analyses are well below the cluster of other Conway and Mt. Osceola zircons. Taken
402 together, the analyses form a steep negative trend with increasing ε_{Hf} values with decreasing age.

403 With the exceptions of the two most negative grains, the Hf model ages obtained for the
404 Mount Osceola Granite range from 400 to 1080 Ma for depleted mantle (T_{DM}) and the Conway
405 Granite has Hf model ages ranging from 380 to 950 Ma (T_{DM}). The two anomalous grains with
406 strongly negative ε_{Hf} values have model ages between 1200 and 1400 Ma.

407

408 **DISCUSSION**

409 The origin of A-type magmas is still the subject of continued research (Shellnutt et al.,
410 2009; Vilalva et al., 2019). Petrogenetic interpretations of A-type magmas are divided into three
411 major models: 1) Fractionation or assimilation-fractional crystallization (AFC) from mantle-
412 derived magmas (Eby, 1990; Turner et al., 1992; Shellnutt et al., 2009); 2) Mixing between crustal
413 melts and mantle-derived magmas (Dailey et al., 2018); and 3) Partial melting of dry, lower crust
414 (granulitic) (Collins et al., 1982; Patiño-Douce, 1997). The data presented in this research together

415 with previous work in the area suggest that the Mount Osceola and Conway granites are the results
416 of highly contaminated mantle-derived magmas or mixing between mantle and crustal melts. This
417 is supported by the mineralogy and whole-rock geochemistry, and zircon isotopic characteristics
418 of both granites.

419 **Mineralogy and whole-rock geochemistry**

420 As it has been previously stated, A-type granites are characterized by high contents of
421 Fe_2O_3T, K_2O, Na_2O, Si_2O, and REE, characteristics of both the Mount Osceola and Conway
422 granites. Electron microprobe analyses conducted on biotite and amphibole of the Mount Osceola
423 and Conway granites confirmed that both granites are Fe-rich (Figures 4 and 5), with values of
424 Fe/(Fe+Mg) close to 1 in the Mount Osceola Granite. In the TAS diagram, they are classified as
425 granites, in the MALI diagram they plot in the alkali-calcic and alkalic fields, and in the
426 FeO/(FeO+MgO) diagram they plot as ferroan (diagrams not shown). These whole-rock and
427 mineralogical compositions are characteristic of A-type granites.

428 Moreover, trace element concentrations from the Mount Osceola and Conway granites
429 show typical patterns of A-type magmas in the spider diagrams with small Nb anomalies and
430 enrichments in HFSE (Figure 7B). A-type magmas plot in the fields of WPG in tectonic
431 discrimination diagrams (Figure 8), and in the OIB of Figure 9, as do the Mount Osceola and
432 Conway granites. Additionally, the Mount Osceola and Conway granites are classified as A_1 in
433 Eby's (1992) diagrams (Figure 10), based on their high Nb/Y, indicating that the Mount Osceola
434 and Conway granites represent differentiation of mantle-derived magmas (Eby, 1992).

435 However, whole-rock major and trace element data do not completely explain the
436 petrogenesis of the granites. Figures 9 and 10 do not reflect the degree of crustal contamination in
437 the granites because the trace elements used in the discriminant diagrams have higher

concentrations than typical crust and their concentrations are less sensitive to continental crustal contamination (Eby, personal communication, 2021). On the other hand, whole-rock isotopic data are sensitive to contamination. Eby et al. (1992) conducted Sr isotopic analyses of several intrusions of the White Mountain Batholith. They found that the Mount Osceola Granite has $^{87}Sr/^{86}Sr_i$ as high as 0.70697, and the Conway Granite up to 0.73641. Similarly, Foland and Allen (1991) conducted whole-rock Sr isotopic analyses of Mesozoic granitic rocks from the White Mountain magma series, obtaining $^{87}Sr/^{86}Sr_i$ values from 0.70310 to 0.7088 and ε_{Nd} from 1.9 to -1.5. They concluded these magmas are mantle-derived with the incorporation of crustal components, but uncertainties about the nature of the parental mafic magma and the contaminant remain.

Zircon isotopic characteristics

O isotopes

$\delta^{18}O$ values for the Mount Osceola and the Conway granites are between 7 and 9‰ (Table 4, Figure 11). The Conway Granite has slightly lower $\delta^{18}O$ values than the Mount Osceola Granite, but both are higher than $\delta^{18}O$ of zircon in uncontaminated mantle-derived magma that has $\delta^{18}O$ values of 5.3±0.3‰ (Valley et al., 2003), demonstrating that either the granites were derived from continental crust or they had mafic, mantle-derived parents that were highly contaminated by continental crust that increased their $\delta^{18}O$ values (Kemp et al., 2007). Given that the rocks consist of approximately 50% oxygen, significant amounts of contamination occurred to drive the $\delta^{18}O$ values from 5.3 to 9‰. The higher $\delta^{18}O$ values of zircon in the Mount Osceola Granite than the Conway Granite indicates either slightly different sources/contaminants, or more extensive contamination of the Mount Osceola Granite as suggested by the Ce/Nb versus Y/Nb and Yb/Ta versus Y/Nb diagrams (Figure 9).

Hf isotopes

Hf isotope ratios in zircon are also sensitive tracers of crustal and mantle inputs to magmatic systems (Shellnutt et al., 2009; Colón et al., 2018). High ε_{Hf} (>0) values in zircon indicate mantle-derived components, whereas marginally low ε_{Hf} (<0) values are evidence of either enriched mantle or crustal contamination (Wong et al., 2009; Shellnutt et al., 2009; Castillo et al., 2017). Strongly negative ε_{Hf} values indicate a dominance of crust which has intrinsically low Lu/Hf ratios.

The most positive ε_{Hf} values for paired zircons from the Redstone Quary are 3.4 for Mount Osceola zircons and 4.7 for the Conway Granite zircons. (Table 5, Figure 11). Even though magmas derived from depleted mantle can have similar ε_{Hf} values, these analyses are paired with $\delta^{18}O$ values between 7 and 9, significantly higher than mantle values near 5.3±0.3‰ (Valley, 2003; Valley et al., 2005) and indicative of a considerable crustal component or source in the continental crust.

The most primitive ε_{Hf} composition for the Mt. Osceola and Conway granites is better preserved in the unpaired zircons from other locations in the White Mountain Batholith. A histogram of these analyses is plotted in Figure 11 (and in more detail in Supplementary Figure 2). Figure 12 plots ε_{Hf} versus age for both the paired and unpaired zircon analyses from the granites (plotted in more detail in Supplementary Figure 1). Also shown are evolution curves for depleted mantle and CHUR (Goodge and Vervoort, 2006; Blitcher-Toft and Puchtel, 2010.). The unpaired ε_{Hf} analyses extend the range of ε_{Hf} values to ~+12. Note the essentially continuous range and simple normal distribution of isotopic values from -5 to +12 (Fig. 11 and Supplementary Figure 2). The high ε_{Hf} values (>10) are consistent with a parental component from the mantle to these A-type granites. Given that these grains are relatively abundant (11% of the spots analyzed had ε_{Hf}>

6; see histogram of Figure 11 and Table 6 and Supplementary Figure 2) and that they are widely distributed in granites across the batholith ($\varepsilon_{Hf} > 6$ is found in 50% of the samples examined), we think they represent an essential endmember composition to the granites; we consider them to be antecrysts.

Most of the zircon isotopic data correlates with the whole-rock analyses of Conway and Mount Osceola granites of Foland and Allen (1991) who reported $\varepsilon_{Nd(188\ Ma)}$ values ranging from 1.9 to -1.5 and $^{87}Sr/^{86}Sr_i$ from 0.70421 to 0.7088, and the $^{87}Sr/^{86}Sr_i$ of Eby et al. (1992) that range from 0.70397 to 0.73641, all demonstrate that the granites contain a high percentage of a crustal component. However, the most positive ε_{Hf} analyses indicate that some zircon grains crystallized before contamination/mixing took place and demonstrate the greater utility of mineral compared to whole-rock isotopic analyses to determine the petrogenesis of these A-type granites.

Petrogenesis of the Mount Osceola and Conway granites

Converted whole-rock $\varepsilon_{Nd\ (413\ Ma)}$ and $\delta^{18}O$ values of metasedimentary rock from the Central Maine terrane (CMT) (Lathrop et al., 1996) are plotted on Figure 11. No Hf isotopic data are available for the CMT metasediments; we approximated ε_{Hf}, fromtheir ε_{Nd} values using: $\varepsilon_{Hf} = 1.55 \times \varepsilon_{Nd} + 1.21$ (Vervoort et al., 2011). Fu et al. (2014) studied the isotopic composition of zircon in Laurentia, Ganderia, and Avalonia, other basement terranes of New England. They deliberately chose zircons from Avalonian rocks with anomalous negative $\delta^{18}O$ whole-rock values to evaluate the regional meteoric water-rock interaction; hence, these data are not completely representative of Avalonian compositions. The rocks and values reported are from Laurentia: Washington and Tyringham gneisses in Massachusetts (ε_{HfT}: -3.1 to 5.8 and $\delta^{18}O$ from 7.1 to 11.9‰); Ganderia: muscovite granite at Bucksport, Maine (ε_{Hf}: -3.1 to 2.1 and $\delta^{18}O$: 8.5 to 11.8‰); and Avalonia: Hope Valley plagioclase gneiss, Connecticut: (ε_{HfT}: 3.9 to 7.5 and

507 $\delta^{18}O$ from 1.6 to 6.2‰) and the Quincy Granite, Massachusetts (ε_{Hf}: 3.2 to 4.7 and $\delta^{18}O$ from 0.3
508 to 3.2‰). These ε_{Hf} values are corroborated with ε_{Hf} zircon analyses from Henderson et al.
509 (2018) and Willner et al. (2014) on similar Avalonian and Ganderian rocks (Figure 12).
510 More broadly representative values for Ganderia and Avalonia are from Fryer et al. (1992)
511 and Potter et al. (2008) who reported whole-rock $\delta^{18}O$ values for igneous rocks of Ganderia and
512 Avalonia in New England and Newfoundland. The values obtained for $\delta^{18}O$ are ~3 to 9‰ in rocks
513 from Avalonia; rocks from Ganderia have predominant values of ~5 to 12‰. The horizontal lines
514 in Figure 11 show these ranges. Fractionation between zircon and its parent magma results in $\delta^{18}O$
515 in zircon being 1 to 1.5‰ lower than the magma (Teixeira et al., 2019). Whole-rock $\delta^{18}O$ values
516 for Ganderia and Avalonia of Potter et al. (2008), Fryer et al. (1992), and whole-rock $\delta^{18}O$ values
517 of metesadimentary rocks of Lathrop et al. (1996) were adjusted by subtracting 1‰.
518 To determine the composition of the crustal component in the Mount Osceola and Conway
519 granites, core and rim analyses were conducted on the zircons (Figure 13). Zircon locks in the ε_{Hf}
520 and $\delta^{18}O$ isotopes and records those isotopic characteristics of the magma from which it
521 crystallized. As zircon crystallizes, isotopic variations in magmas can be preserved in zircon and
522 revealed when both core and rim are analyzed. The black arrows show the isotopic variations of
523 zircon from core to rim. In general, the arrows show that core-rim isotopic evolution in zircon does
524 not have consistent trends of increasing or decreasing in ε_{Hf} and $\delta^{18}O$. However, it should be
525 noted that the core-rim variations do not always exceed the analytical uncertainty at the ± 2 s.e.
526 level. Consequently, many of the analyses are statistically indistinguishable from one another.
527 The lack of consistent directional zoning can be interpreted in two ways. First, if the crustal
528 component was the CMT or Laurentian crust, it might be expected that the core-rim zoning would
529 trend to lower epsilon Hf in this diagram, towards the fields of potential contaminants at lower ε_{Hf}

values. The core-rim differences that exceed the 2 s.e. uncertainty could suggest that the crustal endmember had ε_{Hf} values that were considerably higher than those of the CMT or Laurentia and that neither was the dominant crustal component in the Mount Osceola and Conway granites. If this is the case, then the most probable crust involved in the formation of the Mount Osceola and Conway granites had ε_{Hf} values that were positive or at least, mildly negative. The second and preferred interpretation of the zircon core-rim trends is that contamination/mixing and homogenization of the various magma systems occurred before these zircons crystallized and that the zircons do not provide compositional vectors to define the crustal component.

The temperature of the formation of zircon provides insights into the timing of contamination for the Mount Osceola and Conway granites. Several studies and previous work indicate ranges of temperatures of formation of A-type granites. Some authors propose that A-type magmas are generated by temperatures of 750 ^{o}C and higher (Murphy et al., 2018). The zircon saturation temperatures obtained for the Mount Osceola and Conway granites confirm these high-temperature inferences; they are between 758-838 ^{o}C (with an average of 792 ^{o}C). Importantly, the zircon saturation temperatures suggest that the magmas that formed both granites underwent a process of crustal contamination/mixing at temperatures higher than 838^{o}C because even the cores of the paired zircons indicate crustal contamination and lack mantle-like $\delta^{18}O$ values. Thus, the lack of isotopic zoning in the majority of the zircons with compositional vectors pointing to a specific contaminant hinder precise identification of that contaminant and suggests near complete homogenization of the contaminant and host magma prior to zircon crystallization. Subtle differences in zircon isotopic zoning reflect mixing of different aliquots of hybridized granitic melts with slightly different isotopic values. The unpaired zircon analyses lack corresponding oxygen isotopic analyses, but we infer that zircons with ε_{Hf} values between +6 and +12 would

553 have more mantle-like $\delta^{18}O$ values and that these zircons could better define a potential mantle
554 endmember.

555 In spite of the lack of zircon isotopic zoning to define the crustal components, the ε_{Hf} versus
556 age diagram (Figure 12) allows inferences on its identity. According to Eusden and Lyons (1993),
557 the allochthonous CMT sequence may be as thin as 3 kilometers and we find it unlikely that such
558 a thin sequence could have significantly melted to mix with or to contaminate the inferred mafic
559 endmember of the White Mountain Batholith, leaving Ganderia or Avalonia as preferred crustal
560 endmember. Ganderia and Avalonia are dominated by rocks with ages of ~ 600 Ma. Figure 12
561 includes fields for zircons of this age from these peri-Gondwanan terranes (Willner et al., 2014;
562 Henderson et al., 2018). Crustal evolution fields from Ganderia and Avalonia project below and
563 down through the lower portion of the Conway and Mount Osceola data sets. The Conway and
564 Mount Osceola trends can be explained by mixing of a juvenile mantle component (with ε_{Hf} value
565 of +12) and a peri-Gondwanan component.

566 The strongly negative ε_{Hf} values of -27 for one of the zircons of the Conway Granite and -
567 17 for a Mount Osceola zircon require even older continental crust as a component. The source
568 could be Laurentian crust because such negative ε_{Hf} values were found by Fu et al. (2014).
569 However, Laurentian crust is not required because while such values are rare for both Ganderia or
570 Avalonia (Fu et al., 2014; Willme et al., 2014; Henderson et al., 2018; Severson et al., 2022), a
571 minor component with this isotopic signature is present, thereby permitting the peri-Gondwanan
572 terranes of New England to be the major contaminant in both the Conway and Mount Osceola
573 granites.

574 The inference of contamination by peri-Gondwanan rocks is supported by the histogram in
575 Figure 14 that shows the converted $\delta^{18}O$ values from Ganderia and Avalonia (Potter et al. 2008)

576 that are compared to $\delta^{18}O$ in zircon from the Mount Osceola and Conway granites. Ganderia
577 zircons have predominant values between 6-9‰, whereas predicted $\delta^{18}O$ of Avalonia zircons are
578 mainly between 5-8‰. Although they overlap, Avalonia extends to lower $\delta^{18}O$ than Ganderia.
579 $\delta^{18}O$ values of zircon from the Mount Osceola and Conway granites plot in or near the overlapping
580 area of Ganderia and Avalonia of Potter et al. (2008). Thus, mixing with or contamination of a
581 depleted mantle-derived basaltic magma by peri-Gondwanan rocks can explain the oxygen (and
582 Hf) isotopic compositions of the majority of the analyzed zircons.

583 Wintsch et al. (2014) provided evidence that Avalonia wedged into Ganderian rocks (see
584 inset on Figure 1). How far Avalonia projects under the cover rocks in New England has not been
585 determined, but Ganderian rocks are present as the Massabesic Gneiss Complex of southeastern
586 New Hampshire (Figure 1; Dorais et al., 2012). The Conway and Mount Osceola granites lie
587 inboard of the Massabesic Gneiss Complex, hence, it is more reasonable to infer that Ganderia,
588 rather than Avalonia, was the dominant contaminant to the granites.

589 Choosing Ganderia as the most plausible crustal endmember in the granites of the White
590 Mountain Batholith, we modeled assimilation-fractional crystallization and binary mixing
591 between the inferred mafic endmember and two Ganderian endmembers. The mantle endmember
592 is assumed to have an ε_{Hf} value represented by the most positive of the unpaired zircon analyses-
593 - +12-- and an inferred $\delta^{18}O$ of 5.3 typical of the mantle. Hf and Lu concentrations are those of
594 average OIB (Sun and McDonald, 1989). The Ganderian endmember is inferred to be
595 represented by the average paragneiss compositions of the Massabesic Gneiss Complex, the
596 nearest outcrops of Ganderia to the White Mountain Batholith (Dorais et al., 2012) with a Hf
597 values of 6.12. Two ε_{Hf} values were modeled, one representing the low range of Ganderia at -13;
598 the other the high range at -4. Following Pietranik et al. (2013), we varied the value of D_{Hf} from

599 0·15 for the first 50% of assimilation-fractional crystallization and then it was changed to 1.5 to
600 account for zircon crystallization. The ratio of assimilation to crystallization (r) for the modeling
601 was 0.2.

602 Figure 11 shows AFC and mixing curves for both Ganderian endmembers. Both binary
603 mixing and AFC curves encompass the Conway and Mount Osceola data, hence, either process
604 could account for the isotopic compositions of the granites. It appears that the Mount Osceola
605 Granite is better modeled with the Ganderian composition with the ε_{Hf} value of -4 whereas the
606 Conway Granite data is better encompassed by the -13 endmember. These Hf-O isotopic models
607 are consistent with the incorporation about ~40-60% Ganderian crust into a mantle-derived
608 magma.

609 The steep negative trend of ε_{Hf} versus age in Figure 12 suggests that the Conway and Mount
610 Osceola granites experienced decreasing amounts of the crustal component with time. The oldest
611 zircons analyzed have ages of ~200 Ma (Table 6), very near the age of the tholeiitic flood basalts
612 of the Central Atlantic Magmatic Province that formed during the rifting of Pangea (Hames et al.,
613 2003). The zircons with the strongly negative ε_{Hf} values have model ages greater than 1 Ga and
614 indicate a component from Precambrian crust. With time, that crustal component signature
615 diminished to the point where the youngest zircons preserve hints of larger component from a
616 mafic parent derived from the depleted mantle. This trend suggests that the older granites
617 preserved a stronger crustal signature that evolved to a larger mantle component in the younger
618 granites as rifting proceeded.

619 Hf model ages represent the time since the source of the zircon's host magma separated
620 from the mantle (Vervoort and Kemp, 2016). Model ages have limitations (Payne et al., 2016)
621 that must be carefully considered due to their degree of uncertainty (Vervoort and Kemp, 2016).

Hf model ages require certain parameters for their calculation, especially the $^{176}Lu/^{177}Hf$ ratio for the continental crust component. Several publications suggest a variety of crustal $^{176}Lu/^{177}Hf$ ratios, such as Goodge and Vervoort (2006) and Condie et al. (2011). As a result, the Hf model ages can vary depending on the $^{176}Lu/^{177}Hf$ used. These variations can be of a few hundred million years (Teixeira et al., 2019).

With the exception of the two negative outliers, the T_{DM} model ages obtained for the Mount Osceola and Conway granites are between 380 – 1080 Ma (Figure 12). The older model ages for both granites are close to ages of extraction from the mantle of accreted peri-Gondwanan terranes found in the basement of New Hampshire: Ganderia (950 Ma to 530 Ma; Hibbard et al., 2007), and Avalonia (0.9 – 1.2 Ga; Murphy and Nance, 2002). This evidence also permits an interpretation that peri-Gondwanan rocks were the main contaminant to the mantle-derived magmas that formed the Mount Osceola and Conway granites (Figure 15).

The Hf model ages of the two strongly negative zircon grains range between 1200 to 1400 Ma and suggest that a Precambrian component from Laurentia is present in the oldest crustal contribution to the granites. These ages are similar to those of Grenvillian rocks of the Adirondack Mountains of New York and basement rocks of western New England (McLelland et al., 2004; Walsh et al., 2004), suggesting a minor, early Grenvillian contribution to the Mount Osceola and Conway granites. Alternatively, Ganderia and Avalonia have a minor component with these ages (Willner et al., 2014; Henderson et al., 2018; Severson et al., 2022); hence, peri-Gondwanan rocks could be the exclusive contaminant to the Conway and Mt. Osceola granites. This model is depicted in Figure 15 where mantle-derived basalts traversed Ganderian crust, assimilating or mixing with up to 40-60% of Ganderia, before emplacement into the metasedimentary rocks of the Central Maine Terraine to form the White Mountain Batholith.

CONCLUSIONS

The Mount Osceola and Conway granites are the two most extensive intrusions of the White Mountain Batholith. Understanding their petrogenesis provides deeper insights into the petrogenesis of not only the batholith but also to A-type granites in general.

Both granites have biotite that is Fe-rich; amphiboles in Mount Osceola granite are also Fe-rich. Moreover, whole-rock major and trace elements reveal that both granites have high concentrations of K_2O, Na_2O, SiO_2, FeO_{total}, Zr, Hf, Th, U, and REE, and low contents of Al_2O_3, MgO, and CaO. All this evidence supports the interpretation that the Mount Osceola and the Conway granites are A-types. Specifically, whole-rock trace elements classify the Mount Osceola and Conway granites as A_1 on Eby's (1992) diagrams that see through the crustal contamination that occurred in the magmas.

Oxygen isotopic analyses of zircon show that the Mount Osceola and Conway granites have high degrees of crustal contamination with $\delta^{18}O$ values between 7.01 – 8.84‰, well over 5.3 ± 0.3‰ values for zircon from mantle-derived magmas. ε_{Hf} values for these zircons are between -2.1 and 4.6 and are interpreted as indicating the magmas were derived from parental magmas from the depleted mantle, but these values also indicate large amounts of contamination/mixing because the depleted mantle at this time had values of about +15 (Goodge and Vervoort, 2006). Several unpaired zircons from other locations across the White Mountain Batholith have ε_{Hf} values approaching this depleted mantle value, as high as +12. These zircons crystallized before contamination, confirming the depleted mantle basaltic component to the granites.

Based upon the isotopic values from previous work on Siluro-Devonian Central Maine Terrane metasedimentary rock and the basement rocks found in New England, our ε_{Hf} and $\delta^{18}O$ values, and Hf model ages for the Mount Osceola and Conway granites suggest that the rocks of

668 the Ganderian terrain are potential crustal endmembers in the magmas that formed the White
669 Mountain Batholith. Models involving an inferred mafic endmember and two different Ganderian
670 compositions indicate that the granites contain between 40-60% of a crustal endmember. In the
671 majority of the granites, such contamination/mixing took place at temperatures greater than about
672 850 °C, before zircon crystallization, hence, the primary magma composition is not recorded in the
673 isotopic characteristics of core-rim zoning in most zircon crystals. Some zircons crystallized prior
674 to magma contamination/mixing. Zircon grains inferred to have crystallized before crustal
675 interaction (because of their high eHf values) indicate that basaltic magma that
676 differentiated/hyridized to form the granites was derived from depleted mantle.
677

678 **ACKNOWLEDGEMENTS**

679 We gratefully acknowledge the assistance of Kouki Kitajima and the support to the WiscSIMS
680 lab through NSF grant #EAR-2004618 in obtaining the oxygen isotopic analyses for this study.
681 Very helpful reviews from Bill Collins and an anonymous reviewer are greatly appreciated. This
682 study was partially funded by the College of Physical and Mathematical Sciences, Brigham
683 Young University.

REFERENCES

Andersen, T., Andersson, U.B., Graham, S., Åberg, G., and Simonsen, S.L., 2009. Granitic magmatism by melting of juvenile continental crust: new constraints on the source of Paleoproterozoic granitoids in Fennoscandia from Hf isotopes in zircon: Journal of the Geological Society of London, 166, 233-247.

Billings, M.P., 1956. The Geology of New Hampshire Part II: Bedrock Geology. New Hampshire State Planning and Development Commission., 200 pp.

Blitcher-Toft, J., and Puchtel, I.S., 2010. Depleted mantle sources through time: evidence from Lu-Hf and Sm-Nd isotope systematics of Archean komatiites, Earth and Planetary Science Letters, 297, 598-606.

Boemmels, J.R.C., Crespi, J.M., Webb, L.E., Fosdick, J.C., 2021. $^{40}Ar/^{39}Ar$ and LA-ICP-MS U-Pb geochronology for the New England portion of the Early Cretaceous New England-Quebec Igneous Province: implications for the postrift evolution of the eastern North American margin: American Journal of Science, 321, 365-391.

Boehnke, P., Watson, E., Trail, D., Harrison, T.M., Scmitt, A.K., 2013. Zircon saturation re-visited: Chemical Geology, 351, 324-334.

Bonamici, Fanning, C.M., Kozdon, R., Fournelle, J.H., and Valley, J.W., 2015. Combined oxygen-isotope and U-Pb zoning studies of titanite: New criteria for age preservation: Chemical Geology, 398, 70-84.

Bonin, B., 2007. A-type granites and related rocks: evolution of a concept, problems and prospects, Lithos, 97, 1-29.

Bouvier, A., Vervoort, J.D., and Patchett, P.J., 2008, The Lu-Hf and Sm-Nd isotopic composition of CHUR: Constraints from unequilibrated chondrites and implications for the bulk composition of terrestrial planets. Earth and Planetary Science Letters, 273, 48-57.

Castillo, P., Fanning, C.M., Pankhurst, R.J., Hervé, F., and Rapela, C.W., 2017. Zircon O- and Hf-isotope constraints on the genesis and tectonic significance of Permian magmatism in Patagonia, Journal of the Geological Society, 174, 803-816.

Christiansen, E.H., Sheridan, M.F., and Burt, D.M., 1986. The geology and geochemistry of Cenozoic topaz rhyolites from the western United States: The Geological Society of America Special Paper 205, 1-82.

Clemens, J.D., Holloway, J.R., and White A.J.R., 1986. Origin of an A-type granite: experimental constraints, American Mineralogist, 71, 317-324.

Collins, W.J., Beams, S.D., White, A.J.R., and Chappell, B.W., 1982. Nature and origin of A-type granites with particular reference to southeastern Australia: Contributions to Mineralogy and Petrology, 80, 189-200.

Colón, D.P., Bindeman, I.N., Wotzlaw, J.F., Christiansen, E.H., and Stern, R.A., 2018. Origins and evolution of rhyolitic magmas in the central Snake River Plain: insights from coupled high-precision geochronology, oxygen isotope, and hafnium isotope analyses of zircon: Contributions to Mineralogy and Petrology, 173, 1-18.

Condie, K.C., Bickford, M.E., Aster, R.C., Belousova, E., and Scholl, D.W., 2011. Episodic zircon ages, Hf isotopic composition, and the preservation rate of continental crust, Geological Society of America Bulletin 123, 951-957.

Creaser, R.A., Price, R.C., and Wormald, R.J., 1991. A-type granites revisited: assessment of a residual-source model: Geology, 19, 163-166.

Creasy, J.W., and Eby, G.N., 1993. Ring dikes and plutons: A deeper view of calderas as illustrated by the White Mountain Igneous Province, New Hampshire. Field Trip Guidebook for the Northeastern United States, Geological Society of America, Chapter N.

Dailey, S.R., Christiansen, E.H., Dorais, M.J., Kowallis, B.J., Fernandez, D.P., and Johnson, D.M. 2018. Origin of the fluorine-and beryllium-rich rhyolites of the Spor Mountain Formation, Western Utah. American Mineralogist, 103, 1128-1252.

Dodge, F.C.W., Papike, J.J, and Mays, R.E., 1968. Hornblendes from granitic rocks of the central Sierra Nevada batholith, California. Journal of Petrology, 9, 378-410.

Dorais, M.J., 2003. The petrogenesis and emplacement of the New Hampshire plutonic suite: American Journal of Science, 303, 447-487.

Dorais, M.J., Whitney, J.A, and Roden, M.F., 1990. Origin of mafic enclaves in the Dinkey Creek Pluton, Central Sierra Nevada Batholith, California. Journal of Petrology, 31, 853-881.

Dorais, M.J., Workman, J., and Aggarwal, J., 2008. The petrogenesis of the Highlandcroft and Oliverian plutonic suites, New Hampshire: Implications for the structure of the Taconic orogen. American Journal of Science, 308, 73-99.

Dorais, M.J., Wintsch, R.P., Kunk, M.J., Aleinikoff, J.N., Burton, W., Underdown, C., and Kerwin C.M., 2012. P-T-t conditions, Nd and Pb isotopic compositions and detrital zircon geochronology of the Massabesic Gneiss Complex, New Hampshire: isotopic and metamorphic evidence for the identification of the Gander Basement, Central New England, American Journal of Science, 312, 1049-1097.

Duncan, R.A., 1984. Age progressive volcanism of the New England seamounts and the opening of the central Atlantic Ocean. Journal of Geophysical Reseach –Solid Earth, 89, 9980-9990.

Eby, G.N., 1990. The A-type granitoids: A review of their occurrence and chemical characteristics and speculations on their petrogenesis: Lithos, 26, 115-134.

Eby, G.N., 1992. Chemical subdivision of the A-type granitoids: Petrogenetic and tectonic implications: Geology, 20, 641-644.

Eby, G.N., Krueger, H.W., and Creasy, J.W. 1992. Geology, geochronology, and geochemistry of the White Mountain batholith, New Hampshire, in Puffer, J.H., and Ragland, P.C., (eds.), Eastern North American Mesozoic Magmatism: Geological Society of America Special Paper 268, 379-397.

Eusden, J. D., Jr., and Lyons, J. B., 1993. The sequence of Acadian deformation in central New Hampshire. In; Roy, D. C., and Skehan, J. W., (eds), The Acadian Orogeny: Recent Studies in New England, Maritime Canada, and the Autochthonous Foreland: Geological Society of America Special Paper 275, p. 51-66.

Foland, K.A., and Allen, J.C. 1991. Magma sources for Mesozoic anorogenic granites of the White Mountain magma series, New England, USA: Contributions to Mineralogy and Petrology, 109, 195-211.

Fryer, B.J., Kerr, A., Jenner, G.A., and Longstaffe, F.J., 1992. Probing the crust with plutons: Regional isotopic geochemistry of granitoid intrusions across insular Newfoundland. *In* Current research: Newfoundland Department of Mines and Energy, Geological Survey Branch, Report 92-1, 119-139.

Fu, B., Cliff, J., and Zartman, R.E., 2014. Zircon oxygen isotopic constraints from plutonic rocks on the magmatic and crustal evolution of the northern Appalachians in southern New England, USA: Canadian Journal of Earth Sciences, 51, 485-499.

Goodge, J.W., and Vervoort, J.D., 2006. Origin of Mesoproterozoic A-type granites in Laurentia: Hf isotope evidence: Earth and Planetary Science Letters, 243, 711-731.

Griffin, W.L., Pearson, N.J., Belousova, E., Jackson, S.E, van Achterbergh, E., O'Reilly, S.Y., Shee, S.R., 2000. The Hf isotope composition of cratonic mantle: LAM-MC-ICPMS analysis of zircon megracryst in kimberlites. Geochinica et Cosmochimica Acta, 64, 133-147.

Hames, W., Mchone, J.G., Renne, P., and Ruppel, C., (Editors), 2003. The Central Atlantic Magmatic Province: Insights from Fragments of Pangea. American Geophysical Union Volume 136, 267 pp.

Henderson, B.J., Collins, W.J., Murphy, J.B., and Hand, M., 2018. A hafnium isotopic record of magmatic arcs and continental growth in the Iapetus Ocean: The contrasting evolution of Ganderia and the peri-Laurentian margin: Gondwana Research, 58, 141-160.

Hibbard, J.P., Van Staal, C.R., and Miller, B.V. 2007. Links among Carolinia, Avalonia and Ganderia in the Appalachian peri-Gondwanan realm. In: Sears, J.W., Harms, T.A., and Evenchick, C.A. (eds): When the Mountains? Inquiries into the Evolution of Orogenic Systems: A Volume in Honor of Raymond A. Price: Geological Society of America, Special Paper, 433, 291-312.

Kemp, A. I. S., Hawkesworth, C. K., Foster, G.L., Paterson, B.A., Woodhead, J.D., Hergt, J.M., Gray, C.M., and Whitehouse, M.J., 2007. Magmatic and crustal differentiation history of granitic rocks from Hf-O isotopes in zircon. Science, 315, 980-983.

Kinney, S.T., 2021. Re-evaluating the timescale of rift and post-rift magmatism on the Eastern North American Margin via zircon U-Pb geochronology. PhD diss., Columbia University.

Kinney, S. T., S. A. MacLennan, C. B. Keller, B. Schoene, J. B. Setera, J. A. Van Tongeren, and P. E. Olsen. 2021. Zircon U-Pb geochronology constrains continental expression of Great Meteor Hotspot magmatism. Geophysical Research Letters, e2020GL091390.

Kita, N.T., Ushikubo, T., Fu, B., and Valley, J.W. 2009. High precisión SIMS oxygen isotope analysis and the effect of simple topography. Chemical Geology, 264, 43-57.

Kylander-Clark, A.R.C., Hacker, B.R., and Cottle, J.M., 2013. Laser-Ablation Split-Streat ICP Petrochronology: Chemical Geology, 345, 99-112.

Lathrop, A.S., Blum, J.D. and Chamberlain, C.P., 1996. Nd, Sr and O isotopic study of the petrogenesis of two syntectonic members of the New Hampshire Plutonic Series: Contributions to Mineralogy and Petrology, 124, 126-138.

Leake, B.E., Woolley, A.R., Birch, W.D., Burke, E.A.J., Ferraris, G., Grice, J.D., Hawthorne, F.C., Kisch, H.J., Krivovichev, V.G., Schumacher, J.C., Stephenson, N.C.N., and Whittaker, E.J.W, 1997. Nomenclature of amphiboles: additions and revisions to the International Mineralogical Association's 1997 recommendations: The Canadian Mineralogist, 41, 1355-1362.

Loiselle M.C., and Wones, D.R., 1979. Characteristics and origin of anorogenic granites. Geol Soc Am Abstr with Prog, 11, 468.

Lyons, J.B., Bothner, W.A., Moench, R.H., and Thompson, J.B., Jr., 1997. Bedrock geologic map of New Hampshire: U.S. Geological Survey State Map Series, scales 1:250,000 and 1:500,000.

Matton, G, and Jébrak, M., 2009. The Cretaceous Peri-Atlantic Alkaline Pulse (PAAP): Deep mantle plume origin or shallow lithospheric break-up? Tectonophysics, 469, 1-12.

McHone, J.G., 1996. Constraints on the mantle plume model for Mesozoic alkaline intrusions in northeastern North America: Canadian Mineralogist, 34, 325-334.

McLelland, J.M., Bickford, M., Hill, B.M., Clechenko, C.C., Valley, J.W., and Hamilton, M.A., 2004. Direct dating of Adirondack massif anorthosite by U-Pb SHRIMP analysis of igneous zircon: Implications for AMCG complexes. Geological Society of America Bulletin, 116, 1299–1317.

Menke, W., Skryzalin, P., Levin, V., Darbyshire, F., and Dong, T., 2016. The northern Appalachian anomaly: A modern asthenospheric upwelling. Geophyscal Research Letters, https://doi.org/10.1002/2016GL070918.

Merle, R.E., Jourdan, F., Chiaradia, M., Olierook, H.K.H., and Manatschal, G, 2019. Origin of widespread Cretaceous alkaline magmatism in the Central Atlantic: A single melting anomaly?, Lithos, 342-343, 480-498.

Murphy, J.B., and Nance, R.D., 2002. Sm-Nd isotopic systematics as tectonic tracers: An example from West Avalonia in the Canadian Appalachians. Earth-Science Reviews, 59, 77-100.

Murphy, J.B., Shellnutt, J.G., and Collins, J.C., 2018. Late Neoproterozoic to Carboniferous genesis of A-type magmas in Avalonia of northern Nova Scotia: repeated partial melting of anhydrous lower crust in contrasting tectonic environments: Int J Earth Sci, 107, 587-599.

Nebel, O., Nebel-Jacobsen, Y., Mezger, K., and Berndt, J., 2007. Initial Hf isotope compositions in magmatic zircon from early Proterozoic rocks from the Gawler Craton, Australia: A test for zircon model ages, Chemical Geology, 241, 23-37.

Page, F.Z., Cameron, E.M., Flood, C.M., Dobbins, J.W., Spicuzza, M.J., Kouki, K., Strickland, A., Ushikubo, T., Mattinson, C.G., and Valley, J.W., 2019. Extreme oxygen isotope zoning in garnet and zircon from a metachert block in mélange reveals metasomatism at the peak of subduction metamorphism: Geology, 47, 655-658.

Patchett, P. J., 1983. Importance of the Lu-Hf isotopic system in studies of planetary chronology and chemical evolution. Geochimica et Cosmochimica Acta, 47, 81-91.

Patchett, P. J., and Tatsumoto, M., 1981. A routine high-precision method for Lu-Hf isotope geochemistry and chronology. Contributions to Mineralogy and Petrology, 75, 263-267.

Patiño-Douce, A., 1997. Generation of metaluminous A-type granites by low-pressure melting of calc-alkaline granitoids: Geology, 25, 743-746.

Payne, J.L., McInerney, D.J., Barovich, K.M., Kirkland, C.L., Pearson, N.J., and Hand, M., 2016. Strengths and limitations of zircon Lu-Hf and O isotopes in modeling crustal growth: Lithos, 248-251, 175-192.

Pearce, J. A., 1982. Trace element characteristics of lavas from destructive plate boundaries: In: Thorpe, R. S., ed., Andesites: Chichester, Wiley, 525-548.

Pearce, J.A., Harris, M.B.W., and Tindle, A.G., 1984. Trace element discrimination diagrams for the tectonic interpretation of granitic rocks: Journal of Petrology, 25, 956-983.

Pietranik, A., Odczyk, E.S., Hawkesworth, C.J., Breitkreuz, C., Storey, C.D., Whitehouse, M., and Milke, R., 2013. Heterogeneous zircon cargo in voluminous Late Paleozoic rhyolites: Hf, O isotope and Zr/Hf records of plutonic to volcanic magma evolution. Journal of Petrology, 8, 1483-1501.

Potter, J., Longstaffe, F.J., and Barr, S.M., 2008. Thompson, M.D. and White, C.E., 2008, Altering Avalonia: oxygen isotopes and terrane distinction in the Appalachian peri-Gondwanan realm: Can. J. Earth Sci, 45, 815-825.

Rudnick, R.L., and Gao, S., 2003. Composition of the Continental Crust: Treatise on Geochemistry, 3, 1-64.

Scherer, E., Münker, C., and Mezger, K., 2001. Calibration of the Lutetium-Hafnium Clock. Science, 293, 5530, p. 683-687.

Severson, A.R., Kuiper, Y.D., Eby, G.N., Lee, H.-Y., and Hepburn, J.C., 2022. New detrital zircon U-Pb ages and Lu-Hf isotopic data from metasedimentary rocks along the western boundary of the composite Avalon terrane in the southeastern New England Appalachians. In: New Developments in the Appalachian-Caledonian-Variscan Orogen. Kuiper, Y.D., Murphy, J.B., Nance, R.D., Strachan, R.A., and Thompson, M.D. (Eds.), Geological Society of America Special Paper 554, https://doi.org/10.1130/2021.2554(04).

Shellnutt, J.G., Wang, C.Y., Zhou, M-F., and Yang, Y., 2009. Zircon Lu-Hf isotopic compositions of metaluminous and peralkaline A-type granitic plutons of the Emeishan large igneous province (SW China): Constraints on the mantle source. Journal of Asian Earth Sciences, 35, 45-55.

Söderlund, U., Patchett, P.J., Vervoort, J.D., and Isachsen, C.E., 2004. The ^{176}Lu decay constant determined by Lu-Hf and U-Pb isotope systematics of Precambrian mafic intrusions: Earth and Planetary Science Letters, 219, 311-324.

Taylor, S.R., and McLennan, S.M., 1985. The Continental Crust: its composition and evolution; an examination of the geochemical record preserved in sedimentary rocks, Blackwell Scientific, Oxford, 312 pp.

Texeira, M.F.B., Dall'Agnol, R., Santos, J.O.S., Kemp, O., and Evans, N., 2019. Petrogenesis of the Paleoproterozoic (Orosirian) A-type granites of Carajas Province, Amazon Craton, Brazil: Combined in situ Hf-O isotopes of zircon. Lithos, 332-333, 1-22.

Turner, S.P., Foden, J.D., and Morrison, R.S., 1992. Derivation of some A-type granites magmas by fractionation of basaltic magma: an example from the Padthaway Ridge, South Australia: Lithos, 28, 151-179.

Valley, J.W., 2003. Oxygen isotopes in zircon. In: Hachar, J.M., Hoskin, P.W.O. (Eds), Zircon: Reviews in mineralogy and geochemistry, Mineralogical Society of America and Geochemical Society, 53, 343-385.

Vervoort, J.D., and Kemp, A.I.S., 2016. Clarifying the zircon Hf isotope record of crust-mantle evolution: Chemical Geology, 425, 65-75.

Vervoort, J.D., Plank, T., and Prytulak, J., 2011. The Hf-Nd isotopic composition of marine sediments, Geochimica et Cosmochimica Acta, 75, 5093-5926.

Vervoort, J. D., Patchett, P. J., Söderlund, U., and Baker, M., 2004, Isotopic composition of Yb and the determination of Lu concentrations and Lu/Hf ratios by isotope dilution using MC-ICPMS: Geochemistry, Geophysics, Geosystems, v. 5, no. 11.

Vilalva, F.C.J., Simonetti, A., and Vlach, S.R.F., 2019. Insights on the origin of the Graciosa A-type granites and syenites (Southern Brazil) from zircon U-Pb geochronology, chemistry, and Hf and O isotope compositions: Lithos, 340-341, 20-33.

Walsh, G.J., Aleinikoff, J.N., and Fanning, C.M., 2004. U-Pb geochronology and evolution of Mesoproterozoic basement rocks, western Connecticut. In: Proterozoic Tectonic Evolution of the Grenville Orogen in North America, Tollo, R.P., Corriveau, L., McLelland, J., and Bartholomew, M.J. (eds). Geological Society of America Memoir 197, 729-753.

Watson, E., and Harrison, T.M., 1983. Zircon saturation revisited: temperature and composition effects in a variety of crustal magmas types: Planetary Science Letters, 64, 295-304.

Whalen, J.B., Currie, K.L., and Chappell, B.W., 1987. A-type granite: geochemical characteristics, discrimination and petrogenesis: Contributions to Mineralogy and Petrology, 95, 407-419.

Willner, A.P., Gerdes, A., Massonne, H.J., van Staal, C.R., and Zagorevski, A., 2014. Crustal evolution of the northeast Laurentian margin and the peri-Gondwanan microcontinent Ganderia prior to and during closure of the Iapetus Ocean: detrital zircon U-Pb and Hf isotope evidence from Newfoundland: Geoscience Canada, 41, 345-364.

Wintsch, R.P., Keewok, Y., and Dorais, M.J., 2014. Crustal thickening by tectonic wedging of the Ganderian rocks, southern New England, USA: Evidence from cataclastic zircon microestructures and U-Pb ages: Journal of Structural Geology, 69, 428-448.

Wong, J., Sun, M., Xing, G.F., Li, X.H. Zhao, G.C., Wong, K., Yuan, C., Xia, X.P., Li, L.M., and Wu, F.Y., 2009. Geochemical and zircon U-Pb and Hf isotopic study of the Baijuhuajian metaluminous A-type granite: extension at 125-100 Ma and its tectonic significance for South China: Lithos, 112, 289-305.

Woodhead, J., Hergt, J., Shelley, M., Eggins, S., and Kemp, R., 2004. Zircon Hf-isotope analysis with an excimer laser, depth profiling, ablation of complex geometries, and concomitant age estimation. Chemical Geology, 209, 121-135.

FIGURE CAPTIONS

Figure 1. Simplified geologic map of New England showing the accreted terranes. RH = Rowe-Hawley, MT = Merrimack Trough, P-N = Putnum Nashoba, MGC = Massabesic Gneiss Complex, HB = Hartford Basin.

Figure 2. Simplified geologic map of the White Mountain Batholith and the location of the White Mountain Batholith in New Hampshire, U.S.A.

Figure 3. Cathodoluminescence images of zircon for the Conway (left) and the Mount Osceola Granites (right). They have euhedral shapes and oscillatory zoning patterns of igneous zircons.

Figure 4. Al vs Fe/(Fe+Mg) diagram showing the A-type field (modified from Christiansen et al., 1986).

Figure 5. Si versus Mg/(Mg+Fe) diagram for amphiboles (Leake et al., 1997) of the Mount Osceola Granite(green) and amphiboles of the Sierra Nevada Batholith of Dorais et al. (1990) (blue).

Figure 6. Variation diagrams of major elements for the Mount Osceola (green) and Conway (red) granites.

Figure 7A. Chondrite-normalized REE patterns for the Mount Osceola (green) and Conway granites (red). 7B. Primitive-mantle normalized trace element patterns for the Mount Osceola (green) and Conway granites (red).

Figure 8. Tectonic discrimination diagrams from Pearce et al. (1984) with the A_1 and A_2 discriminant line from Eby (1992).

Figure 9. Ce/Nb versus Y/Nb and Yb/Ta versus Y/Nb discrimination diagrams for ocean island basalts (OIB) and island arc basalts (IAB) from Eby (1992). The Mount Osceola (green) and Conway (red) granites plot in the OIB field. Continental crust of Rudnick and Gao (2003) is plotted in blue.

Figure 10. Ternary (A) Nb-Y-Ce and (B) Nb-Y-Ga diagrams for distinguishing between A_1 and A_2 granites (Eby, 1992).

Figure 11. ε_{Hf} vs $\delta^{18}O$ for zircon of the Mount Osceola and Conway granites compared to whole-rock ε_{Nd} values of Lathrop et al. (1996) calculated from whole-rock ε_{Nd} values using Vervoort et al. (2011), zircon isotopic values of Laurentia, Ganderia and Avalonia from Fu et al. (2014), and predicted zircon values of Ganderia and Avalonia from Potter et al. (2008). A histogram of ε_{Hf} for the unpaired zircons is plotted along the X axis of the diagram. Both AFC and binary mixing curves are plotted.

Figure 12. Epsilon Hf versus age for the Mount Osceola (green) and Conway (red) granites. The $^{176}Lu/^{177}Hf$ values (0.015) used in the calculation of this diagram was taken from Goodge and Vervoort (2006). Depleted Mantle values from Griffin et al. (2000).

Figure 13. Core-rim isotopic evolution of zircon. Arrows point to the rim. Estimates of the analytical uncertainly are plotted in the upper right corner of the diagram.

Figure 14. Histogram showing zircon $\delta^{18}O$ values of the Mount Osceola and the Conway granites, and the converted $\delta^{18}O$ values from whole rock to zircon from Ganderia and Avalonia (Potter et al., 2008).

Figure 12. Schematic cross-section of the White Mountain Batholith area showing the process of contamination/mixing in Ganderia and emplacement into the metasedimentary rocks of the Central Maine Terraine (CMT; modified after Wintsch et al., 2014).

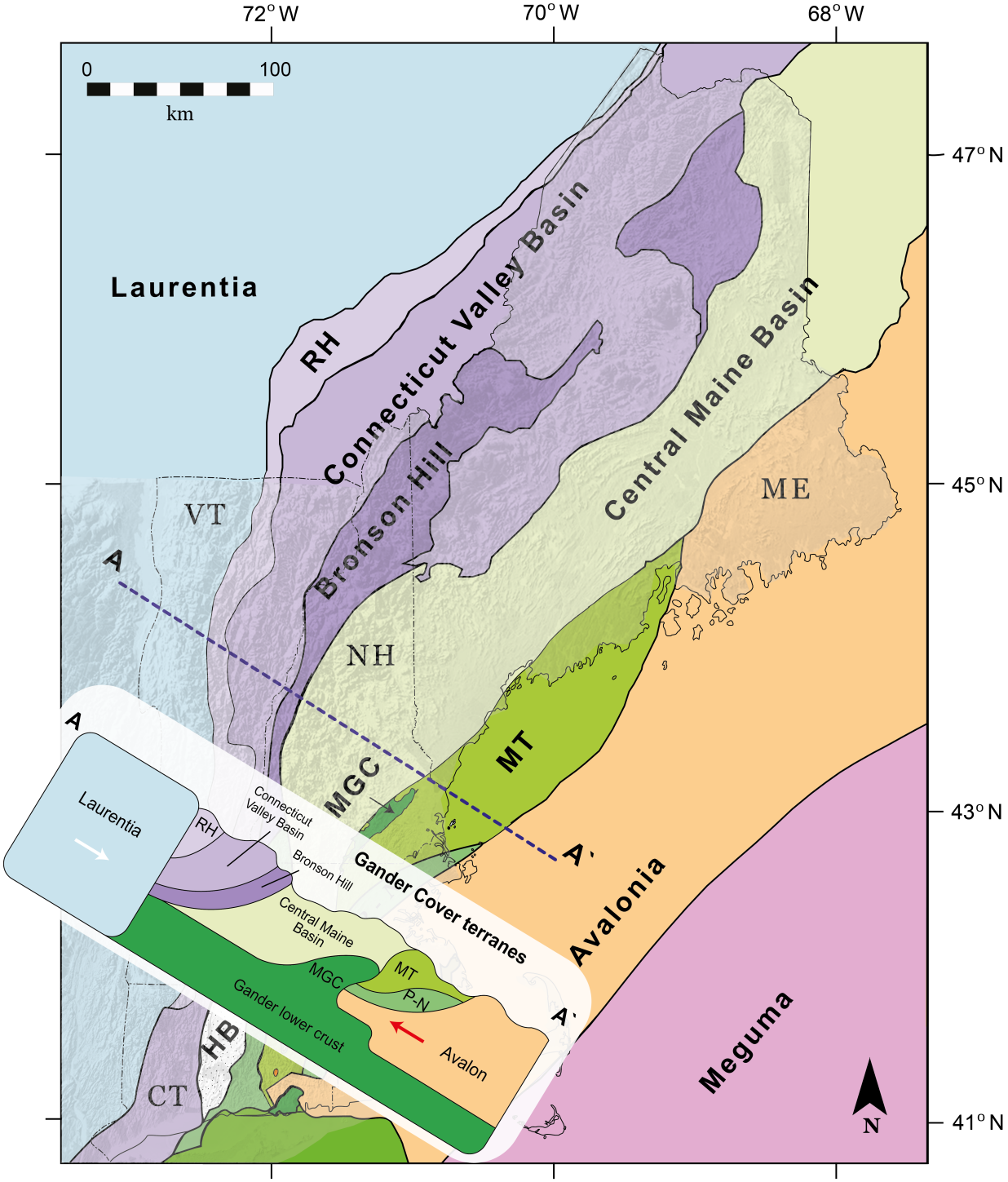
72° W
70° W
68° W
47° N
45° N
43° N
41° N
0
100
km
Laurentia
RH
Connecticut Valley Basin
Bronson Hill
Central Maine Basin
VT
NH
ME
MGC
MT
A
A'
Avalonia
Meguma
CT
HB
N
Laurentia
RH
Connecticut Valley Basin
Bronson Hill
Central Maine Basin
MGC
MT
P-N
Gander lower crust
Avalon
Gander Cover terranes

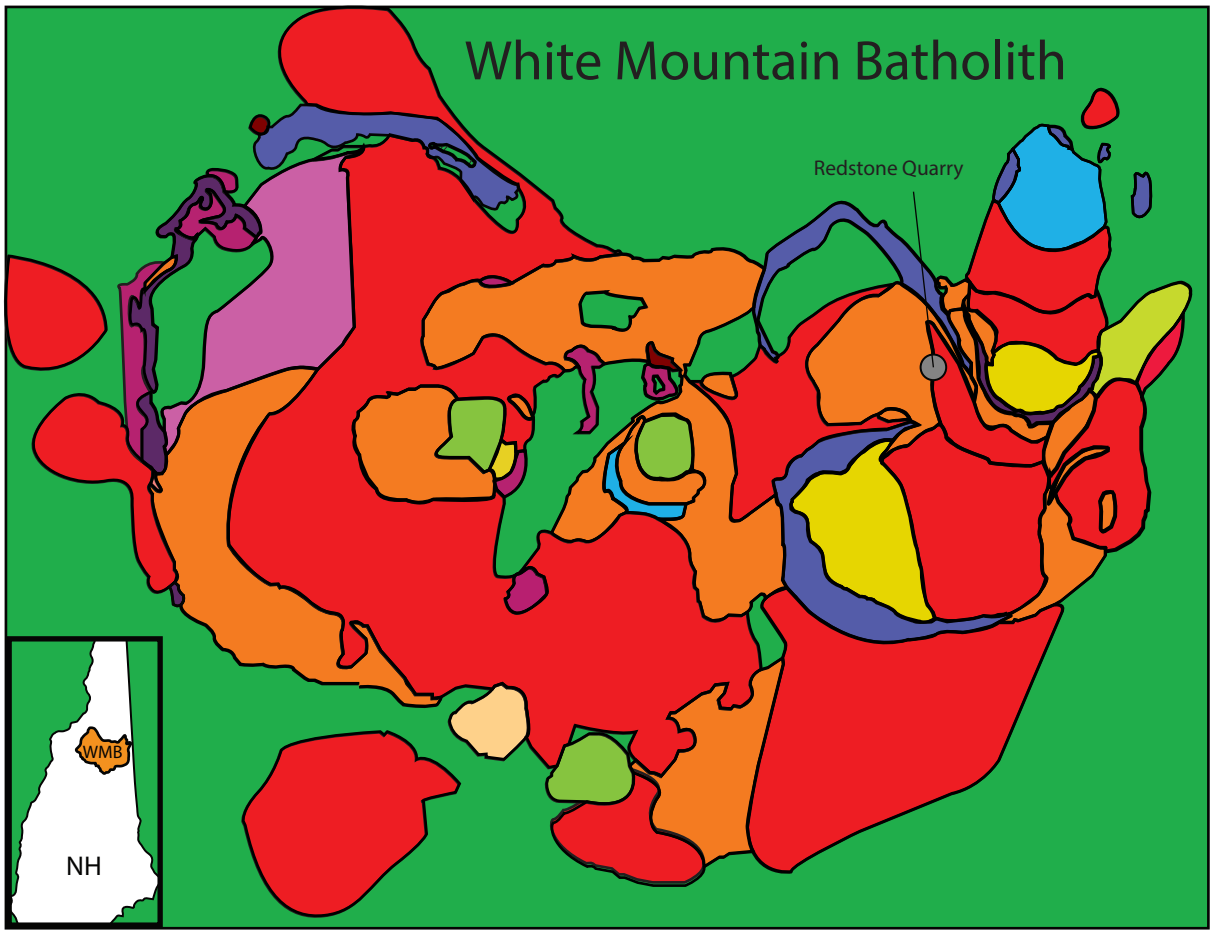

Conway Granite
Mt Osceola Granite
Porphyric Amph Granite
Mt Tripyramid Complex
Moat Volcanics
Syenite
Granite Porphyry
Country Rocks
Mt Lafayette Granite Porphyry
Mt Garfield Granite Porphyry
Albany Quartz Syenite
Quartz Syenite

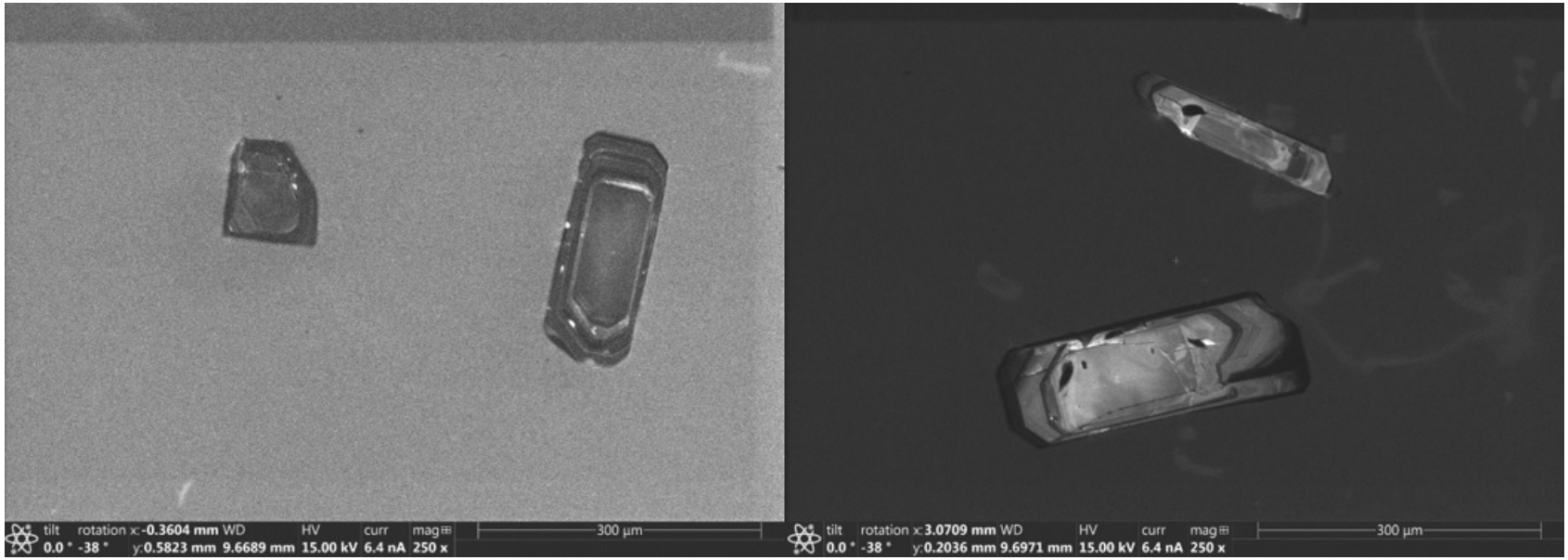
tilt rotation x:-0.3604 mm WD HV curr mag
0.0 ° -38 ° y:0.5823 mm 9.6689 mm 15.00 kV 6.4 nA 250 x
300 µm
tilt rotation x:3.0709 mm WD HV curr mag
0.0 ° -38 ° y:0.2036 mm 9.6971 mm 15.00 kV 6.4 nA 250 x
300 µm

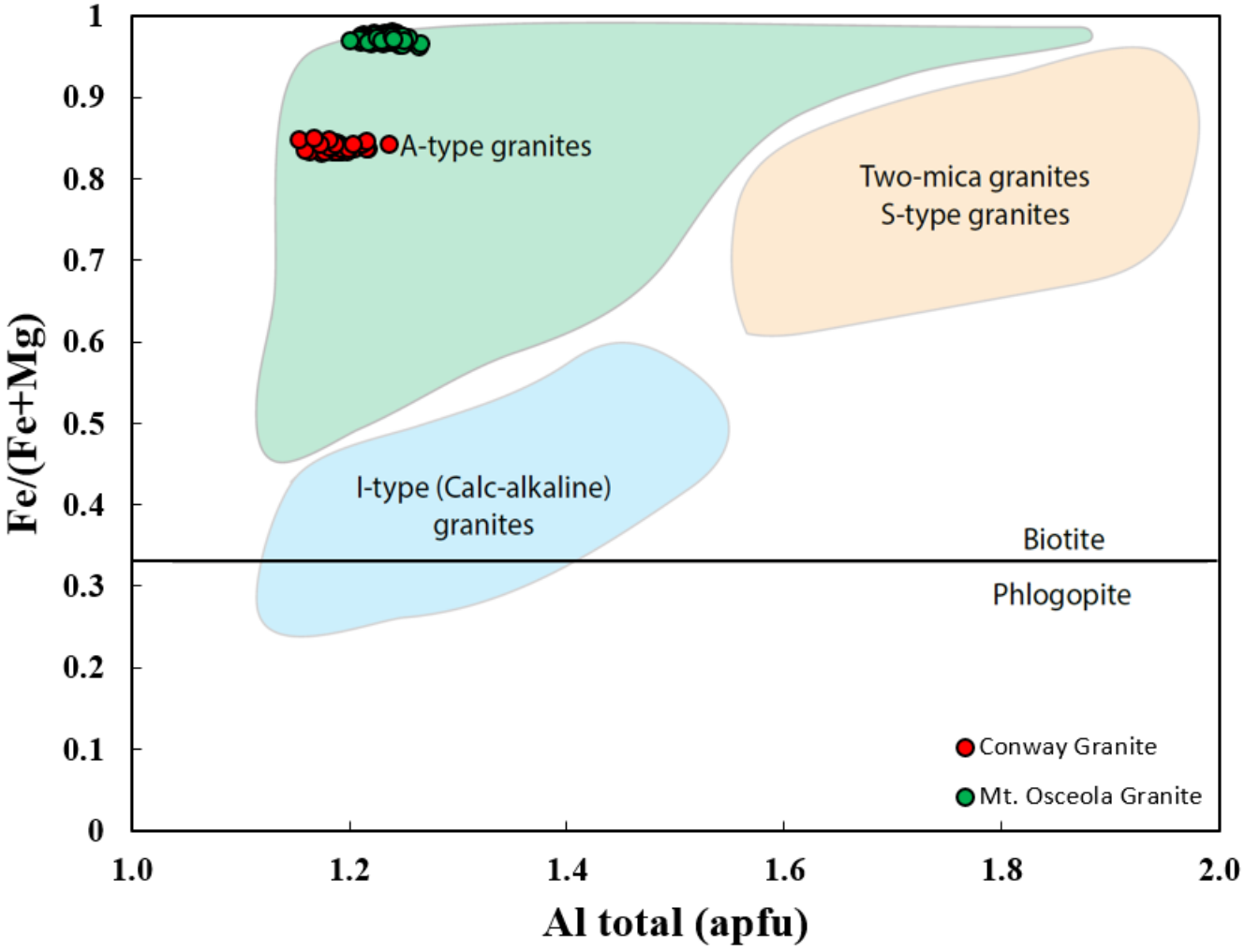
1
0.9
0.8
0.7
0.6
0.5
0.4
0.3
0.2
0.1
0
Fe/(Fe+Mg)
A-type granites
Two-mica granites
S-type granites
I-type (Calc-alkaline)
granites
Biotite
Phlogopite
Conway Granite
Mt. Osceola Granite
1.0
1.2
1.4
1.6
1.8
2.0
Al total (apfu)

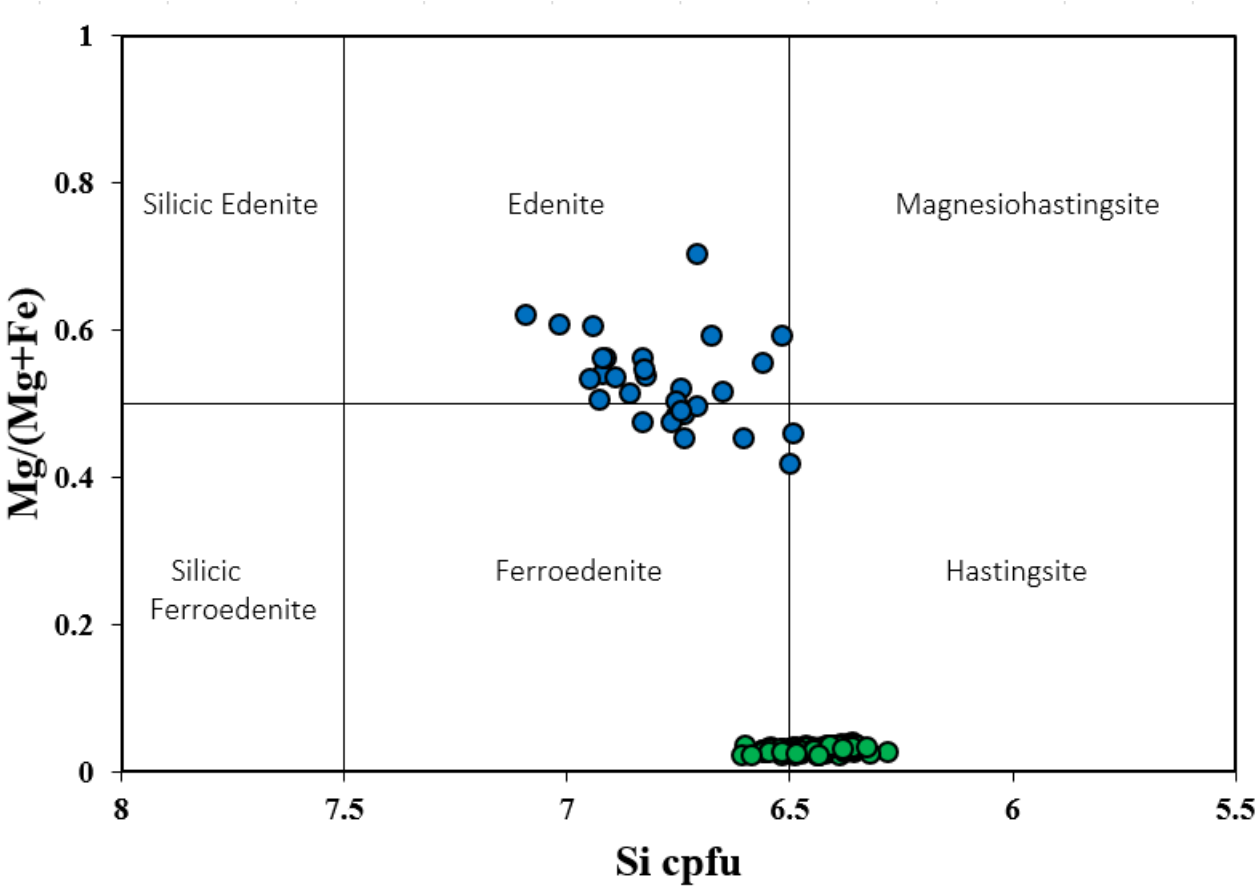
Silicic Edenite
Edenite
Magnesiohastingsite
Silicic Ferroedenite
Ferroedenite
Hastingsite
Mg/(Mg+Fe)
Si cpfu
1
0.8
0.6
0.4
0.2
0
8
7.5
7
6.5
6
5.5

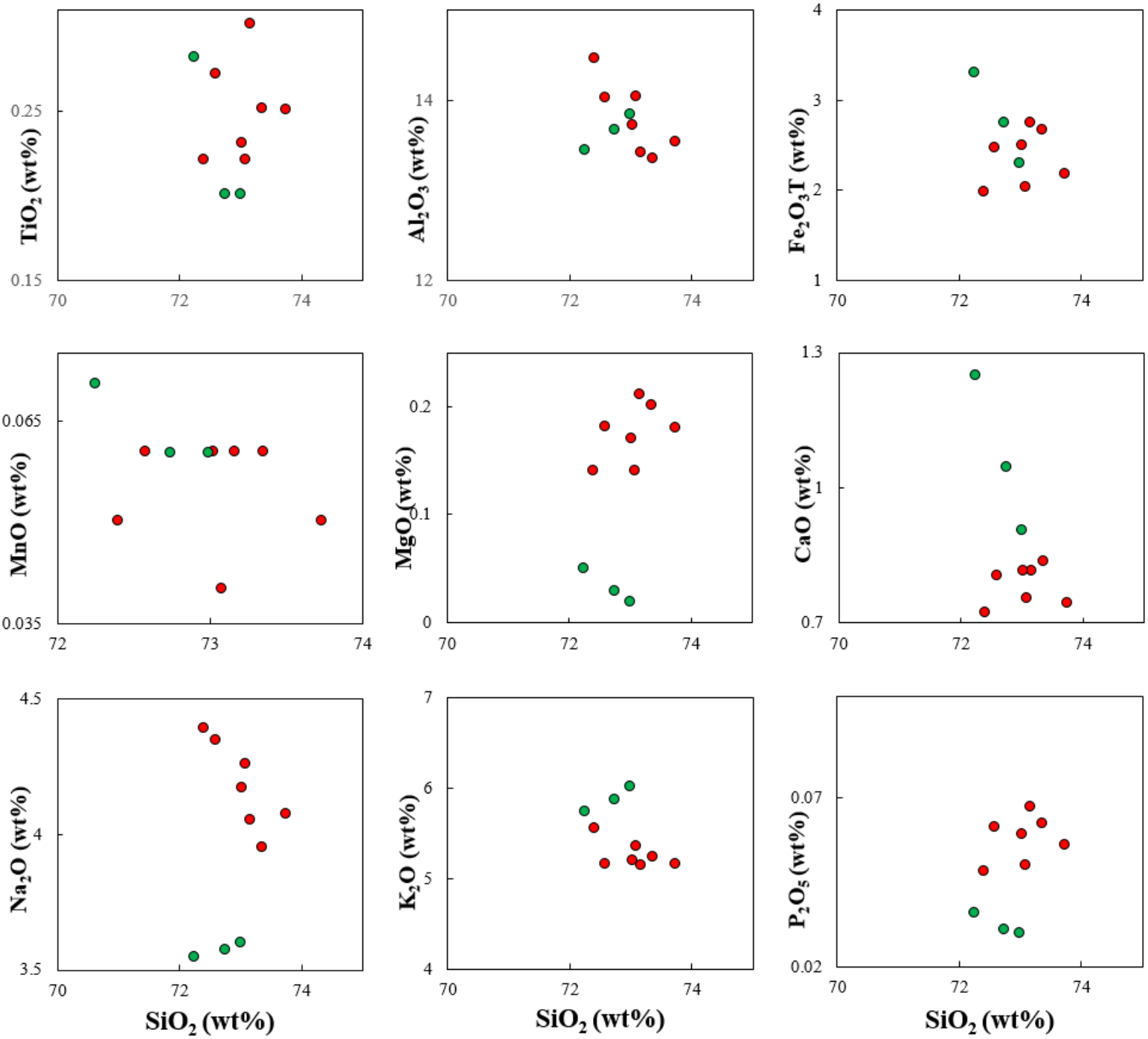
TiO2 (wt%)
0.25
0.15
Al2O3 (wt%)
14
12
Fe2O3T (wt%)
4
3
2
1
MnO (wt%)
0.065
0.035
MgO (wt%)
0.2
0.1
0
CaO (wt%)
1.3
1
0.7
Na2O (wt%)
4.5
4
3.5
K2O (wt%)
7
6
5
4
P2O5 (wt%)
0.07
0.02
70
72
73
74
SiO2 (wt%)

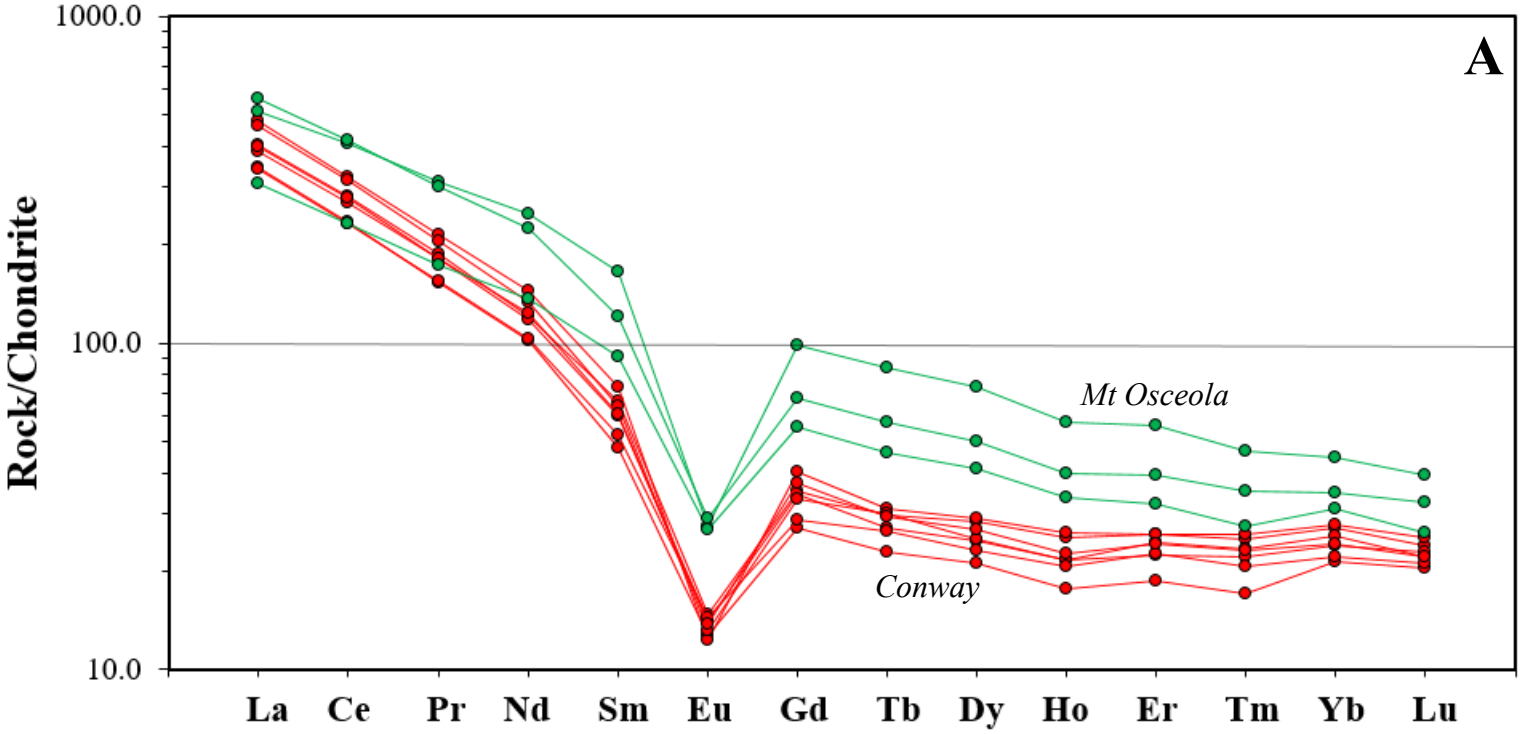
A
1000.0
100.0
10.0
Rock/Chondrite
Mt Osceola
Conway
La Ce Pr Nd Sm Eu Gd Tb Dy Ho Er Tm Yb Lu

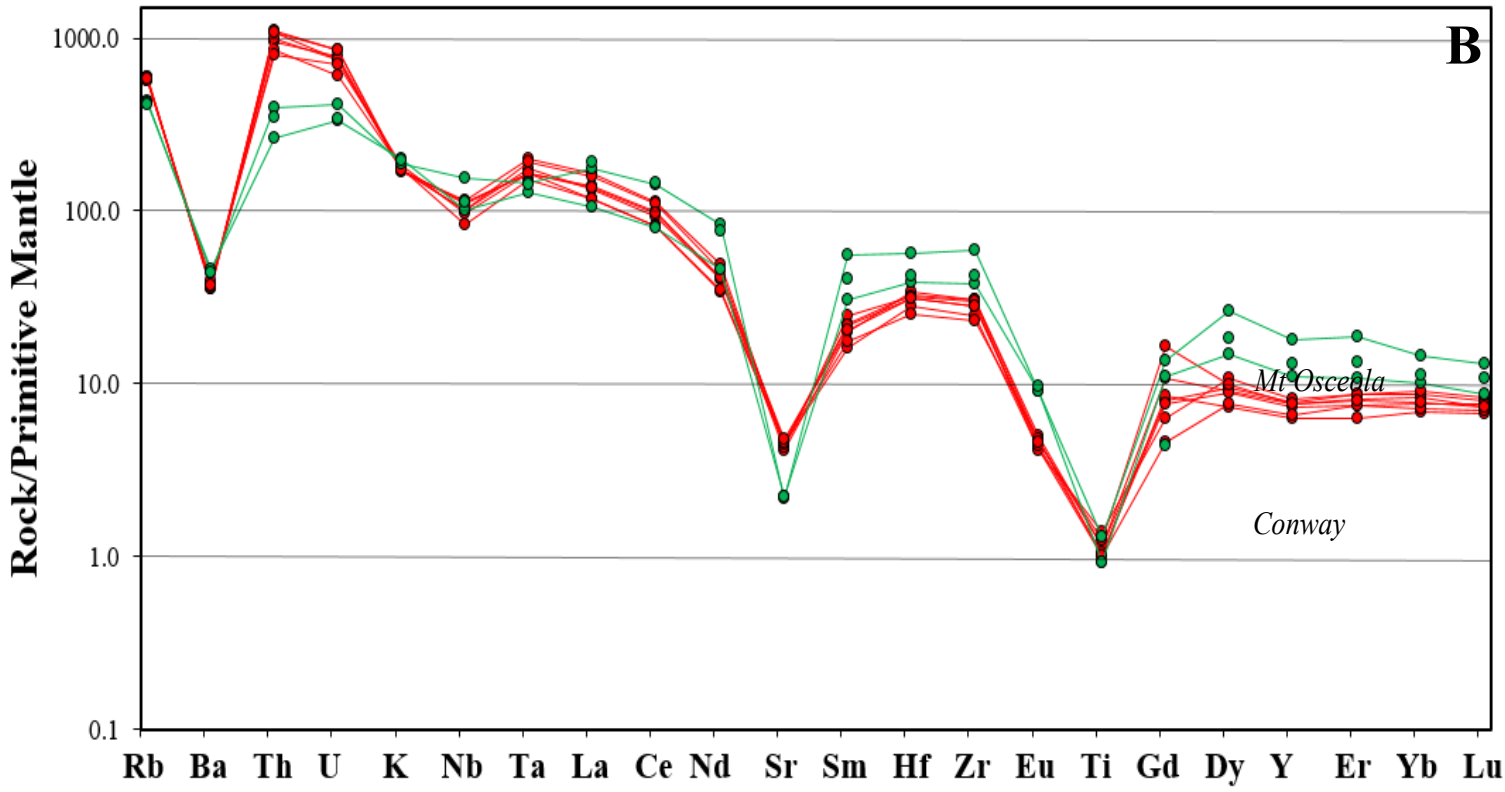
B
1000.0
100.0
10.0
1.0
0.1
Rock/Primitive Mantle
Mt Osceola
Conway
Rb Ba Th U K Nb Ta La Ce Nd Sr Sm Hf Zr Eu Ti Gd Dy Y Er Yb Lu

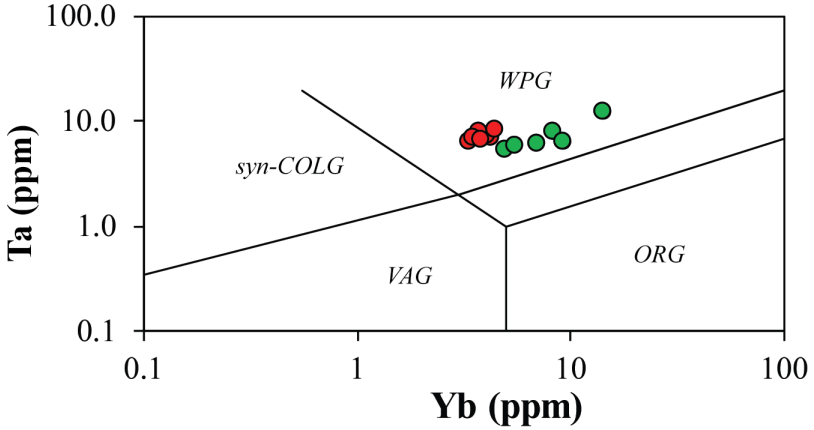
100.0
10.0
1.0
0.1
Ta (ppm)
0.1
1
10
100
Yb (ppm)
WPG
syn-COLG
VAG
ORG

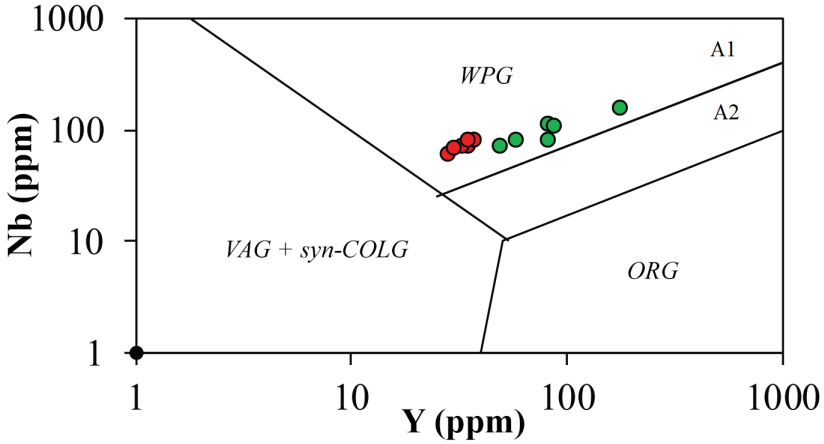
1000
100
10
1
Nb (ppm)
1
10
100
1000
Y (ppm)
A1
A2
WPG
VAG + syn-COLG
ORG

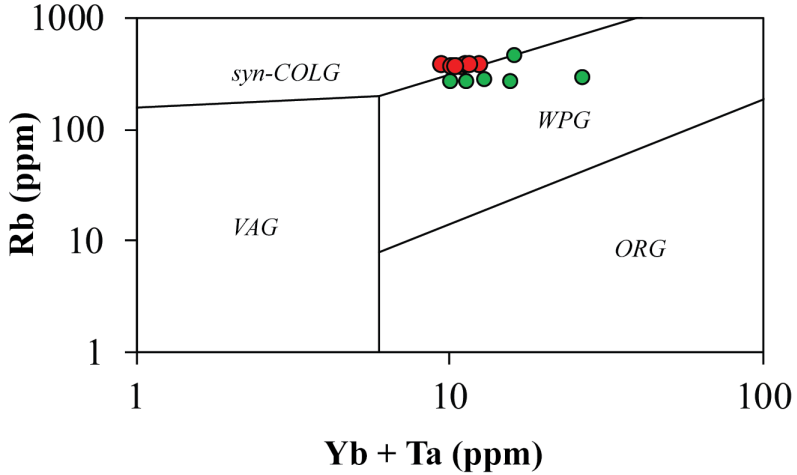
1000
100
10
1
Rb (ppm)
1
10
100
Yb + Ta (ppm)
syn-COLG
WPG
VAG
ORG

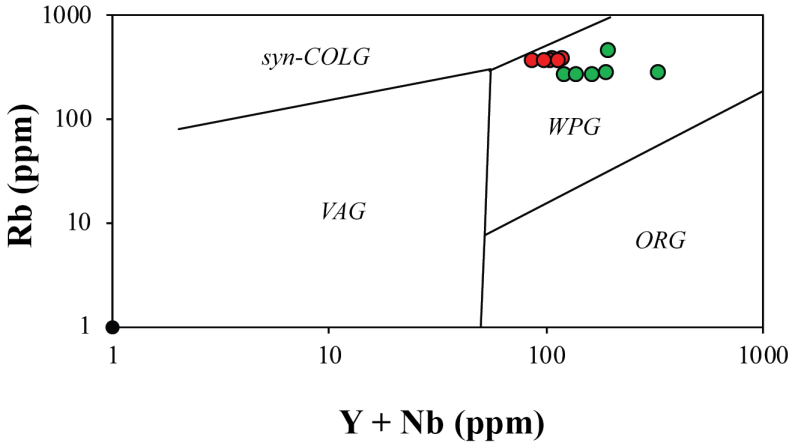
1000
100
10
1
Rb (ppm)
1
10
100
1000
Y + Nb (ppm)
syn-COLG
WPG
VAG
ORG

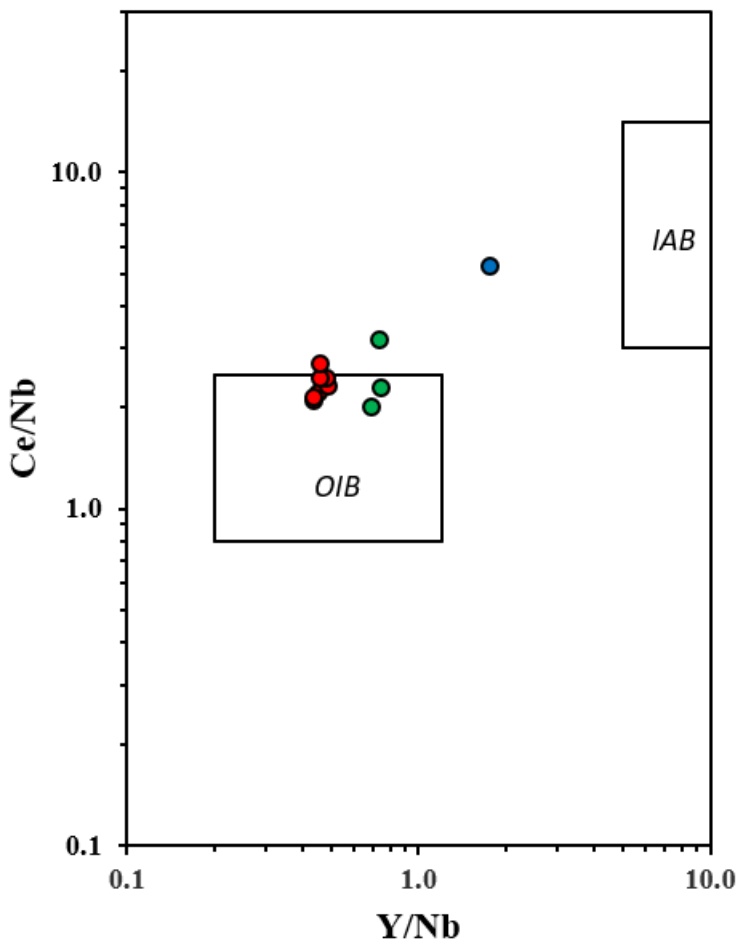
10.0
1.0
0.1
Ce/Nb
IAB
OIB
0.1
1.0
10.0
Y/Nb

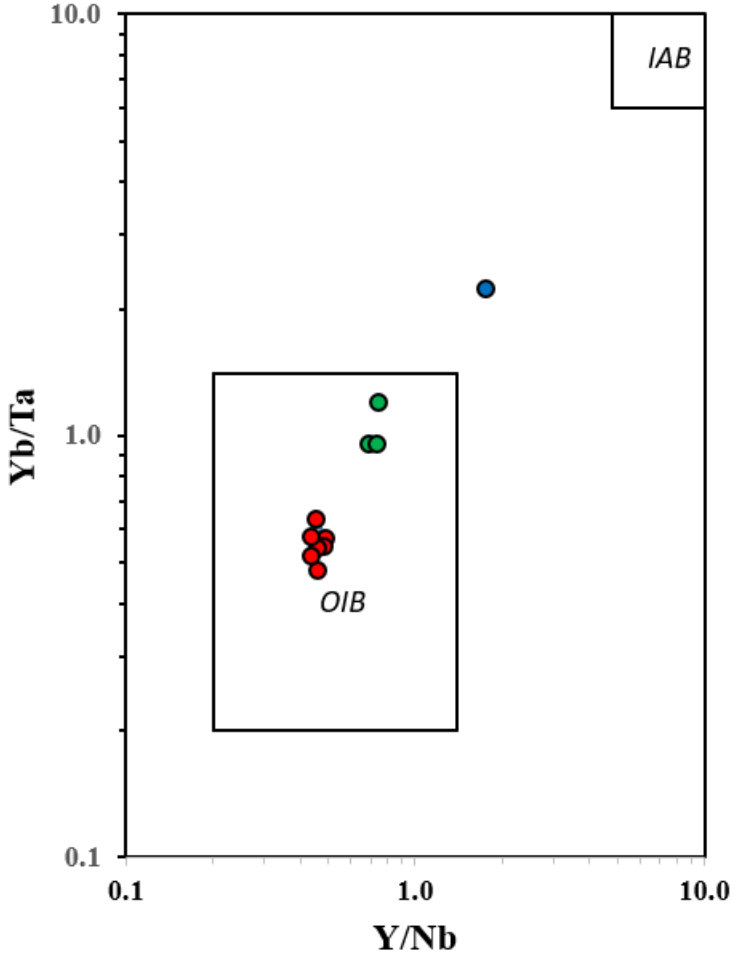
10.0
1.0
0.1
Yb/Ta
IAB
OIB
0.1
1.0
10.0
Y/Nb

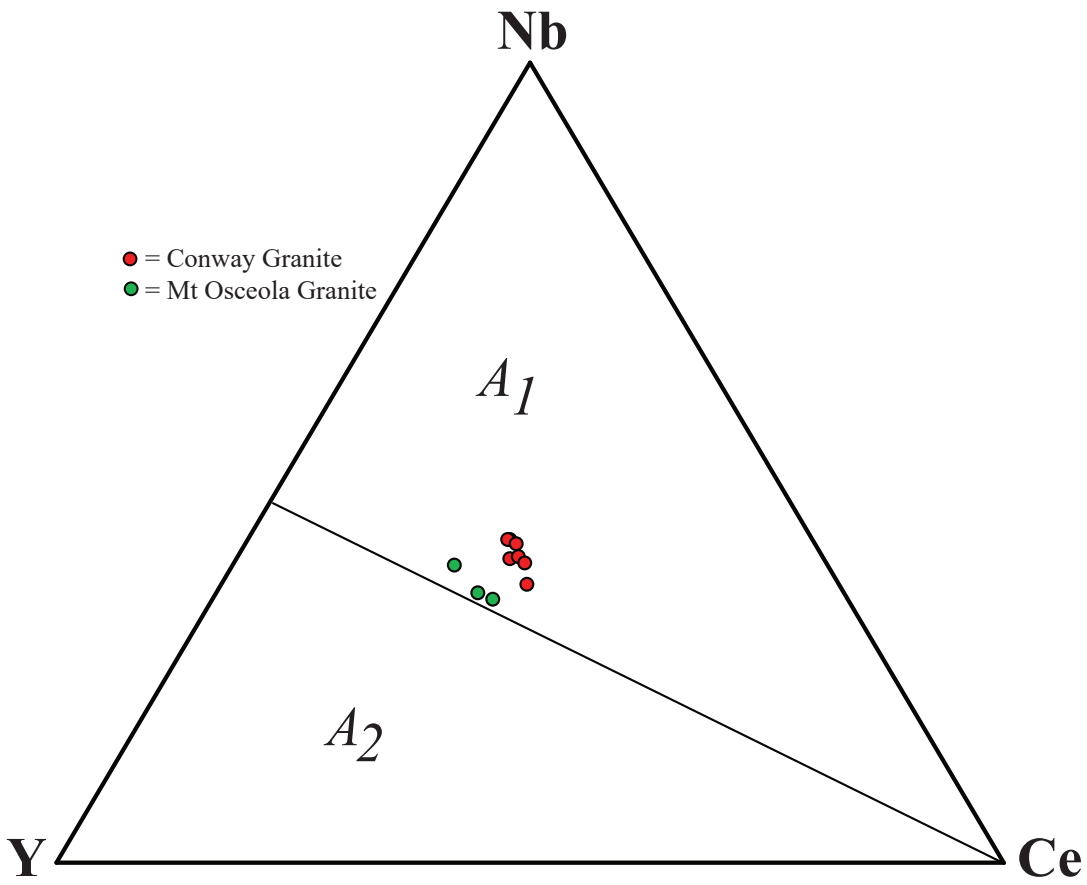
Nb
= Conway Granite
= Mt Osceola Granite
A_1
A_2
Y
Ce

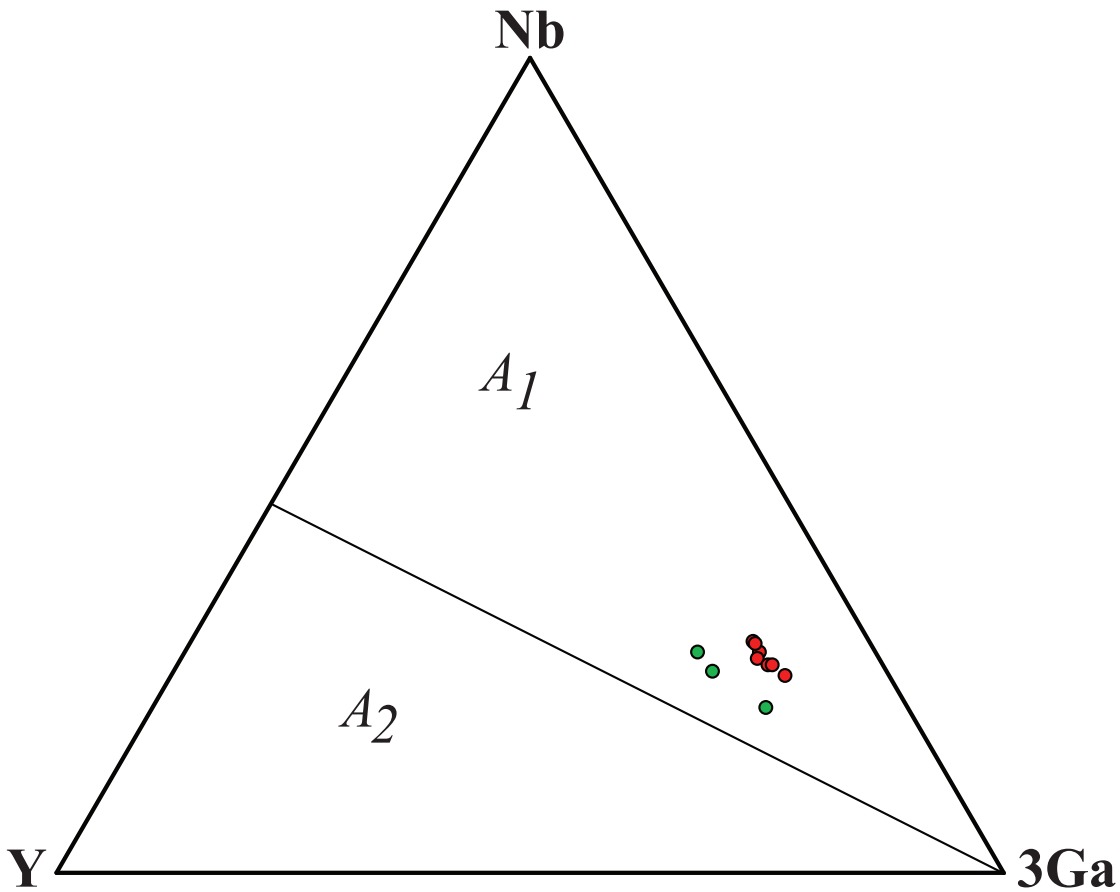
Nb
A_1
A_2
Y
3Ga

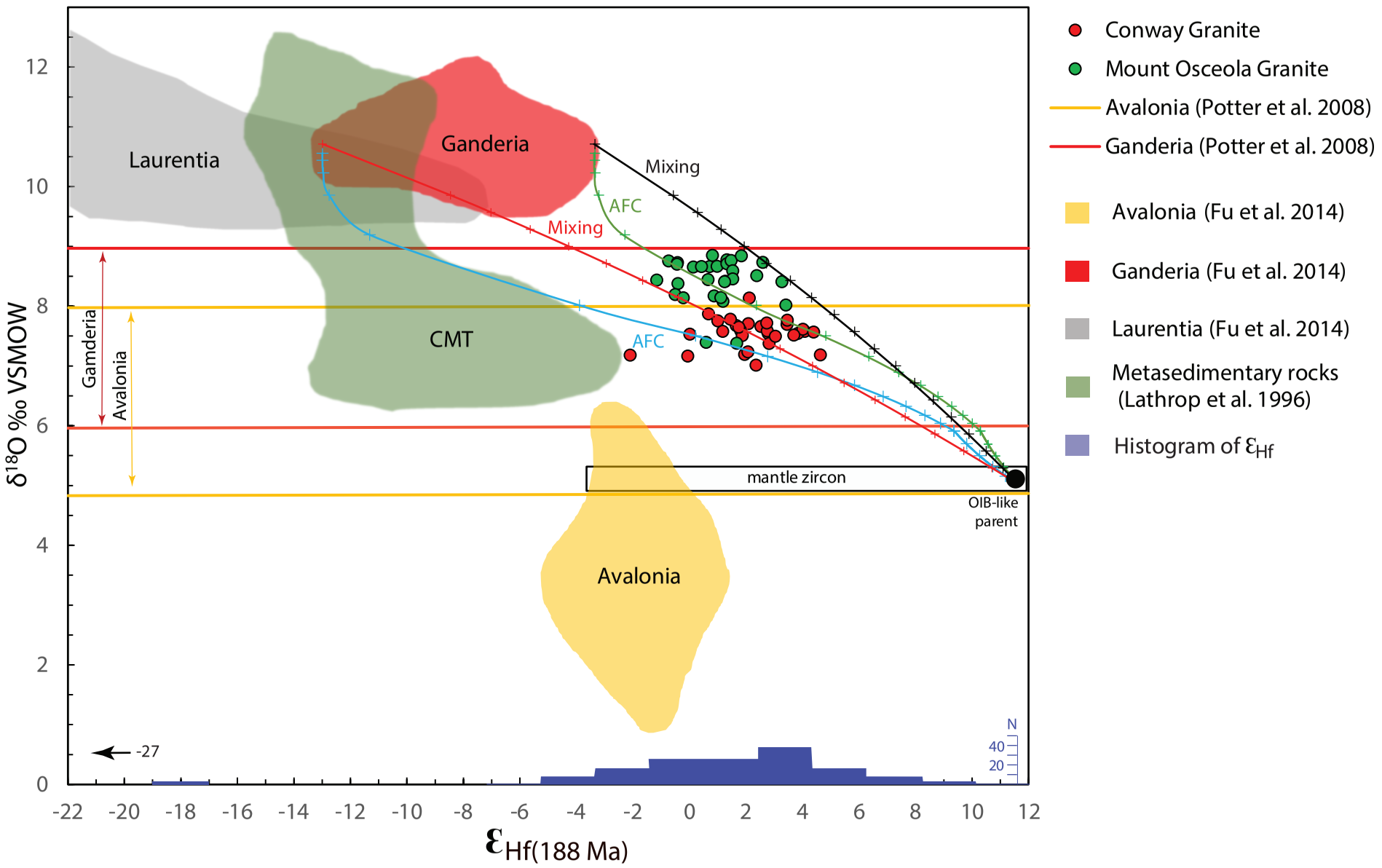
Laurentia
Ganderia
CMT
Avalonia
Mixing
AFC
Mixing
AFC
Gamderia
Avalonia
mantle zircon
OIB-like
parent
-27
N
40
20
δ18O ‰ VSMOW
εHf(188 Ma)
12
10
8
6
4
2
0
-22
-20
-18
-16
-14
-12
-10
-8
-6
-4
-2
0
2
4
6
8
10
12
Conway Granite
Mount Osceola Granite
Avalonia (Potter et al. 2008)
Ganderia (Potter et al. 2008)
Avalonia (Fu et al. 2014)
Ganderia (Fu et al. 2014)
Laurentia (Fu et al. 2014)
Metasedimentary rocks
(Lathrop et al. 1996)
Histogram of εHf

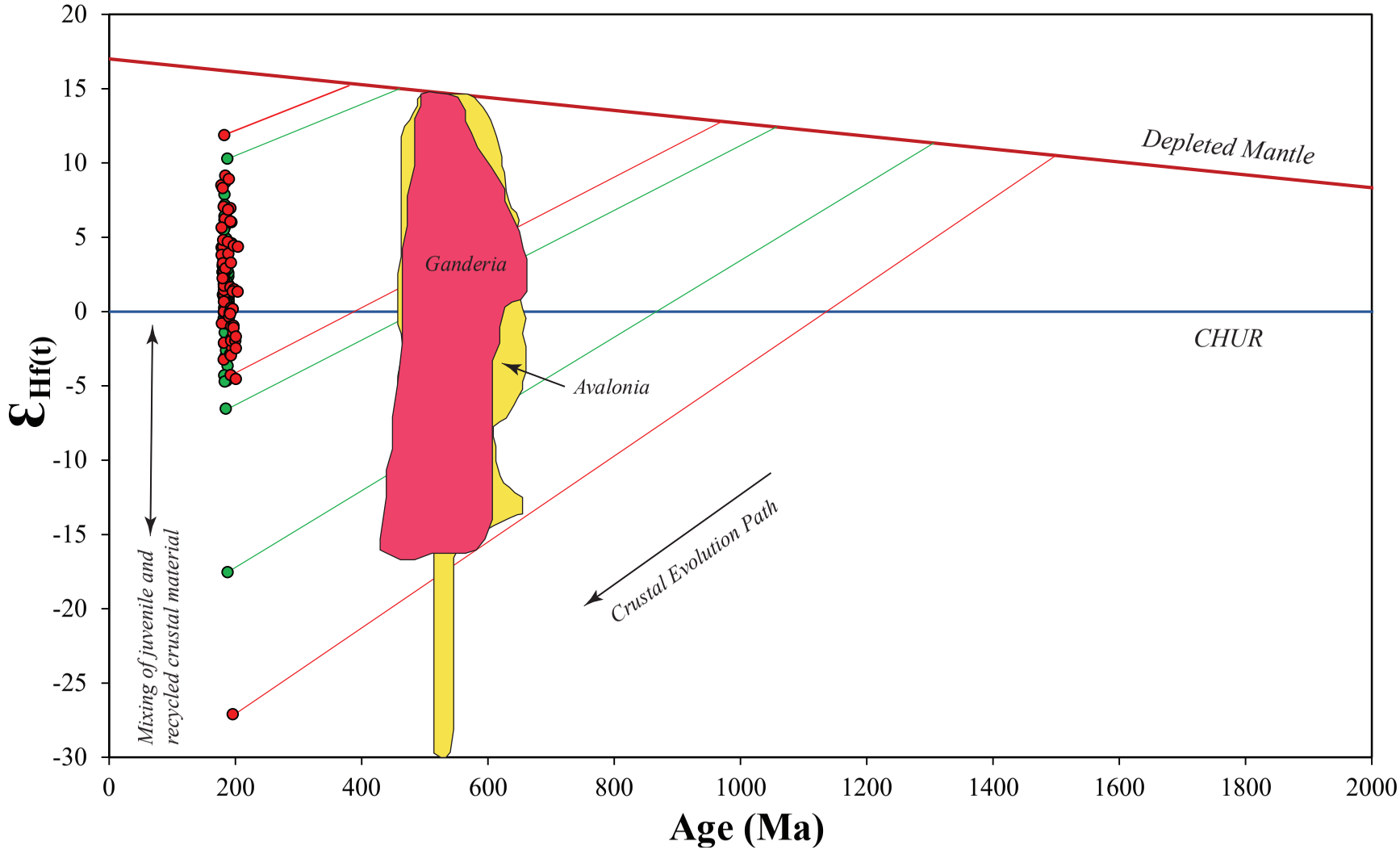
20
15
10
5
0
-5
-10
-15
-20
-25
-30
εHf(t)
0
200
400
600
800
1000
1200
1400
1600
1800
2000
Age (Ma)
Depleted Mantle
CHUR
Ganderia
Avalonia
Crustal Evolution Path
Mixing of juvenile and recycled crustal material

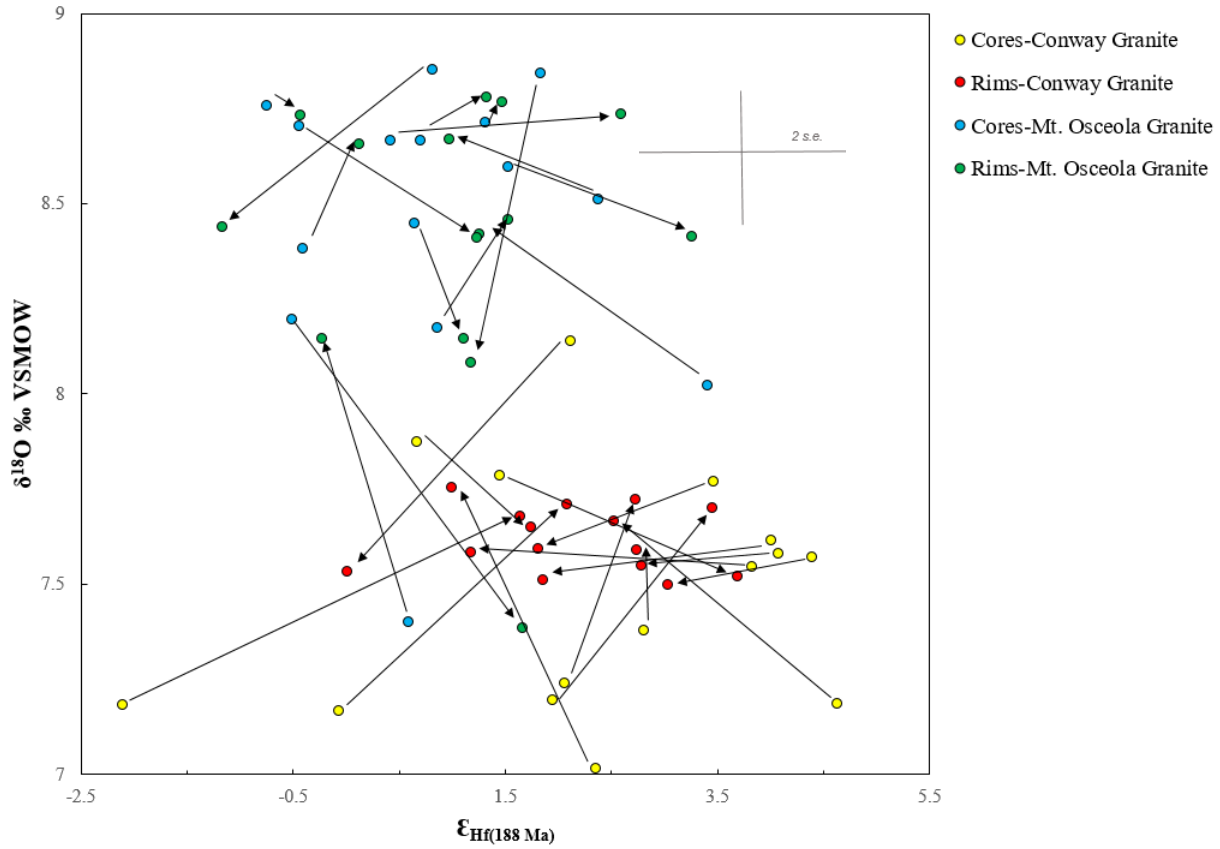
9
8.5
8
7.5
7
-2.5
-0.5
1.5
3.5
5.5
δ18O ‰ VSMOW
εHf(188 Ma)
2 s.e.
Cores-Conway Granite
Rims-Conway Granite
Cores-Mt. Osceola Granite
Rims-Mt. Osceola Granite

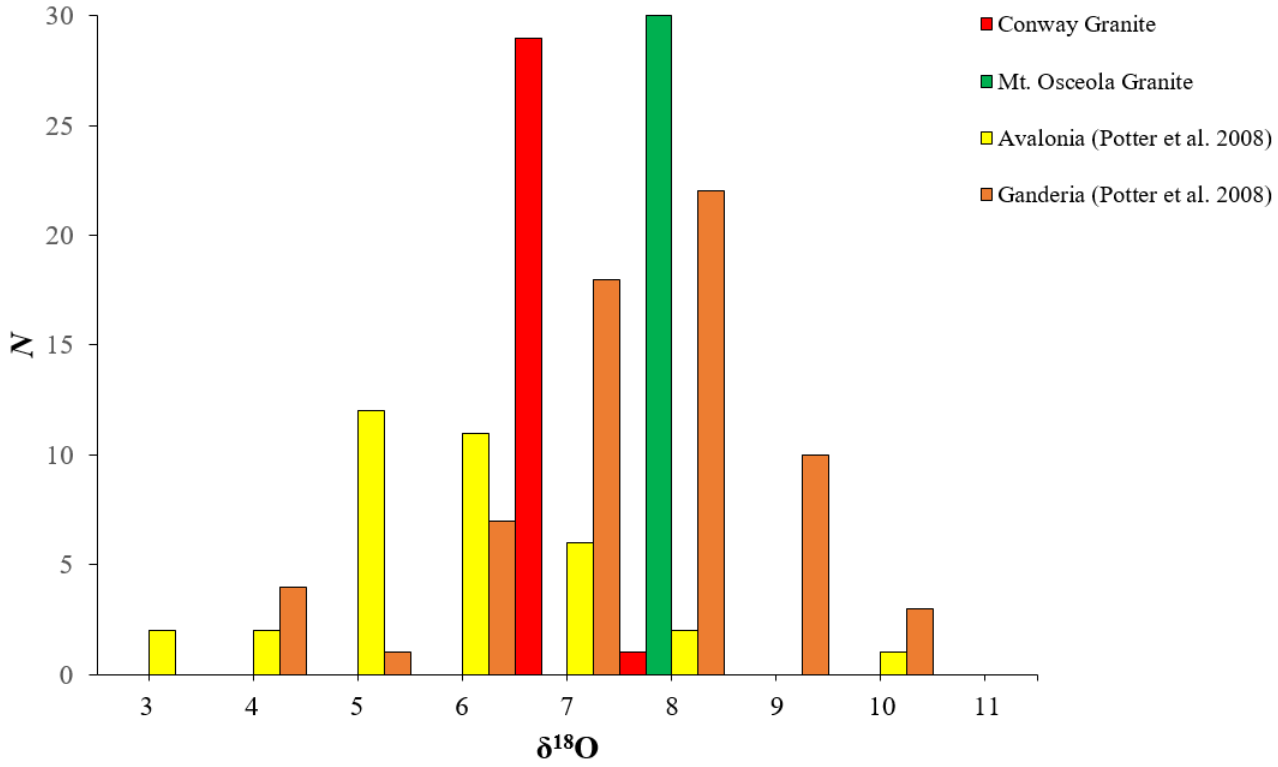
30
25
20
15
10
5
0
N
3
4
5
6
7
8
9
10
11
δ18O
Conway Granite
Mt. Osceola Granite
Avalonia (Potter et al. 2008)
Ganderia (Potter et al. 2008)

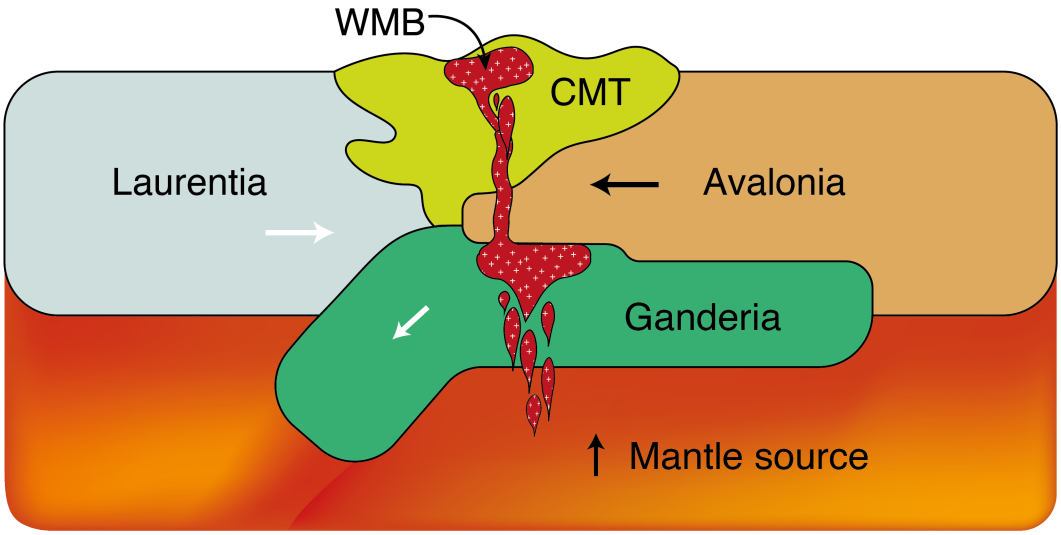
WMB
CMT
Laurentia
Avalonia
Ganderia
Mantle source

Table 1. Representative biotite analyses, Conway and Mount Osceola Granites

	F	Na2O	MgO	Al2O3	SiO2	Cl	K2O	CaO	TiO2	MnO	FeO	Total	F=O	Cl=O	Total
C-1 Bio-1	1.238	0.106	3.491	12.213	35.259	0.312	9.599	0.005	3.452	0.735	31.727	98.137	-0.521	-0.071	97.545
C-1 Bio-1	1.309	0.126	3.336	12.061	34.889	0.291	9.755	0.008	3.678	0.65	31.761	97.864	-0.551	-0.066	97.247
C-1 Bio-1	1.296	0.135	3.502	12.157	35.179	0.282	9.778	0	3.694	0.587	31.247	97.857	-0.546	-0.064	97.247
C-1 Bio-1	1.343	0.127	3.304	12.072	35.143	0.29	9.642	0	3.695	0.738	31.253	97.607	-0.566	-0.065	96.976
C-1 Bio-1	1.427	0.13	3.353	12.185	34.836	0.263	9.703	0.006	3.768	0.636	31.015	97.322	-0.601	-0.059	96.662
C-1 Bio-1	1.388	0.13	3.418	11.988	35.414	0.292	9.6	0.003	3.69	0.679	30.606	97.208	-0.584	-0.066	96.558
C-1 Bio-1	1.369	0.147	3.505	12.125	35.279	0.259	9.764	0	3.723	0.597	31.124	97.892	-0.577	-0.059	97.256
C-1 Bio-1	1.301	0.145	3.54	11.975	35.407	0.307	9.724	0.007	3.689	0.633	31.154	97.882	-0.548	-0.069	97.265
C-1 Bio-1	1.342	0.137	3.326	12.087	35.154	0.289	9.712	0.003	3.649	0.619	30.969	97.287	-0.565	-0.065	96.657
C-1 Bio-1	1.258	0.094	3.469	12.159	35.752	0.323	9.752	0	3.552	0.636	30.966	97.961	-0.53	-0.073	97.358
C-1 Bio-1	1.33	0.145	3.434	12.112	34.976	0.317	9.766	0	3.556	0.639	31.129	97.404	-0.56	-0.071	96.773
C-1 Bio-1	1.286	0.155	3.369	12.048	35.475	0.308	9.805	0	3.492	0.654	30.718	97.31	-0.541	-0.069	96.7
C-1 Bio-1	1.261	0.104	3.373	12.023	35.653	0.307	9.677	0.016	3.256	0.696	31.437	97.803	-0.531	-0.069	97.203
C-1 Bio-2	1.559	0.189	3.433	12.164	35.251	0.278	9.841	0	3.895	0.728	30.663	98.001	-0.657	-0.063	97.281
C-1 Bio-2	1.481	0.155	3.284	11.911	34.739	0.299	9.562	0.003	3.802	0.645	32.24	98.121	-0.624	-0.067	97.43
C-1 Bio-2	1.421	0.104	3.391	12.163	35.22	0.289	9.731	0	3.77	0.682	31.208	97.979	-0.598	-0.065	97.316
C-1 Bio-2	1.394	0.123	3.323	12.038	35.487	0.295	9.806	0	3.704	0.64	30.351	97.161	-0.587	-0.066	96.508
C-1 Bio-2	1.373	0.108	3.433	11.834	35.947	0.271	9.631	0.019	3.683	0.643	31.045	97.987	-0.578	-0.061	97.348
C-1 Bio-2	1.162	0.058	3.36	12.374	35.285	0.286	9.438	0.038	3.777	0.443	31.022	97.243	-0.489	-0.064	96.69
C-1 Bio-2	1.183	0.066	3.258	12.34	35.072	0.29	9.749	0	3.905	0.671	31.203	97.737	-0.498	-0.066	97.173
C-1 Bio-2	1.092	0.11	3.166	12.433	36.307	0.261	8.63	0.14	3.234	0.556	30.879	96.808	-0.46	-0.059	96.289
C-1 Bio-3	1.49	0.142	3.446	12.082	35.306	0.258	9.61	0.008	3.758	0.731	30.952	97.783	-0.627	-0.058	97.098
C-1 Bio-3	1.315	0.134	3.341	12.152	34.86	0.254	9.773	0	3.802	0.829	31.497	97.957	-0.554	-0.057	97.346
C-1 Bio-3	1.258	0.171	3.299	12.209	34.599	0.259	9.644	0.001	3.803	0.72	31.07	97.033	-0.53	-0.058	96.445
C-1 Bio-3	1.13	0.121	3.426	12.14	35.307	0.268	9.59	0	3.754	0.608	31.391	97.735	-0.476	-0.06	97.199
C-6 bio-1	1.123	0.097	3.645	11.867	35.503	0.38	9.673	0.012	3.365	0.567	31.576	97.808	-0.473	-0.086	97.249
C-6 bio-1	1.208	0.124	3.654	12.056	35.334	0.374	9.652	0.02	3.388	0.663	31.523	97.996	-0.509	-0.084	97.403
C-6 bio-1	1.171	0.138	3.722	12.187	35.443	0.369	8.842	0.01	3.208	0.662	32.224	97.976	-0.493	-0.083	97.4
C-6 bio-1	1.329	0.155	3.66	11.741	35.629	0.376	9.418	0	3.428	0.67	31.339	97.745	-0.56	-0.085	97.1
C-6 bio-1	1.19	0.137	3.664	11.993	35.334	0.412	9.708	0.012	3.508	0.62	31.247	97.825	-0.501	-0.093	97.231
C-6 bio-1	1.088	0.063	3.626	12.269	34.824	0.384	9.361	0	3.392	0.478	31.487	96.972	-0.458	-0.087	96.427
C-6 bio-2	1.539	0.176	3.369	12.105	35.318	0.384	9.647	0.006	3.86	0.677	30.784	97.865	-0.648	-0.087	97.13
C-6 bio-2	1.403	0.178	3.464	12.079	34.876	0.415	9.713	0	3.738	0.719	31.284	97.869	-0.591	-0.094	97.184
C-6 bio-2	1.404	0.146	3.422	12.05	35.237	0.426	9.558	0	3.644	0.79	31.213	97.89	-0.591	-0.096	97.203
C-6 bio-2	1.432	0.142	3.454	12.048	35.554	0.404	9.704	0	3.581	0.773	30.869	97.961	-0.603	-0.091	97.267
C-6 bio-2	1.366	0.175	3.362	11.944	35.165	0.403	9.494	0	3.714	0.67	31.485	97.778	-0.575	-0.091	97.112
C-6 bio-2	1.414	0.143	3.397	11.973	35.248	0.416	9.636	0.005	3.562	0.588	31.768	98.15	-0.595	-0.094	97.461
C-6 bio-3	1.181	0.097	3.501	12.088	34.893	0.451	9.768	0	3.169	0.666	31.918	97.732	-0.497	-0.102	97.133
C-6 bio-3	1.085	0.056	3.453	12.102	34.792	0.438	9.635	0	3.259	0.711	31.993	97.524	-0.457	-0.099	96.968
C-6 bio-3	0.952	0.036	3.433	12.467	34.693	0.468	9.21	0.01	3.145	0.601	32.757	97.772	-0.401	-0.106	97.265
C-6 bio-3	0.993	0.062	3.425	12.246	34.746	0.477	9.366	0.085	3.309	0.534	32.552	97.795	-0.418	-0.108	97.269
C-6 bio-3	1.137	0.121	3.334	12.116	35.087	0.458	9.787	0	3.378	0.664	31.286	97.368	-0.479	-0.103	96.786
C-6 bio-3	1.112	0.097	3.391	12.017	35.012	0.408	9.541	0.027	3.53	0.553	31.695	97.383	-0.468	-0.092	96.823

MTO-1 bio-1	0.51	0.132	0.617	12.303	34.07	0.307	9.467	0	3.449	0.47	35.071	96.396	-0.215	-0.069	96.112
MTO-1 bio-1	0.45	0.168	0.627	12.292	34.106	0.345	9.304	0.025	3.455	0.47	36.302	97.544	-0.19	-0.078	97.276
MTO-1 bio-1	0.446	0.132	0.646	12.44	34.491	0.337	9.415	0.003	3.421	0.491	35.802	97.624	-0.188	-0.076	97.36
MTO-1 bio-1	0.541	0.081	0.611	12.275	34.393	0.307	9.257	0.015	3.54	0.491	35.761	97.272	-0.228	-0.069	96.975
MTO-1 bio-1	0.546	0.168	0.572	12.32	34.05	0.248	9.297	0.012	3.561	0.491	35.841	97.106	-0.23	-0.056	96.82
MTO-1 bio-1	0.461	0.193	0.62	12.229	34.133	0.279	9.42	0	3.546	0.522	35.464	96.867	-0.194	-0.063	96.61
MTO-1 bio-1	0.486	0.127	0.652	12.425	33.972	0.323	9.348	0.003	3.468	0.519	35.767	97.09	-0.205	-0.073	96.812
MTO-1 bio-1	0.258	0.046	0.63	12.322	34.246	0.262	9.184	0.037	3.477	0.224	36.065	96.751	-0.109	-0.059	96.583
MTO-1 bio-1	0.34	0.092	0.687	12.452	34.134	0.232	9.35	0.008	3.528	0.368	35.488	96.679	-0.143	-0.052	96.484
MTO-1 bio-1	0.401	0.077	0.624	12.306	33.677	0.274	9.284	0.033	3.536	0.42	35.818	96.45	-0.169	-0.062	96.219
MTO-1 bio-1	0.335	0.092	0.729	12.561	34.118	0.226	9.343	0	3.606	0.343	36.046	97.399	-0.141	-0.051	97.207
MTO-1 bio-1	0.292	0.08	0.656	12.516	34.044	0.318	9.412	0.018	3.82	0.263	35.435	96.854	-0.123	-0.072	96.659
MTO-1 bio-1	0.394	0.169	0.733	12.558	34.309	0.285	9.308	0.01	3.534	0.413	35.702	97.415	-0.166	-0.064	97.185
MTO-1 bio-1	0.375	0.163	0.67	12.609	34.104	0.293	9.086	0.114	3.412	0.504	35.076	96.406	-0.158	-0.066	96.182
MTO-1 bio-2	0.701	0.11	0.394	12.406	33.977	0.394	9.238	0.016	3.572	0.728	36.157	97.693	-0.295	-0.089	97.309
MTO-1 bio-2	0.694	0.148	0.48	12.324	33.83	0.329	9.353	0.015	3.6	0.539	36.071	97.383	-0.292	-0.074	97.017
MTO-1 bio-2	0.677	0.129	0.447	12.076	34.187	0.32	9.393	0.023	3.599	0.532	35.785	97.168	-0.285	-0.072	96.811
MTO-1 bio-2	0.664	0.09	0.469	12.326	34.079	0.308	9.472	0.02	3.242	0.662	35.444	96.776	-0.28	-0.069	96.427
MTO-1 bio-2	0.614	0.069	0.438	12.175	33.666	0.314	9.156	0.037	2.958	0.706	36.77	96.903	-0.258	-0.071	96.574
MTO-1 bio-2	0.664	0.067	0.512	12.088	33.938	0.306	9.266	0.068	3.485	0.531	36.373	97.298	-0.279	-0.069	96.95
MTO-1 bio-2	0.624	0.057	0.511	12.48	34.158	0.294	9.349	0.024	3.409	0.529	35.778	97.213	-0.263	-0.066	96.884
MTO-1 bio-2	0.571	0.046	0.498	12.371	33.97	0.305	9.223	0.052	3.298	0.472	36.012	96.818	-0.24	-0.069	96.509
MTO-1 bio-2	0.586	0.114	0.486	12.209	33.829	0.322	9.255	0.029	3.155	0.622	36.377	96.984	-0.247	-0.073	96.664
MTO-1 bio-2	0.68	0.134	0.521	12.388	34.307	0.312	9.221	0.046	3.265	0.588	35.571	97.033	-0.286	-0.07	96.677
MTO-1 bio-2	0.642	0.141	0.538	12.565	33.992	0.313	9.214	0.003	3.168	0.64	36.04	97.256	-0.27	-0.071	96.915
MTO-1 bio-2	0.615	0.073	0.498	12.403	34.038	0.311	9.181	0.043	2.955	0.591	35.74	96.448	-0.259	-0.07	96.119
MTO-1 bio-2	0.662	0.118	0.556	12.252	33.946	0.326	9.213	0.002	3.027	0.577	36.345	97.024	-0.279	-0.073	96.672
MTO-1 bio-2	0.719	0.123	0.502	12.318	34.454	0.328	9.44	0.03	2.906	0.598	36.052	97.47	-0.303	-0.074	97.093
MTO-1 bio-2	0.623	0.077	0.494	12.352	34.324	0.293	9.287	0.051	2.916	0.577	36.224	97.218	-0.262	-0.066	96.89
MTO-1 bio-3	0.733	0.183	0.559	12.15	34.39	0.29	9.32	0	3.742	0.385	35.654	97.406	-0.309	-0.066	97.031
MTO-1 bio-3	0.653	0.128	0.639	12.154	34.203	0.292	9.423	0	3.518	0.55	35.739	97.299	-0.275	-0.066	96.958
MTO-1 bio-3	0.567	0.156	0.572	12.306	34.071	0.334	9.333	0.003	3.445	0.504	36.29	97.581	-0.239	-0.075	97.267
MTO-1 bio-3	0.561	0.17	0.548	12.194	34.152	0.28	9.325	0	3.467	0.382	35.722	96.801	-0.236	-0.063	96.502
MTO-1 bio-3	0.578	0.219	0.622	12.316	34.012	0.3	9.435	0.006	3.442	0.441	36.181	97.552	-0.244	-0.068	97.24
MTO-1 bio-3	0.545	0.161	0.596	12.523	34.127	0.325	9.342	0.011	3.463	0.483	35.755	97.331	-0.229	-0.073	97.029

Table 2. Representative amphibole analyses, Mount Osceola Granite

	F	Na2O	MgO	Al2O3	SiO2	Cl	K2O	CaO	TiO2	MnO	FeO	Total	O=F	O=Cl	Total
MTO-1-1	0.74	1.963	0.686	8.876	38.63	0.488	1.622	10.107	1.999	0.581	32.482	98.174	-0.312	-0.11	97.752
MTO-1-1	0.763	1.967	0.606	8.753	38.858	0.513	1.721	10.277	2.086	0.627	32.67	98.841	-0.321	-0.116	98.404
MTO-1-1	0.656	1.951	0.633	8.751	38.267	0.495	1.636	10.265	2.034	0.687	31.562	96.937	-0.276	-0.112	96.549
MTO-1-1	0.64	2.019	0.571	8.864	38.059	0.39	1.593	10.061	1.7	0.686	32.087	96.67	-0.269	-0.088	96.313
MTO-1-1	0.723	1.989	0.62	9.067	39.027	0.5	1.566	10.01	2.059	0.546	32.559	98.666	-0.304	-0.113	98.249
MTO-1-1	0.72	1.912	0.648	8.994	38.828	0.496	1.572	10.275	1.98	0.634	32.254	98.313	-0.303	-0.112	97.898
MTO-1-1	0.729	1.942	0.679	8.913	39.376	0.493	1.619	10.169	2.018	0.627	32.248	98.813	-0.307	-0.111	98.395
MTO-1-1	0.746	1.811	0.666	9.182	38.482	0.509	1.597	9.914	1.917	0.68	32.013	97.517	-0.314	-0.115	97.088
MTO-1-1	0.732	1.898	0.6	9.097	38.875	0.497	1.633	10.179	2.009	0.592	31.811	97.923	-0.308	-0.112	97.503
MTO-1-1	0.792	1.905	0.67	8.744	38.975	0.487	1.557	10.232	2.003	0.595	32.08	98.04	-0.334	-0.11	97.596
MTO-1-1	0.777	1.931	0.674	8.771	39.074	0.468	1.58	10.354	1.979	0.529	31.699	97.836	-0.327	-0.106	97.403
MTO-1-2	0.641	1.981	0.528	8.409	39.659	0.474	1.586	9.976	1.986	0.764	32.168	98.172	-0.27	-0.107	97.795
MTO-1-2	0.503	1.779	0.426	8.216	40.428	0.357	1.52	9.624	1.331	0.738	33.502	98.424	-0.212	-0.081	98.131
MTO-1-2	0.629	1.888	0.45	8.701	39.902	0.424	1.45	9.917	1.433	0.834	32.676	98.304	-0.265	-0.096	97.943
MTO-1-2	0.611	1.935	0.529	8.578	39.691	0.221	1.353	9.56	1.285	0	33.511	97.274	-0.257	-0.05	96.967
MTO-1-2	0.463	1.544	0.475	8.346	39.469	0.19	1.278	7.83	1.045	0.815	35.339	96.794	-0.195	-0.043	96.556
MTO-1-2	0.719	1.98	0.471	8.576	39.689	0.349	1.469	9.917	1.434	0.764	32.907	98.275	-0.303	-0.079	97.893
MTO-1-2	0.584	1.962	0.463	8.526	39.756	0.456	1.485	9.967	1.64	0.887	32.979	98.705	-0.246	-0.103	98.356
MTO-1-2	0.568	1.916	0.517	8.666	39.648	0.307	1.415	9.674	1.397	0.806	32.831	97.745	-0.239	-0.069	97.437
MTO-1-2	0.633	1.976	0.474	8.669	39.672	0.333	1.43	9.799	1.55	0.725	33.196	98.457	-0.267	-0.075	98.115
MTO-1-2	0.715	2.007	0.465	8.688	39.483	0.365	1.484	10.004	1.637	0.855	33.355	99.058	-0.301	-0.082	98.675
MTO-1-3	0.782	1.882	0.621	8.791	38.986	0.51	1.628	10.011	2.177	0.461	33.012	98.861	-0.329	-0.115	98.417
MTO-1-3	0.801	1.847	0.634	8.875	39.113	0.505	1.611	10.077	2.13	0.493	33.067	99.153	-0.337	-0.114	98.702
MTO-1-3	0.722	1.941	0.627	8.826	39.271	0.48	1.647	10.212	2.154	0.472	32.778	99.13	-0.304	-0.108	98.718
MTO-3-1	0.573	1.821	0.538	8.704	39.208	0.426	1.402	9.104	1.846	0.687	34.266	98.575	-0.241	-0.096	98.238
MTO-3-1	0.542	1.636	0.591	9.231	38.098	0.356	1.303	8.344	1.677	0.635	36.565	98.978	-0.228	-0.08	98.67
MTO-3-1	0.523	1.731	0.588	8.679	38.568	0.356	1.361	8.512	1.67	0.732	36.236	98.956	-0.22	-0.08	98.656
MTO-3-1	0.604	1.822	0.583	9.023	39.185	0.345	1.379	8.877	1.526	0.668	34.784	98.796	-0.254	-0.078	98.464
MTO-3-1	0.642	1.974	0.558	8.818	38.814	0.306	1.357	8.918	1.52	0.744	34.744	98.395	-0.27	-0.069	98.056
MTO-3-1	0.672	1.974	0.536	8.24	38.104	0.37	1.438	9.458	1.785	0.662	33.323	96.562	-0.283	-0.083	96.196
MTO-3-2	0.683	1.796	0.438	8.986	39.274	0.437	1.443	9.258	1.638	0.749	33.661	98.363	-0.288	-0.099	97.976
MTO-3-2	0.64	1.824	0.575	8.86	38.988	0.422	1.413	9.119	1.703	0.647	34.874	99.065	-0.269	-0.095	98.701
MTO-3-2	0.768	2.079	0.605	8.641	39.404	0.408	1.5	9.826	1.635	0.673	32.858	98.397	-0.323	-0.092	97.982
MTO-3-1	0.649	2.054	0.535	8.586	40.064	0.297	1.506	9.718	1.815	0.755	31.531	97.51	-0.273	-0.067	97.17
MTO-3-1	0.681	1.998	0.547	8.277	40.05	0.348	1.522	9.835	1.822	0.552	32.056	97.688	-0.287	-0.079	97.322
MTO-3-1	0.685	1.98	0.503	8.255	39.883	0.403	1.554	9.778	1.95	0.702	31.699	97.392	-0.289	-0.091	97.012
MTO-3-1	0.767	1.984	0.56	8.188	39.882	0.397	1.525	9.815	1.992	0.724	31.666	97.5	-0.323	-0.09	97.087
MTO-3-1	0.689	1.956	0.585	8.19	39.925	0.418	1.533	9.823	1.9	0.72	31.896	97.635	-0.29	-0.094	97.251
MTO-3-1	0.697	2.01	0.55	8.463	39.45	0.427	1.594	9.869	2.016	0.713	32.076	97.865	-0.294	-0.096	97.475
MTO-3-1	0.757	1.955	0.605	8.514	39.79	0.449	1.554	9.934	1.979	0.63	31.536	97.703	-0.319	-0.101	97.283
MTO-3-1	0.734	1.919	0.659	8.04	40.311	0.453	1.493	9.98	1.906	0.658	31.299	97.452	-0.309	-0.102	97.041
MTO-3-1	0.679	1.962	0.62	8.437	40.095	0.454	1.515	10.034	2.022	0.623	31.374	97.815	-0.286	-0.102	97.427
MTO-3-1	0.695	1.957	0.65	8.373	39.794	0.46	1.55	10.038	2.009	0.762	32.049	98.337	-0.293	-0.104	97.94
MTO-3-2	0.723	1.937	0.581	8.545	39.582	0.469	1.625	10.153	1.951	0.808	31.804	98.178	-0.304	-0.106	97.768
MTO-3-2	0.662	1.909	0.517	8.484	39.314	0.466	1.507	9.95	1.959	0.724	31.804	97.296	-0.279	-0.105	96.912
MTO-3-2	0.691	1.92	0.465	8.635	39.491	0.48	1.559	9.95	2.029	0.713	31.868	97.801	-0.291	-0.108	97.402
MTO-3-2	0.657	1.909	0.594	8.736	39.578	0.484	1.577	10.139	1.987	0.658	31.684	98.003	-0.277	-0.109	97.617
MTO-3-2	0.726	1.919	0.579	8.559	39.741	0.374	1.518	9.924	1.722	0.772	32.379	98.213	-0.306	-0.084	97.823
MTO-3-2	0.69	1.968	0.612	8.643	39.438	0.491	1.528	9.96	2.065	0.752	31.582	97.729	-0.291	-0.111	97.327
MTO-3-2	0.804	2.017	0.651	8.604	39.361	0.455	1.542	10.073	2.018	0.689	32.231	98.445	-0.338	-0.103	98.004
MTO-3-2	0.756	1.993	0.577	8.622	39.89	0.296	1.4	9.875	1.75	0.685	32.751	98.595	-0.318	-0.067	98.21
MTO-3-2	0.805	2.003	0.579	8.469	39.547	0.256	1.402	9.882	1.593	0.689	31.34	96.565	-0.339	-0.058	96.168
MTO-3-2	0.679	1.972	0.567	8.676	39.521	0.446	1.502	10.092	1.794	0.619	31.787	97.655	-0.286	-0.101	97.268
MTO-3-3	0.675	1.945	0.567	8.798	39.116	0.494	1.641	10.129	2.102	0.55	31.025	97.042	-0.284	-0.112	96.646
MTO-3-3	0.752	1.916	0.657	8.793	39.365	0.501	1.575	10.026	2.026	0.529	31.266	97.406	-0.317	-0.113	96.976
MTO-3-3	0.667	1.959	0.649	8.823	39.072	0.495	1.603	10.182	2.14	0.603	31.439	97.632	-0.281	-0.112	97.239
MTO-3-3	0.72	1.948	0.69	8.785	38.898	0.522	1.631	10.17	2.079	0.574	31.684	97.701	-0.303	-0.118	97.28
MTO-3-3	0.773	1.964	0.618	8.876	39.076	0.503	1.646	10.171	2.041	0.62	32.079	98.367	-0.326	-0.114	97.927
MTO-3-3	0.757	1.97	0.607	8.91	38.855	0.55	1.692	10.213	2.039	0.602	31.644	97.839	-0.319	-0.124	97.396
MTO-3-3	0.719	1.886	0.694	8.938	38.846	0.572	1.71	10.153	2.033	0.508	31.928	97.987	-0.303	-0.129	97.555
MTO-3-3	0.679	1.932	0.663	8.83	38.942	0.559	1.629	10.195	2.134	0.613	31.189	97.365	-0.286	-0.126	96.953
MTO-3-3	0.816	1.917	0.744	8.919	38.764	0.56	1.676	10.188	2.036	0.585	31.853	98.058	-0.344	-0.126	97.588
MTO-3-3	0.757	1.911	0.703	8.928	38.848	0.532	1.724	10.163	2.074	0.501	31.954	98.095	-0.319	-0.12	97.656
MTO-3-3	0.768	2.025	0.699	8.917	38.797	0.515	1.667	10.2	1.95	0.525	32.1	98.163	-0.323	-0.116	97.724
MTO-3-3	0.725	2.2	0.696	8.693	38.594	0.727	1.992	9.936	2.08	0.554	31.117	97.314	-0.305	-0.164	96.845
MTO-3-3	0.777	1.933	0.681	8.834	38.772	0.508	1.654	10.196	2.111	0.494	31.665	97.625	-0.327	-0.115	97.183
MTO-3-3	0.773	1.993	0.64	8.648	38.895	0.496	1.656	10.093	2.097	0.627	32.08	97.998	-0.325	-0.112	97.561
MTO-3-4	0.592	2.036	0.616	8.671	39.577	0.457	1.535	10.137	1.916	0.634	32.052	98.223	-0.249	-0.103	97.871
MTO-3-4	0.611	2	0.565	8.637	39.561	0.421	1.584	9.986	1.918	0.767	32.114	98.164	-0.257	-0.095	97.812
MTO-3-4	0.569	2.119	0.574	8.439	39.087	0.473	1.542	9.882	1.915	0.714	31.78	97.094	-0.239	-0.107	96.748
MTO-3-4	0.61	2.009	0.593	8.615	39.738	0.413	1.569	9.883	1.962	0.686	32.071	98.149	-0.257	-0.093	97.799
MTO-3-4	0.671	2.016	0.593	8.537	39.461	0.423	1.58	9.772	1.911	0.718	31.557	97.239	-0.283	-0.095	96.861

MTO-3-4	0.67	2.023	0.613	8.66	39.146	0.423	1.565	9.867	1.971	0.613	31.84	97.391	-0.282	-0.095	97.014
MTO-3-4	0.639	1.969	0.576	8.494	39.743	0.427	1.599	9.993	1.934	0.589	31.593	97.556	-0.269	-0.096	97.191
MTO-3-4	0.61	2.005	0.639	8.462	39.509	0.393	1.57	9.952	1.975	0.672	32.01	97.797	-0.257	-0.089	97.451
MTO-3-4	0.672	1.943	0.584	8.512	39.511	0.425	1.584	10.046	1.935	0.718	32.073	98.003	-0.283	-0.096	97.624
MTO-3-4	0.687	1.982	0.522	8.494	39.463	0.446	1.573	10.041	2.013	0.673	31.756	97.65	-0.289	-0.101	97.26
MTO-3-4	0.692	1.994	0.641	8.662	39.501	0.48	1.613	9.951	1.963	0.743	31.88	98.12	-0.291	-0.108	97.721
MTO-3-4	0.592	1.969	0.554	8.542	39.691	0.357	1.549	9.898	1.95	0.71	32.548	98.36	-0.249	-0.081	98.03
MTO-3-4	0.641	2.071	0.561	8.452	39.527	0.443	1.625	10.052	1.962	0.75	31.74	97.824	-0.27	-0.1	97.454
MTO-3-4	0.613	1.962	0.55	8.772	39.648	0.462	1.544	10.114	2.009	0.603	31.695	97.972	-0.258	-0.104	97.61
MTO-3-4	0.67	2.021	0.607	8.441	39.228	0.431	1.54	10.042	1.961	0.718	32.291	97.95	-0.282	-0.097	97.571
MTO-3-4	0.668	1.932	0.546	8.655	39.28	0.425	1.576	10.031	1.997	0.578	32.265	97.953	-0.281	-0.096	97.576
MTO-3-4	0.636	1.944	0.545	8.607	39.777	0.46	1.57	9.96	1.978	0.54	31.956	97.973	-0.268	-0.104	97.601

Table 3. Representative Whole-rock analyses of the Conway and Mount Osceola Granites

	C-1	C-2	C-3	C-4	C-5	C-6	C-7	MTO-1	MTO-2	MTO-3
SiO2	73.23	72.70	72.53	72.55	72.39	71.85	71.93	71.64	72.47	72.16
TiO2	0.25	0.25	0.22	0.30	0.23	0.22	0.27	0.28	0.20	0.20
Al2O3	13.46	13.24	13.94	13.31	13.62	14.37	13.91	13.34	13.75	13.57
Fe2O3	2.18	2.65	2.03	2.73	2.49	1.97	2.46	3.29	2.29	2.74
MnO	0.05	0.06	0.04	0.06	0.06	0.05	0.06	0.07	0.06	0.06
MgO	0.18	0.20	0.14	0.21	0.17	0.14	0.18	0.05	0.02	0.03
CaO	0.74	0.83	0.75	0.81	0.81	0.72	0.80	1.24	0.90	1.04
Na2O	4.05	3.92	4.23	4.02	4.14	4.36	4.31	3.52	3.58	3.55
K2O	5.13	5.21	5.33	5.11	5.17	5.52	5.13	5.70	5.99	5.83
P2O5	0.06	0.06	0.05	0.07	0.06	0.05	0.06	0.04	0.03	0.03
SUM	99.33	99.12	99.26	99.17	99.14	99.25	99.11	99.17	99.29	99.21
Ba	248	248	259	240	242	263	248	294	320	305
Ce	157	157	139	181	176	132	160	232	147	219
Cl	131	143	146	156	146	125	132	156	108	111
Cr	5	9	5	6	5	5	6	1	0	2
Cu	0	0	0	0	0	0	0	0	0	0
F	2077	2772	2446	2434	2483	1879	2357	2614	1798	2016
Ga	17	14	16	16	18	18	17	25	23	23
La	111	114	102	129	120	93	111	120	88	132
Nb	67	68	54	76	68	58	73	96	63	76
Nd	49	51	42	59	55	43	52	100	58	87
Ni	9	10	11	9	9	9	8	8	7	8
Pb	18	21	20	19	19	20	18	33	33	33
Rb	364	382	377	379	372	365	370	280	279	271
Sc	0	0	0	1	0	0	0	8	2	3
Sm	9	9	8	11	11	8	10	14	9	14
Sr	91	85	93	88	91	93	96	46	46	46
Th	75	78	72	89	90	65	86	34	25	31
U	13	14	13	14	14	13	14	10	9	9
V	3	4	2	4	4	1	5	3	0	0
Y	35	38	30	40	36	31	36	81	50	60
Zn	42	50	37	50	45	38	45	116	79	95
Zr	263	276	239	288	272	215	270	473	323	412

Table 4. Representative Zircon Oxygen Isotopic Analyses

Sample	$\delta^{18}O$ ‰ measured	2SE (int.)	^{16}O (Gcps)	$\delta^{18}O$ ‰ VSMOW
C-01C	3.81	0.13	2.51	7.18
C-01R	4.28	0.11	2.42	7.66
C-02C	3.82	0.2	2.5	7.19
C-02R	4.32	0.2	2.43	7.7
C-03C	3.64	0.18	2.51	7.01
C-03R	4.37	0.22	2.39	7.75
C-04C	3.79	0.16	2.5	7.17
C-04R	4.33	0.16	2.41	7.71
C-05C	4.2	0.2	2.43	7.58
C-05R	4.17	0.19	2.39	7.55
C-06C	4.39	0.16	2.41	7.77
C-06R	4.21	0.17	2.48	7.59
C-07C	3.8	0.14	2.59	7.18
C-07R	4.3	0.12	2.55	7.68
C-08C	4.16	0.16	2.59	7.54
C-08R	4.24	0.19	2.51	7.58
C-09C	4.04	0.16	2.56	7.38
C-09R	4.25	0.15	2.52	7.59
C-10C	4.28	0.17	2.51	7.61
C-10R	4.17	0.18	2.52	7.51
C-11C	4.8	0.16	2.51	8.14
C-11R	4.19	0.19	2.52	7.53
C-12C	3.9	0.16	2.65	7.24
C-12R	4.38	0.16	2.48	7.72
C-13C	4.23	0.17	2.48	7.57
C-13R	4.16	0.21	2.47	7.5
C-14C	4.45	0.17	2.49	7.78
C-14R	4.18	0.16	2.47	7.52
C-15C	4.53	0.13	2.48	7.87
C-15R	4.31	0.17	2.45	7.65
MTO-01C	4.95	0.19	2.46	8.38
MTO-01R	5.23	0.17	2.43	8.66
MTO-02C	5.24	0.09	2.4	8.67
MTO-02R	5.35	0.2	2.5	8.78
MTO-03C	5.42	0.15	2.54	8.85
MTO-03R	5.01	0.16	2.54	8.44
MTO-04C	4.77	0.16	2.58	8.19
MTO-04R	3.96	0.2	2.59	7.38
MTO-05C	3.97	0.18	2.63	7.4
MTO-05R	4.72	0.13	2.55	8.14
MTO-06C	5.08	0.16	2.57	8.51
MTO-06R	5.24	0.19	2.52	8.67
MTO-07C	5.28	0.17	2.53	8.71
MTO-07R	5.34	0.18	2.5	8.77
MTO-08C	5.33	0.19	2.52	8.76
MTO-08R	5.36	0.22	2.48	8.73
MTO-09C	5.34	0.14	2.48	8.7
MTO-09R	5.05	0.14	2.47	8.42
MTO-10C	5.23	0.2	2.47	8.6
MTO-10R	5.05	0.17	2.47	8.41
MTO-11C	4.81	0.14	2.48	8.17
MTO-11R	5.09	0.14	2.47	8.46
MTO-12C	5.48	0.19	2.47	8.84
MTO-12R	4.72	0.14	2.46	8.08
MTO-13C	5.08	0.14	2.45	8.45
MTO-13R	4.78	0.19	2.45	8.14
MTO-14C	5.3	0.2	2.44	8.66
MTO-14R	5.37	0.17	2.42	8.73
MTO-15C	4.66	0.11	2.46	8.02
MTO-15R	5.05	0.15	2.41	8.41

Table 5. Zircon Hafnium isotopic Analyses, Conway and Mount Osceola Granites

Sampl	$^{176}Hf/^{177}Hf$	2s	$^{176}Lu/^{177}Hf$	2s	T (Ma)	$^{176}Hf/^{177}Hf(t)$	$\varepsilon_{Hf}(t)$	$\varepsilon_{Hf}(0)$	T_{DM} (Hf) (Ma)	T_{DM}^{2} (cont. crust)(Ma)
C-01C	0.28282	0.00016	0.00633	0.0003	188	0.282797743	4.63	1.24	704.66	1795.94
C-01R	0.282743	0.00007	0.001323	0.000057	188	0.282738348	2.53	-1.49	719.74	1926.95
C-02C	0.282731	0.000083	0.00258	0.00024	188	0.282721928	1.95	-1.91	762.05	1963.12
C-02R	0.28277	0.000062	0.001586	0.000087	188	0.282764423	3.45	-0.53	686.44	1869.47
C-03C	0.282744	0.000087	0.003019	0.000085	188	0.282733385	2.35	-1.45	752.14	1937.89
C-03R	0.282699	0.00005	0.001119	0.000044	188	0.282695065	1	-3.04	777.55	2022.23
C-04C	0.282679	0.000068	0.00396	0.00013	188	0.282665076	-0.06	-3.75	870.72	2088.14
C-04R	0.28273	0.000051	0.001188	0.00005	188	0.282725823	2.09	-1.94	735.44	1954.54
C-05C	0.2828	0.00014	0.00511	0.00019	188	0.282782033	4.07	0.53	710.69	1830.62
C-05R	0.282749	0.000051	0.00096	0.000011	188	0.282745625	2.79	-1.27	704.5	1910.92
C-06C	0.282772	0.000067	0.00206	0.00013	188	0.282764757	3.46	-0.46	692.36	1868.74
C-06R	0.282722	0.00007	0.001117	0.000028	188	0.282718072	1.81	-2.23	745.28	1971.6
C-07C	0.28262	0.0001	0.00354	0.00054	188	0.282607553	-2.1	-5.83	948.56	2214.34
C-07R	0.282718	0.00005	0.001284	0.000049	188	0.282713485	1.65	-2.37	754.21	1981.7
C-08C	0.282785	0.000085	0.0028	0.00011	188	0.282775155	3.83	0	687.41	1845.8
C-08R	0.282705	0.000094	0.001393	0.000049	188	0.282700102	1.18	-2.83	774.74	2011.15
C-09C	0.28276	0.00011	0.00387	0.00052	188	0.282746393	2.81	-0.88	746.15	1909.23
C-09R	0.282749	0.000089	0.001269	0.000067	188	0.282744538	2.75	-1.27	710.27	1913.31
C-10C	0.282789	0.000089	0.0025	0.00039	188	0.28278021	4.01	0.14	675.94	1834.65
C-10R	0.282723	0.000052	0.000967	0.000022	188	0.2827196	1.87	-2.19	740.95	1968.24
C-11C	0.282732	0.000058	0.001506	0.000039	188	0.282726705	2.12	-1.87	738.84	1952.6
C-11R	0.282671	0.000044	0.001073	0.000029	188	0.282667227	0.01	-4.03	815.78	2083.41
C-12C	0.28276	0.00011	0.00988	0.00053	188	0.282725261	2.07	-0.88	899.91	1955.78
C-12R	0.282747	0.000054	0.000788	0.000012	188	0.282744229	2.74	-1.34	704.12	1913.99
C-13C	0.282798	0.000063	0.001962	0.000025	188	0.282791101	4.4	0.46	653.2	1810.6
C-13R	0.282756	0.000053	0.0009	0.000001	188	0.282752835	3.04	-1.03	693.63	1895.03
C-14C	0.282715	0.00008	0.002051	0.000086	188	0.282707788	1.45	-2.48	774.14	1994.24
C-14R	0.282775	0.000043	0.001091	0.000045	188	0.282771164	3.69	-0.35	670.48	1854.61
C-15C	0.282694	0.000087	0.00235	0.00039	188	0.282685737	0.67	-3.22	810.85	2042.74
C-15R	0.282722	0.00007	0.001651	0.000037	188	0.282716195	1.75	-2.23	755.92	1975.74

MTO-01C	0.28266	0.000055	0.001326	0.000068	188	0.282655338	-0.41	-4.42	836.72	2109.52
MTO-01R	0.282674	0.000057	0.00097	0.00012	188	0.282670589	0.13	-3.93	809.39	2076.03
MTO-02C	0.282689	0.000063	0.000597	0.000014	188	0.282686901	0.71	-3.39	780.82	2040.18
MTO-02R	0.282706	0.000057	0.000468	0.000003	188	0.282704354	1.33	-2.79	754.8	2001.79
MTO-03C	0.282692	0.000078	0.000593	0.000012	188	0.282689915	0.82	-3.29	776.6	2033.55
MTO-03R	0.282636	0.00004	0.000559	0.000005	188	0.282634035	-1.16	-5.27	853.16	2156.28
MTO-04C	0.282659	0.000096	0.00185	0.00018	188	0.282652495	-0.51	-4.46	849.92	2115.76
MTO-04R	0.282719	0.000088	0.00139	0.00015	188	0.282714113	1.67	-2.33	754.92	1980.32
MTO-05C	0.28269	0.000071	0.00185	0.0001	188	0.282683495	0.59	-3.36	805.67	2047.66
MTO-05R	0.282665	0.000065	0.00123	0.00013	188	0.282660675	-0.22	-4.24	827.58	2097.8
MTO-06C	0.282742	0.000047	0.002216	0.000093	188	0.282734208	2.38	-1.52	738.64	1936.07
MTO-06R	0.282696	0.000061	0.000429	0.000015	188	0.282694492	0.98	-3.15	767.8	2023.49
MTO-07C	0.282706	0.000071	0.000505	0.000003	188	0.282704224	1.32	-2.79	755.52	2002.08
MTO-07R	0.282711	0.000048	0.00072	0.000029	188	0.282708468	1.47	-2.62	752.82	1992.74
MTO-08C	0.282648	0.00007	0.000581	0.000018	188	0.282645957	-0.74	-4.84	837.09	2130.12
MTO-08R	0.282657	0.000055	0.000631	0.00002	188	0.282654781	-0.43	-4.53	825.75	2110.75
MTO-09C	0.282656	0.00006	0.000472	0.000014	188	0.28265434	-0.44	-4.56	823.72	2111.71
MTO-09R	0.282705	0.000044	0.000702	0.000046	188	0.282702532	1.26	-2.83	760.79	2005.8
MTO-10C	0.282715	0.000065	0.001416	0.000075	188	0.282710021	1.53	-2.48	761.09	1989.32
MTO-10R	0.282763	0.000058	0.001073	0.000013	188	0.282759227	3.27	-0.78	686.98	1880.93
MTO-11C	0.2827	0.00013	0.00245	0.00025	188	0.282691385	0.87	-3.01	804.36	2030.32
MTO-11R	0.282714	0.000059	0.001119	0.000074	188	0.282710065	1.53	-2.51	756.53	1989.23
MTO-12C	0.282729	0.000073	0.0029	0.000004	188	0.282718803	1.84	-1.98	771.73	1970
MTO-12R	0.282703	0.000057	0.000799	0.00018	188	0.28270019	1.18	-2.9	765.5	2010.95
MTO-13C	0.282692	0.000078	0.001911	0.000081	188	0.282685281	0.65	-3.29	804.13	2043.74
MTO-13R	0.282703	0.000075	0.001354	0.000035	188	0.282698239	1.11	-2.9	776.76	2015.25
MTO-14C	0.282681	0.000047	0.000641	0.000002	188	0.282678747	0.42	-3.68	792.77	2058.1
MTO-14R	0.282742	0.000047	0.000525	0.000004	188	0.282740154	2.59	-1.52	706.22	1922.97
MTO-15C	0.282778	0.000075	0.00421	0.00011	188	0.282763197	3.41	-0.25	725.94	1872.18
MTO-15R	0.282707	0.000062	0.00142	0.00012	188	0.282702007	1.24	-2.76	772.47	2006.96

Table 6. Zircon Hf isotopic analyses, Conway and Mount Osceola Granites

Unit	Locality	Sample	(176Yb + 176Lu) / 176Hf (%)	176Hf/177Hf	± (1s)	176Lu/177Hf	176Hf/177Hf (T)	E-Hf (0)	E-Hf (0) ± (1s)	E-Hf (T)	Age (Ma)
Osceola Granite	Rattlesnake Mtn	2_05-29-19-02_Spot01	54.95259563	0.282544899	2.48228E-05	0.002436561	0.2825364	-8.49	0.88	-4.66	186.2
Osceola Granite	Rattlesnake Mtn	2_05-29-19-02_Spot02	52.34414441	0.282755617	1.74396E-05	0.002354703	0.282747448	-1.04	0.62	2.79	185.2
Osceola Granite	Rattlesnake Mtn	2_05-29-19-02_Spot04	36.46769898	0.282793578	2.64363E-05	0.001794779	0.282787405	0.30	0.93	4.17	183.6
Osceola Granite	Rattlesnake Mtn	2_05-29-19-02_Spot05	55.69199622	0.282661201	2.73079E-05	0.002615048	0.282652021	-4.38	0.97	-0.54	187.4
Osceola Granite	Rattlesnake Mtn	2_05-29-19-02_Spot08	131.761185	0.282505937	5.01075E-05	0.006188547	0.282484525	-9.87	1.77	-6.52	184.7
Osceola Granite	Rattlesnake Mtn	2_05-29-19-02_Spot10	51.57861079	0.282855919	2.60799E-05	0.002350248	0.282847757	2.51	0.92	6.34	185.4
Osceola Granite	Rattlesnake Mtn	2_05-29-19-02_Spot11	50.25962188	0.282770969	3.3481E-05	0.002247965	0.282763136	-0.50	1.18	3.36	186
Osceola Granite	Rattlesnake Mtn	2_05-29-19-02_Spot13	35.19492945	0.282790366	4.12485E-05	0.001531101	0.282784994	0.19	1.46	4.16	187.3
Osceola Granite	Rattlesnake Mtn	2_05-29-19-02_Spot15	36.11714226	0.282864517	2.9993E-05	0.001743513	0.28285841	2.81	1.06	6.75	187
Osceola Granite	Rattlesnake Mtn	2_05-29-19-02_Spot16	41.90766803	0.282766258	2.57302E-05	0.002090417	0.282758983	-0.66	0.91	3.21	185.8
Osceola Granite	Rattlesnake Mtn	2_05-29-19-02_Spot19	36.14468141	0.282778111	2.17995E-05	0.001700049	0.282772184	-0.24	0.77	3.68	186.1
Osceola Granite	Rattlesnake Mtn	2_05-29-19-02_Spot20	55.18780511	0.282592245	3.14137E-05	0.0025445	0.28258347	-6.82	1.11	-3.04	184.1
Osceola Granite	Rattlesnake Mtn	2_05-29-19-02_Spot22	107.1537895	0.282648754	6.53319E-05	0.005784782	0.282628706	-4.82	2.31	-1.42	185
Osceola Granite	Rattlesnake Mtn	2_05-29-19-02_Spot23	38.64383144	0.282778172	1.88787E-05	0.001812296	0.282771813	-0.24	0.67	3.70	187.3
Osceola Granite	Rattlesnake Mtn	2_05-29-19-02_Spot26	49.31286476	0.282662058	3.31583E-05	0.002225629	0.282654374	-4.35	1.17	-0.52	184.3
Osceola Granite	Rattlesnake Mtn	2_05-29-19-02_Spot28	26.21489542	0.28296239	2.18358E-05	0.001052726	0.282958697	6.27	0.77	10.31	187.3
Osceola Granite	Rattlesnake Mtn	2_05-29-19-02_Spot36	55.22427888	0.282572921	3.34158E-05	0.002491989	0.282564159	-7.50	1.18	-3.64	187.7
Osceola Granite	Rattlesnake Mtn	2_05-29-19-02_Spot37	43.59031978	0.282754856	2.14115E-05	0.002105362	0.282747465	-1.07	0.76	2.84	187.4
Osceola Granite	Rattlesnake Mtn	2_05-29-19-02_Spot38	23.15794518	0.282835167	2.13796E-05	0.001155628	0.282831188	1.77	0.76	5.72	183.8
Osceola Granite	Rattlesnake Mtn	2_05-29-19-02_Spot41	44.53817113	0.282664675	2.98831E-05	0.002098255	0.282657408	-4.25	1.06	-0.40	184.9
Osceola Granite	Rattlesnake Mtn	2_05-29-19-02_Spot43	38.46460635	0.282757556	1.75333E-05	0.001937824	0.282750884	-0.97	0.62	2.88	183.8
Osceola Granite	Rattlesnake Mtn	2_05-29-19-02_Spot44	108.3991711	0.282188126	2.6972E-05	0.004781318	0.282171305	-21.11	0.95	-17.54	187.8
Osceola Granite	Rattlesnake Mtn	2_05-29-19-02_Spot46	38.60243739	0.282729467	2.03587E-05	0.00182681	0.28272317	-1.96	0.72	1.90	184
Osceola Granite	Rattlesnake Mtn	2_05-29-19-02_Spot48	50.15679294	0.282660398	2.35687E-05	0.002365333	0.282652205	-4.41	0.83	-0.59	184.9
Osceola Granite	Rattlesnake Mtn	2_05-29-19-02_Spot50	83.1086668	0.282723813	3.71108E-05	0.004216244	0.282709201	-2.16	1.31	1.43	185
Osceola Granite	Humphrey's Ledge	4_05-29-19-04_Spot04	21.67057734	0.282791292	1.94842E-05	0.00114336	0.282787343	0.22	0.69	4.18	184.4
Osceola Granite	Humphrey's Ledge	4_05-29-19-04_Spot06	35.82212011	0.282555854	2.31692E-05	0.001897153	0.282549375	-8.10	0.82	-4.28	182.3
Osceola Granite	Humphrey's Ledge	4_05-29-19-04_Spot07	32.99902505	0.28268867	2.48282E-05	0.00167206	0.282682888	-3.41	0.88	0.49	184.6
Osceola Granite	Humphrey's Ledge	4_05-29-19-04_Spot08	37.46745052	0.282684272	2.66536E-05	0.00184922	0.282677863	-3.56	0.94	0.32	185
Osceola Granite	Humphrey's Ledge	4_05-29-19-04_Spot11	31.76320158	0.282787994	4.13621E-05	0.001872435	0.282781582	0.11	1.46	3.94	182.8
Osceola Granite	Humphrey's Ledge	4_05-29-19-04_Spot13	43.38076052	0.28289993	2.70855E-05	0.002040484	0.282892939	4.06	0.96	7.88	182.9
Osceola Granite	Humphrey's Ledge	4_05-29-19-04_Spot16	27.54002399	0.282849982	2.16368E-05	0.001445048	0.28284504	2.30	0.77	6.18	182.6
Osceola Granite	Humphrey's Ledge	4_05-29-19-04_Spot18	23.4045735	0.28269209	2.16138E-05	0.001221841	0.28268786	-3.29	0.76	0.67	184.8
Osceola Granite	Humphrey's Ledge	4_05-29-19-04_Spot20	21.75261918	0.282783614	2.26794E-05	0.001070575	0.282779942	-0.05	0.80	3.89	183.1
Osceola Granite	Humphrey's Ledge	4_05-29-19-04_Spot21	12.70783317	0.282853948	2.33955E-05	0.000658851	0.282851689	2.44	0.83	6.43	183
Osceola Granite	Humphrey's Ledge	4_05-29-19-04_Spot22	19.9700982	0.282919067	3.59689E-05	0.001083057	0.282915336	4.74	1.27	8.70	183.9
Osceola Granite	Humphrey's Ledge	4_05-29-19-04_Spot25	20.39945754	0.282768253	1.92008E-05	0.000938762	0.282765017	-0.59	0.68	3.38	184
Osceola Granite	Humphrey's Ledge	4_05-29-19-04_Spot28	42.35518377	0.282736059	1.73499E-05	0.002152944	0.282728707	-1.73	0.61	2.06	182.3
Osceola Granite	Humphrey's Ledge	4_05-29-19-04_Spot31	21.25953864	0.282726603	2.32338E-05	0.001077065	0.282722879	-2.07	0.82	1.91	184.6
Osceola Granite	Humphrey's Ledge	4_05-29-19-04_Spot32	41.27960469	0.28261707	2.41135E-05	0.002097873	0.282609902	-5.94	0.85	-2.14	182.4
Osceola Granite	Humphrey's Ledge	4_05-29-19-04_Spot33	21.42840857	0.282773523	2.68783E-05	0.000935187	0.282770312	-0.41	0.95	3.56	183.3
Osceola Granite	Humphrey's Ledge	4_05-29-19-04_Spot34	76.92158518	0.282548811	2.80485E-05	0.003416477	0.282537087	-8.35	0.99	-4.70	183.2
Osceola Granite	Humphrey's Ledge	4_05-29-19-04_Spot35	25.68928356	0.282757324	1.81427E-05	0.001226683	0.282753098	-0.98	0.64	2.96	183.9
Osceola Granite	Humphrey's Ledge	4_05-29-19-04_Spot36	24.99915669	0.282746183	2.83536E-05	0.001315927	0.282741685	-1.37	1.00	2.52	182.5
Osceola Granite	Humphrey's Ledge	4_05-29-19-04_Spot40	36.62435662	0.282673705	2.35941E-05	0.00185302	0.28266729	-3.94	0.83	-0.06	184.8
Osceola Granite	Humphrey's Ledge	4_05-29-19-04_Spot41	31.89195677	0.282879408	2.18394E-05	0.001742616	0.282873431	3.34	0.77	7.20	183.1
Osceola Granite	Humphrey's Ledge	4_05-31-19-04_Spot01	27.22732321	0.282791678	3.11419E-05	0.001384703	0.282786913	0.24	1.10	4.15	183.7
Osceola Granite	Humphrey's Ledge	4_05-31-19-04_Spot03	16.24244617	0.28283234	2.32584E-05	0.000936759	0.282829178	1.67	0.82	5.57	180.2

Osceola Granite	Humphrey's Ledge	4_05-31-19-04_Spot05	15.41655255	0.282749884	2.18524E-05	0.000758477	0.282747325	-1.24	0.77	2.67	180.1
Osceola Granite	Humphrey's Ledge	4_05-31-19-04_Spot06	14.05889528	0.282750001	2.16701E-05	0.000709948	0.282747607	-1.24	0.77	2.68	180
Osceola Granite	Humphrey's Ledge	4_05-31-19-04_Spot07	44.62364458	0.282774534	2.46557E-05	0.002292639	0.282766627	-0.37	0.87	3.44	184.1
Osceola Granite	Humphrey's Ledge	4_05-31-19-04_Spot08	27.49624676	0.282760888	2.37024E-05	0.001504768	0.282755738	-0.85	0.84	3.03	182.7
Osceola Granite	Humphrey's Ledge	4_05-31-19-04_Spot10	64.99367481	0.282819519	3.15172E-05	0.003518466	0.282807273	1.22	1.11	4.92	185.8
Osceola Granite	Humphrey's Ledge	4_05-31-19-04_Spot13	27.36776769	0.282755917	1.86578E-05	0.00137204	0.282751266	-1.03	0.66	2.83	181
Osceola Granite	Humphrey's Ledge	4_05-31-19-04_Spot14	31.41379818	0.282683419	2.13525E-05	0.001558576	0.282678097	-3.59	0.76	0.27	182.3
Osceola Granite	Humphrey's Ledge	4_05-31-19-04_Spot15	14.19283533	0.282775417	1.74921E-05	0.000739898	0.282772907	-0.34	0.62	3.60	181.1
Osceola Granite	Humphrey's Ledge	4_05-31-19-04_Spot19	22.4576934	0.282661855	2.48579E-05	0.001116285	0.282658058	-4.35	0.88	-0.45	181.6
Osceola Granite	Humphrey's Ledge	4_05-31-19-04_Spot21	41.18280676	0.282705866	3.58592E-05	0.002562207	0.282697122	-2.80	1.27	0.94	182.2
Osceola Granite	Humphrey's Ledge	4_05-31-19-04_Spot23	18.65185506	0.282762156	1.61107E-05	0.000936904	0.282758997	-0.81	0.57	3.08	180
Osceola Granite	Humphrey's Ledge	4_05-31-19-04_Spot24	62.93870712	0.282737845	2.92219E-05	0.003582749	0.282725368	-1.67	1.03	2.02	185.9
Osceola Granite	Humphrey's Ledge	4_05-31-19-04_Spot25	32.46383172	0.282769504	3.30127E-05	0.001517689	0.282764335	-0.55	1.17	3.31	181.8
Osceola Granite	Humphrey's Ledge	4_05-31-19-04_Spot26	66.05484525	0.282737104	2.31898E-05	0.003182664	0.282726212	-1.69	0.82	1.98	182.7
Osceola Granite	Humphrey's Ledge	4_05-31-19-04_Spot27	14.06331325	0.282829745	2.54051E-05	0.000792517	0.282827046	1.58	0.90	5.53	181.8
Osceola Granite	Humphrey's Ledge	4_05-31-19-04_Spot29	20.64588793	0.282842816	1.36557E-05	0.001029671	0.282839264	2.04	0.48	6.01	184.2
Osceola Granite	Humphrey's Ledge	4_05-31-19-04_Spot30	40.00529442	0.28272481	2.31918E-05	0.002019304	0.28271785	-2.13	0.82	1.71	184
Osceola Granite	Humphrey's Ledge	4_05-31-19-04_Spot31	69.59870409	0.282640713	2.19607E-05	0.003078691	0.282630142	-5.10	0.78	-1.40	183.3
Osceola Granite	Humphrey's Ledge	4_05-31-19-04_Spot32	51.75644295	0.282604062	2.93237E-05	0.002641545	0.282594888	-6.40	1.04	-2.60	185.4
Osceola Granite	Humphrey's Ledge	4_05-31-19-04_Spot36	47.9405205	0.282808763	2.7215E-05	0.002695255	0.282799398	0.84	0.96	4.63	185.5
Osceola Granite	Humphrey's Ledge	4_05-31-19-04_Spot39	19.09028369	0.282707117	1.57047E-05	0.000978324	0.282703815	-2.75	0.56	1.13	180.2
Osceola Granite	Humphrey's Ledge	4_05-31-19-04_Spot40	55.47728435	0.282658408	2.48439E-05	0.002862383	0.282648446	-4.48	0.88	-0.70	185.8
Conway Granite	Middle Mtn	6_05-29-19-01_Spot04	32.37449305	0.282852023	2.81513E-05	0.001579353	0.282846594	2.37	1.00	6.26	183.5
Conway Granite	Middle Mtn	6_05-29-19-01_Spot07	39.54445342	0.282801735	3.25771E-05	0.001835212	0.282795551	0.59	1.15	4.37	179.9
Conway Granite	Middle Mtn	6_05-29-19-01_Spot11	59.67288832	0.283016572	4.52383E-05	0.003014025	0.283006279	8.19	1.60	11.88	182.3
Conway Granite	Middle Mtn	6_05-29-19-01_Spot12	26.94402334	0.28283731	2.94594E-05	0.001297095	0.282832973	1.85	1.04	5.67	178.5
Conway Granite	Middle Mtn	6_05-29-19-01_Spot14	66.08240701	0.282591081	3.91572E-05	0.00330802	0.282579835	-6.86	1.38	-3.22	181.5
Conway Granite	Middle Mtn	6_05-29-19-01_Spot20	25.81143212	0.282651424	3.25719E-05	0.001229841	0.28264718	-4.72	1.15	-0.78	184.2
Conway Granite	Middle Mtn	6_05-29-19-01_Spot22	26.90877107	0.282875226	2.49323E-05	0.001321887	0.282870734	3.19	0.88	7.07	181.4
Conway Granite	Middle Mtn	6_05-29-19-01_Spot25	34.03561485	0.282793113	2.74964E-05	0.001622188	0.282787521	0.29	0.97	4.18	184
Conway Granite	Middle Mtn	6_05-29-19-01_Spot27	54.83802796	0.282803974	3.06105E-05	0.00270325	0.282794935	0.67	1.08	4.32	178.5
Conway Granite	Middle Mtn	6_05-29-19-01_Spot28	33.89925598	0.282800428	2.81402E-05	0.001722513	0.282794598	0.55	1.00	4.36	180.7
Conway Granite	Middle Mtn	6_05-29-19-01_Spot30	34.49682063	0.282785886	2.85147E-05	0.001540858	0.282780743	0.03	1.01	3.81	178.2
Conway Granite	Middle Mtn	6_05-29-19-01_Spot31	26.13381536	0.282767702	2.53846E-05	0.001087504	0.282764029	-0.61	0.90	3.27	180.3
Conway Granite	Middle Mtn	6_05-29-19-01_Spot33	22.51022862	0.282917435	3.63656E-05	0.001116102	0.282913714	4.68	1.29	8.51	178
Conway Granite	Middle Mtn	6_05-29-19-01_Spot35	36.36263351	0.282757399	2.96397E-05	0.001719801	0.282751455	-0.98	1.05	2.91	184.5
Conway Granite	Middle Mtn	6_05-29-19-01_Spot40	24.95572325	0.282911765	2.80945E-05	0.001425335	0.282906959	4.48	0.99	8.32	180
Conway Granite	Middle Mtn	6_05-29-19-01_Spot42	82.08604453	0.282663137	2.77051E-05	0.003826566	0.282650314	-4.31	0.98	-0.79	178.9
Conway Granite	Middle Mtn	6_05-29-19-01_Spot43	22.91789914	0.28273936	2.58418E-05	0.001169892	0.282735418	-1.61	0.91	2.25	179.9
Conway Granite	Middle Mtn	6_05-29-19-01_Spot44	77.1842648	0.282820111	3.24422E-05	0.003701162	0.282807569	1.24	1.15	4.82	180.9
Conway Granite	Middle Mtn	6_05-29-19-01_Spot45	28.5769555	0.282933164	2.4935E-05	0.001365544	0.28292846	5.24	0.88	9.16	183.9
Conway Granite	Kancamangus Hwy	14_06-21-15-01_Spot05	23.48414458	0.282838947	3.46349E-05	0.001566353	0.282833257	1.91	1.22	6.02	193.9
Conway Granite	Kancamangus Hwy	14_06-21-15-01_Spot09	41.08545684	0.282870076	3.51918E-05	0.002417718	0.282861376	3.01	1.24	6.97	192.1
Conway Granite	Kancamangus Hwy	14_06-21-15-01_Spot10	39.89544291	0.28284561	4.10373E-05	0.002608021	0.282836225	2.14	1.45	6.08	192.1
Conway Granite	Kancamangus Hwy	14_06-21-15-01_Spot17	31.79875075	0.282716162	1.76726E-05	0.001468868	0.282710876	-2.43	0.62	1.65	192.1
Conway Granite	Kancamangus Hwy	14_06-21-15-01_Spot18	26.26541083	0.28279832	3.5001E-05	0.001416737	0.282793169	0.47	1.24	4.60	194.1
Conway Granite	Kancamangus Hwy	14_06-21-15-01_Spot19	59.59968304	0.282683193	3.86644E-05	0.003326587	0.282671172	-3.60	1.37	0.26	192.9
Conway Granite	Kancamangus Hwy	14_06-21-15-01_Spot20	21.10308304	0.282587797	3.35764E-05	0.001023805	0.282584118	-6.97	1.19	-2.84	191.8
Conway Granite	Kancamangus Hwy	14_06-21-15-01_Spot22	15.04931525	0.282658608	2.5583E-05	0.000777568	0.28265584	-4.47	0.90	-0.35	190
Conway Granite	Kancamangus Hwy	14_06-21-15-01_Spot23	12.27118956	0.282920418	2.06797E-05	0.000660684	0.282918069	4.79	0.73	8.93	189.8

Conway Granite	Kancamangus Hwy	14_06-21-15-01_Spot26	32.51846962	0.282782107	3.23052E-05	0.001604649	0.282776422	-0.10	1.14	3.90	189.1
Conway Granite	Kancamangus Hwy	14_06-21-15-01_Spot27	17.00579109	0.282615439	2.68783E-05	0.000930034	0.282612071	-6.00	0.95	-1.82	193.3
Conway Granite	Kancamangus Hwy	14_06-21-15-01_Spot29	14.00265574	0.282667427	3.29754E-05	0.000738934	0.282664752	-4.16	1.17	0.04	193.2
Conway Granite	Kancamangus Hwy	14_06-21-15-01_Spot30	65.72275214	0.282555311	4.43721E-05	0.003234785	0.282543645	-8.12	1.57	-4.26	192.5
Conway Granite	Kancamangus Hwy	14_06-21-15-01_Spot33	64.44315239	0.282609199	6.15861E-05	0.004415535	0.28259306	-6.22	2.18	-2.45	195.1
Conway Granite	Kancamangus Hwy	14_06-21-15-01_Spot34	13.19061814	0.282638192	1.91572E-05	0.000696105	0.282635668	-5.19	0.68	-0.98	193.5
Conway Granite	Kancamangus Hwy	14_06-21-15-01_Spot38	12.76737247	0.282759254	2.35862E-05	0.000657868	0.282756873	-0.91	0.83	3.30	193.2
Conway Granite	Kancamangus Hwy	14_06-21-15-01_Spot42	14.10144428	0.282665687	3.096E-05	0.000697132	0.282663195	-4.22	1.09	-0.07	190.8
Conway Granite	Kancamangus Hwy	14_06-21-15-01_Spot43	41.56024776	0.282806729	2.90494E-05	0.001949135	0.282799854	0.77	1.03	4.71	188.3
Conway Granite	Kancamangus Hwy	14_06-21-15-01_Spot44	12.61473203	0.282862889	2.0206E-05	0.000656584	0.282860568	2.75	0.71	6.87	188.7
Conway Granite	Kancamangus Hwy	14_06-21-15-01_Spot45	32.51143872	0.282614271	3.83176E-05	0.001628697	0.282608367	-6.04	1.36	-1.95	193.5
Conway Granite	Kancamangus Hwy	14_06-21-15-01_Spot47	110.7176364	0.282685655	5.36153E-05	0.005039608	0.282667178	-3.51	1.90	0.18	195.7
Conway Granite	Kancamangus Hwy	14_06-21-15-01_Spot48	15.75388154	0.28266297	3.1658E-05	0.000748521	0.28266028	-4.32	1.12	-0.15	191.9
Conway Granite	Kancamangus Hwy	14_06-21-15-01_Spot50	76.0962579	0.282598136	5.02731E-05	0.004903051	0.282580408	-6.61	1.78	-2.95	193
Conway Granite	Mt Willard	1_08-26-15-01_Spot03	31.53466203	0.282793509	3.1512E-05	0.001832766	0.282786731	0.30	1.11	4.45	197.4
Conway Granite	Mt Willard	1_08-26-15-01_Spot05	34.2778701	0.282628295	2.00536E-05	0.001950983	0.282621102	-5.54	0.71	-1.42	196.8
Conway Granite	Mt Willard	1_08-26-15-01_Spot07	31.31461281	0.2826407	1.79862E-05	0.001692329	0.282634448	-5.10	0.64	-0.94	197.2
Conway Granite	Mt Willard	1_08-26-15-01_Spot10	28.45806286	0.282708887	2.42376E-05	0.001505744	0.282703304	-2.69	0.86	1.51	197.9
Conway Granite	Mt Willard	1_08-26-15-01_Spot15	39.18706777	0.27862213	0.000119857	0.002690004	0.278611954	-147.21	4.24	-143.15	201.9
Conway Granite	Mt Willard	1_08-26-15-01_Spot19	27.4566948	0.282705668	2.12285E-05	0.001443482	0.282700373	-2.81	0.75	1.36	195.8
Conway Granite	Mt Willard	1_08-26-15-01_Spot21	51.49045744	0.281908331	5.30467E-05	0.003232795	0.281896479	-31.00	1.88	-27.08	195.7
Conway Granite	Mt Willard	1_08-26-15-01_Spot23	27.72212417	0.282636984	2.18224E-05	0.00169395	0.282630729	-5.23	0.77	-1.08	197.1
Conway Granite	Mt Willard	1_08-26-15-01_Spot24	39.54457078	0.282611168	2.39836E-05	0.001921976	0.282603962	-6.15	0.85	-1.96	200.1
Conway Granite	Mt Willard	1_08-26-15-01_Spot25	57.17489961	0.282541337	3.40694E-05	0.002743276	0.282531016	-8.62	1.20	-4.52	200.8
Conway Granite	Mt Willard	1_08-26-15-01_Spot27	44.40064535	0.282702291	3.00945E-05	0.001843442	0.282695259	-2.92	1.06	1.35	203.6
Conway Granite	Mt Willard	1_08-26-15-01_Spot30	19.48281254	0.282593334	2.00508E-05	0.001068734	0.282589309	-6.78	0.71	-2.45	201
Conway Granite	Mt Willard	1_08-26-15-01_Spot33	20.85170553	0.282615714	1.90376E-05	0.001129344	0.282611467	-5.99	0.67	-1.68	200.7
Conway Granite	Mt Willard	1_08-26-15-01_Spot36	32.10652762	0.282790456	3.5948E-05	0.002635503	0.282780378	0.19	1.27	4.37	204.1